Nuclear Reactor Physics Experiments

Misawa, Tsuyoshi; Unesaki, Hironobu; Pyeon, Cheolho

Nuclear Reactor Physics Experiments

Tsuyoshi Misawa, Hironobu Unesaki and Cheolho Pyeon

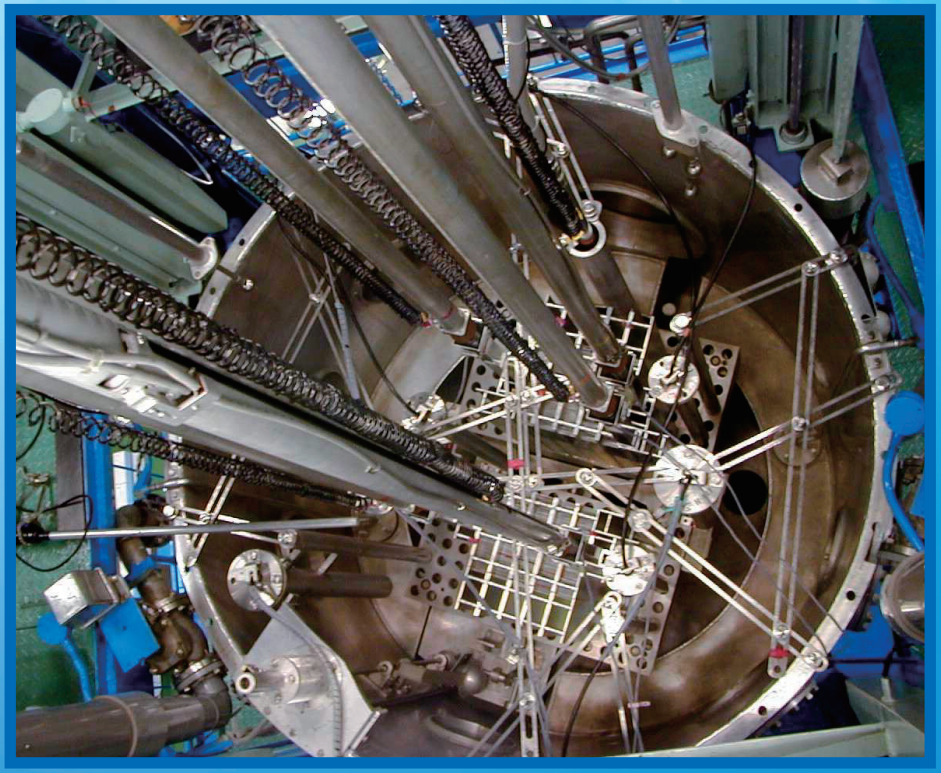

Nuclear Reactor Physics Experiments Tsuyoshi Misawa, Hironobu Unesaki and Cheolho Pyeon

Nuclear Reactor Physics Experiments

Nuclear Reactor Physics Experiments

Tsuyoshi Misawa, Hironobu Unesaki and Cheolho Pyeon

Kyoto University Press

First published in 2010
Reprinted 2018
Kyoto University Press
Yoshida South Campus, Kyoto University
69 Konoe-cho Yoshida
Sakyo, Kyoto 606−8315

Japan
Telephone: +81−75−761−6182
Fax: +81−75−761−6190
Email: sales@kyoto-up.or.jp
Web: http://www.kyoto-up.or.jp

Printed in Japan by Kwix co., Ltd.

ISBN 978−4−87698−959−1

Contents

Preface

This is a laboratory instructions book for the "Joint Reactor Laboratory Course for Students" (mainly graduate school and partly undergraduate school students), which we prepared over the course of thirty years since 1975 at the Kyoto University Critical Assembly (KUCA); this book has been translated from Japanese to English.

The major objective of this course is to help students understand the essence of nuclear reactor physics and radiation detection through experiments conducted at the KUCA C-core (water-moderated- and -reflected-core). At the same time, it is expected that by the end of the course, students would be able to gain substantial knowledge related to nuclear engineering.

Thus, students who have studied courses on subjects such as reactor physics, reactor engineering, and radiation detection in their schools will find this book exciting, and it will help them broaden their horizon. A multitude of experiences over the past thirty years have demonstrated that students majoring in nuclear engineering must have at least a rough knowledge of reactor physics and radiation detection fields before they can work effectively with other scientists and engineers in a team. Consequently, the present book contains information on a wide variety of reactor physics and radiation detection experiments. The experiments have been collated to emphasize on unique ideas or concepts by many professors and professors emeriti of the following Japanese universities: Hokkaido University, Tohoku University, Tokyo Institute of Technology, Tokyo City University (the former Musashi Institute of Technology), Tokai University, Nagoya University, Osaka University, Kinki University, Kobe University (the former Kobe University of Mercantile Marine), Fukui University, Kyushu University, and Kyoto University.

We would like to especially thank many professors and professors emeriti of the abovementioned Japanese universities for their support and patience throughout the many years in which the manuscript for the Japanese version of the textbook was finalized. The careful review of the manuscript and figure preparation by Prof. Jae-Yong Lim of KUCA was invaluable in preparing the final manuscript.

We gratefully acknowledge the meticulous efforts of Mr. Itaru Saito of the Kyoto University Press for his contribution in finalizing the entire manuscript.

This book was partly supported under the "Energy Science in the Age of Global Warming" of Global Center of Excellence (G-COE) program (J−051) of the Ministry of Education, Culture, Sports, Science and Technology of Japan.

Osaka, Japan
25th February, 2010

Tsuyoshi Misawa
Hironobu Unesaki
Cheolho Pyeon

List of Contributors

Tsuyoshi Misawa (BS, 1984; MS, 1986; Ph. D., 1989, nuclear engineering, Kyoto University, Japan) is Professor of Nuclear Engineering Science Division, Institute for Integrated Radiation and Nuclear Science, Kyoto University. His background includes reactor physics, nuclear design calculations, and nuclear education.

Hironobu Unesaki (BS, 1985; MS, 1987, nuclear engineering, Osaka University, Japan; Ph. D., 2001, energy science, Kyoto University, Japan) is Professor of Nuclear Engineering Science Division, Institute for Integrated Radiation and Nuclear Science, Kyoto University. His background includes reactor physics, nuclear design calculations, and nuclear fuel management.

Cheolho Pyeon (BS, 1995; MS, 1997, nuclear engineering, Nagoya University, Japan; Ph. D., 2000, energy science, Kyoto University, Japan) is Associate Professor of Nuclear Engineering Science Division, Institute for Integrated Radiation and Nuclear Science, Kyoto University. His background includes reactor physics, nuclear design calculations, and nuclear education.

Introduction to Kyoto University Critical Assembly (KUCA)

1. General Description of KUCA Facility

1−1 KUCA Facility

The Kyoto University Critical Assembly (KUCA) is a multi-core-type critical assembly developed by the Kyoto University, Japan, as a facility that can be used by researchers from all the universities in Japan to carry out studies in the field of reactor physics. KUCA was established in 1974 as one of the main facilities of the Institute for Integrated Radiation and Nuclear Science (former the Research Reactor Institute), Kyoto University, located at Kumatori-cho, Sennan-gun, Osaka.

Fig. 1 View of the KUCA building

KUCA is a multi-core-type critical assembly consisting of two solid-moderated cores (A- and B-cores) and one light-water-moderated core (C-core). However, only a single core can attain the critical state at a given time because the assembly is equipped with a single control mechanism that prevents the simultaneous operation of multiple cores. Users can select the core that is

the most appropriate for their experiment. A pulsed neutron source is also installed, which can be used in combination with the critical assembly.

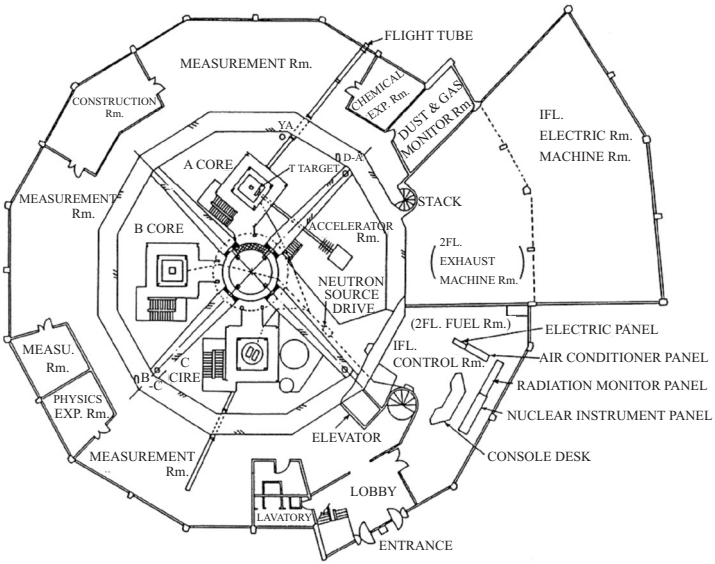

Fig. 2 Horizontal cross section of the KUCA building

Owing to the compatibility of KUCA, a wide variety of research and education is being performed at the facility. Currently, KUCA is being used for the following research activities:

- basic studies on new reactor concepts
- basic studies on thorium-fueled reactors
- basic studies on fusion-fission hybrid systems
- basic studies on subcritical systems
- basic studies on accelerator-driven systems (ADS)
- basic studies on nuclear characteristics of minor actinides
- experimental education course[1–7] for students majoring in nuclear engineering

Experimental and analytical studies on the validation of nuclear data and codes and the development of new detector systems are also conducted.

1–2 Solid-Moderated-Cores (A- and B-cores)

Two solid-moderated cores (A- and B-cores) are installed at KUCA.

Square-shaped coupon-type uranium fuel plates (93% enriched) of length 2″, breadth 2″, and thickness 1/16″ covered with a thin plastic coating are used as the fuel material. Solid moderator materials such as polyethylene and graphite are combined with enriched uranium, thorium, and natural uranium plates to form the fuel elements. Polyethylene, graphite, and beryllium are used as the reflector elements.

A wide variety of neutron spectra could be achieved by varying the composition of fuel and moderator plates in the fuel element, and also by varying the reflector elements.

Fig. 3 Solid-moderated and -reflected core

The A-core can be used in combination with the pulsed neutron generator. Currently, it is used for carrying out studies on accelerator-driven systems (ADS) and fission-fusion hybrid reactor systems (see Sec. 1−4).

1−3 Light-Water-Moderated Core (C-core)

A single light-water-moderated core (C-core) is installed at KUCA. Plate-type uranium fuel (93% enriched) of length 600 mm, width 62 mm, and thickness 1.5 mm with an aluminum (Al) cladding of thickness 0.5 mm is used in the C-core. In addition, there are two types of curved fuel plates − one 93% and the other 45% enriched − of length 650 mm and thickness 1.4 mm with an Al cladding of thickness 0.45 mm; 32 plates with different curvatures and widths are used.

The fuel element is formed by assembling the fuel plates in aluminum fuel frames. The fuel elements are loaded in a core tank of diameter

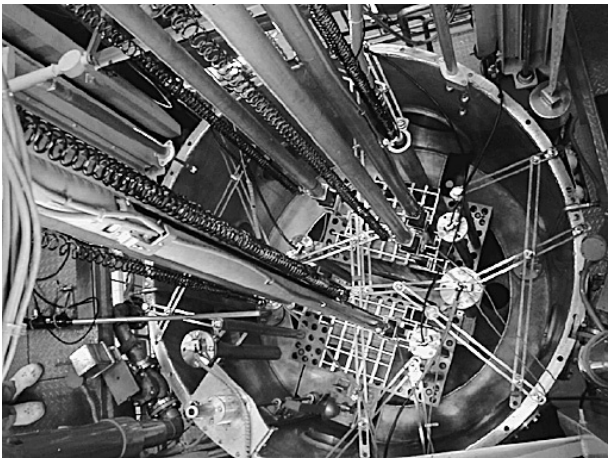

Fig. 4 Light-water-moderated core (C-core)

2,000 mm, and then immersed in light water to form the core. A part of the reflector region can be substituted with a heavy-water reflector. Three types of fuel frames, each having different fuel loading pitch and thus providing different neutron spectra in the core, are available. The core can be separated into two parts with an arbitrary gap width, and it is suitable for coupled core and criticality safety studies.

The C-core is used for carrying out a wide variety of basic studies on light-water-moderated systems, such as development of a high-flux research reactor, enrichment reduction in a research reactor, criticality safety, and study of coupled core theory.

The C-core is also used for conducting a graduate-level joint reactor laboratory course in affiliation with ten Japanese universities in addition to conducting an undergraduate-level reactor laboratory course in affiliation with the Kyoto University. International reactor laboratory courses for students in Korea and Sweden are also being conducted since 2003 and 2007, respectively.

1−4 Pulsed Neutron Source

A pulsed neutron generator (see Fig. 5) is attached to KUCA. Deuteron ion beam is injected onto a tritium target to generate the pulsed neutrons through $^{3}H(d, n)^{4}He$ reactions. The pulsed neutron generator can be used in combination with the critical assembly (A-core). The system consists of a duoplasmatron-type ion source, a high-voltage generator with a capacity of 300 kV, an acceleration tube, a beam pulsing system, and a tritium target.

The maximum acceleration voltage is 300 kV with an ion beam current of approx. 5 mA. A neutron pulse with pulse width in the range of 100 ns to 300 μs, a pulse repetition rate of 0.1 Hz to 30 kHz (max. duty ratio 1%) can be achieved.

Fig. 5 Pulsed neutron generator

The pulse neutron generator is currently being used in combination with the A-core, and it has been used for carrying out basic studies on ADS and fission-fusion hybrid reactor systems.

1−5 Control Room

Reactor operations and most of the measurements (except activation measurements) are performed in the control room (see Fig. 6). The control room is designed to enable user-friendly operation, and it is suited for educational and training purposes.

2. Details of the Light-Water-Moderated Core (C-core)

This experimental course is conducted using the light-water-moderated core (C-core) of KUCA. In this section, detailed information on the C-core is described.

2−1 Overall Structure

The overall structure of the C-core is shown in Fig. 7. The core assembly (reactor core) is placed inside the core tank, as shown in Fig. 4. Control

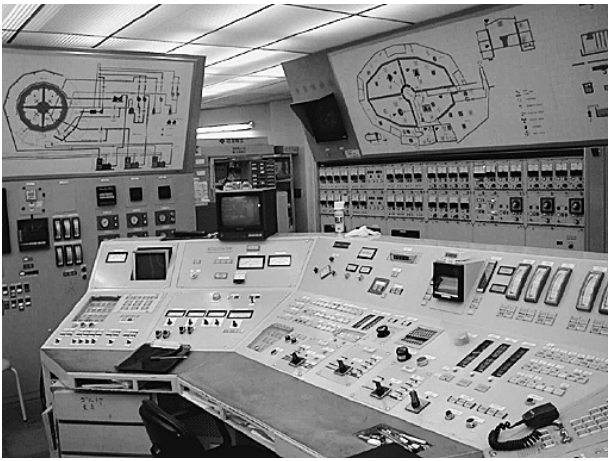

Fig. 6 Control room

and safety rods, and neutron detectors are placed around the reactor core. The core tank is supported by a three-floored support. A dump tank containing light water is placed at the height of the lower pit. Light water is first pumped up into the core tank, from which it is then supplied to the moderator and reflector during the reactor operation.

2−2 Core Tank and Grid Plate

The core tank (see Fig. 4) is made of aluminum, and its diameter is 2,000 mm and depth is 2,000 mm. Light water is fed from the bottom of the core tank. A grid plate is placed in the core tank, in which the fuel elements, control and safety rods, and neutron detectors are placed. The grid plate can be separated manually into two sections, thereby enabling to carry out experiments on coupled core reactors.

2−3 Fuel Plate and Fuel Frame

The fuel used in the C-core is a plate-type fuel (see Fig. 8) made of a U-Al alloy (thickness: 0.5 mm) that is cladded with a thick aluminum layer (thickness: 0.5 mm). The overall length, width, and thickness of the fuel plate are 600 mm, 62 mm, and 1.5 mm, respectively. The region containing uranium (U-Al alloy) is called fuel meat, and its length, width, and thickness are 570 mm, 52.8 mm, and 0.5 mm, respectively. Each fuel plate contains 8.89 g of ^{235}U.

The fuel plates are inserted in the fuel frame (see Fig. 9), which consists of side plates with grooves for inserting the fuel plates, frame base, and

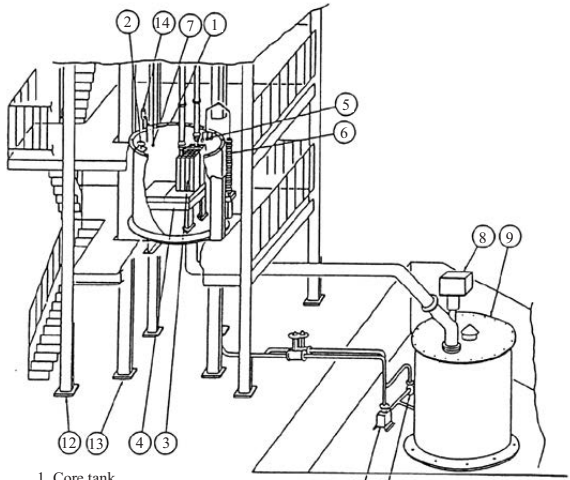

1. Core tank
2. Handl for the core separation mechanism
3. Core assembly
4. Core separation mechanism
5. Float switch to detect the core overflow
6. Overflow tube
7. Water level switch
8. Dump valve
9. Dump tank
10. High-flow feed pump
11. Low-flow feed pump
12. Supporting structure of the scaffold
13. Supporting structure of the core tank
14. Water feed tank for brecision control

Fig. 7 Sketch of the KUCA light-water-moderated core (C-core)

handles. Three kinds of side plates with different groove pitches can be used in order to vary the water-to-uranium ratio of the core and thus the neutron spectrum of the core.

The detailed structure of the fuel frame is shown in Fig. 10. The horizontal cross section is a rectangle of 70 mm by 140 mm. Three types of fuel frames − corresponding to the number of grooves in the side plate and thus the fuel pitch p − are available; they are referred to as C30, C35, and C45, which corresponds to a fuel pitch p of 3.0 mm, 3.5 mm, and 4.5 mm, respectively. The number of fuel plates loaded in the fuel frame can be adjusted by adding or removing the fuel plates one by one. Note that the maximum number of fuel plates loaded in a single fuel frame depends on the type of the frame; the maximum number of fuel plates for C30, C35, and C45 frames is 47, 40, and 31, respectively.

After loading the appropriate number of fuel plates, the fuel frames are loaded into the core tank. They are arranged on a grid plate with a pitch of 71 mm × 142 mm to form the reactor core. Control and safety rods, neutron

source, and neutron detectors are also arranged on the grid plate.

It should be noted that, after arranging the fuel plates on the grid plate, certain gaps are formed between the neighboring fuel frames, as shown in Fig. 11. These gaps are filled with light water during the reactor operation.

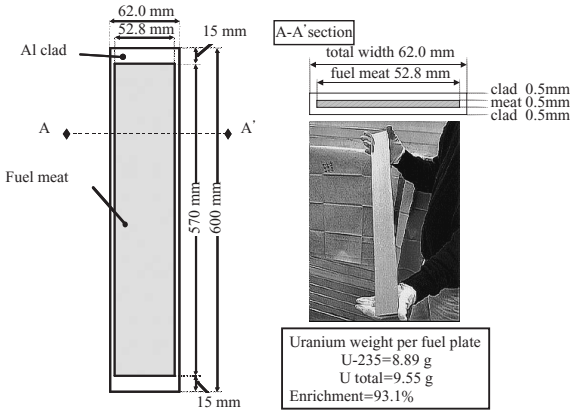

Fig. 8 Fuel plate

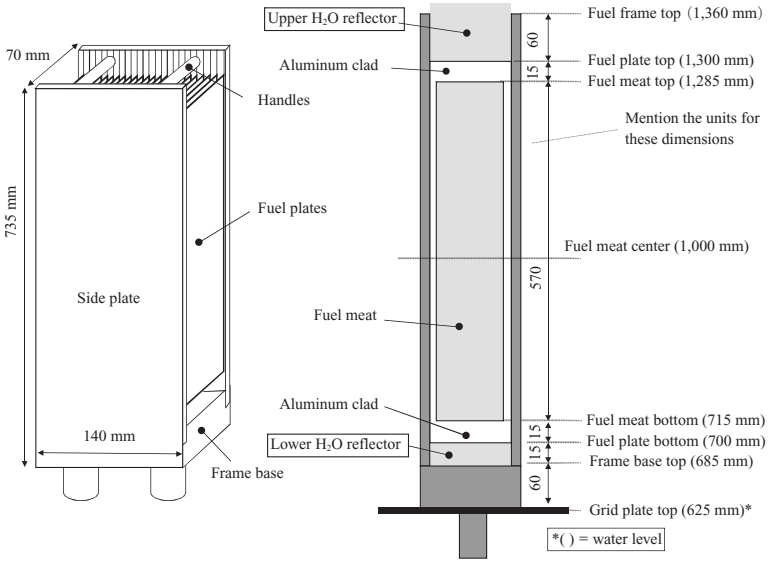

Fig. 9 Fuel frame

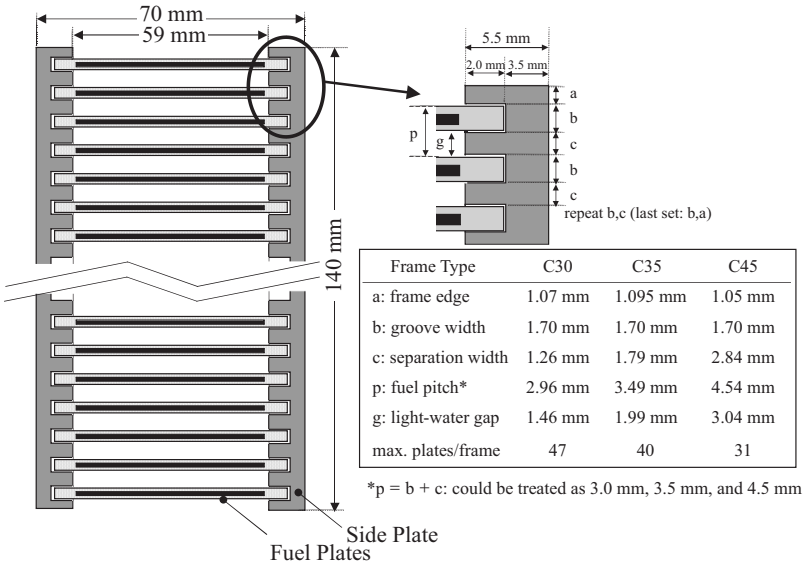

Frame Type	C30	C35	C45
a: frame edge	1.07 mm	1.095 mm	1.05 mm
b: groove width	1.70 mm	1.70 mm	1.70 mm
c: separation width	1.26 mm	1.79 mm	2.84 mm
p: fuel pitch*	2.96 mm	3.49 mm	4.54 mm
g: light-water gap	1.46 mm	1.99 mm	3.04 mm
max. plates/frame	47	40	31

*p = b + c: could be treated as 3.0 mm, 3.5 mm, and 4.5 mm

Fig. 10 Horizontal cross section of fuel frame and detailed dimensions

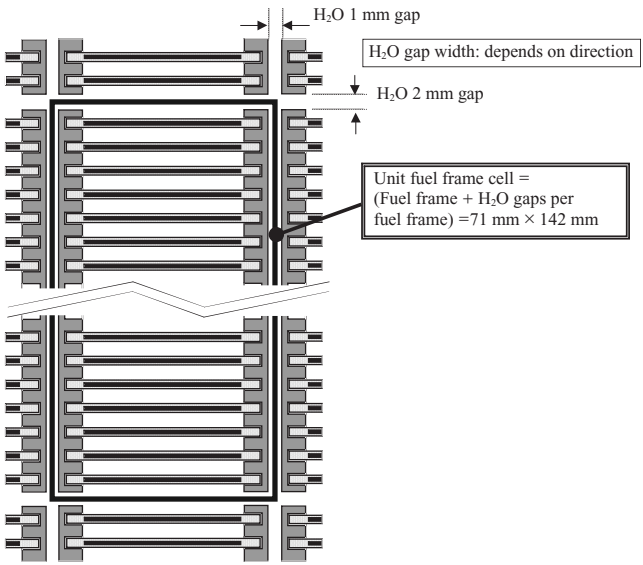

Fig. 11 Unit fuel frame cell and light-water-filled gaps between neighboring fuel frames

2−4 Core Configuration

A typical core configuration is shown in Fig. 12. In this example, 12 fuel frames are arranged in four rows, each row containing three fuel frames. Eight fuel frames are fully loaded and four are partially loaded with fuel plates in order to adjust the critical mass. Three control rods (C1, C2, C3) and three safety rods (S4, S5, S6) surround the core. Detailed structure of the control rod is given in Chapter 2 (Control Rod Calibration). Three fission chambers (#1, #2, #3) and three uncompensated ionization chambers (#4, #5, #6) are used for monitoring the neutron level. The neutron source (N: Am-Be, 7.4×10^{10} Bq and 2 Ci, Neutron yield 5.0×10^{6} *n*/s) is used for supplying the initial neutrons for startup. During operation, light water surrounds the core and acts as a reflector.

The KUCA cores are named with identical core IDs. The core ID consists of three parts, namely, fuel frame type, separation gap of the core in cm, and number of rows in the core in parenthesis. Assuming that the C35 fuel frame is used in Fig. 12, the core ID would be **C35G0(4R)**, as the core consists of C35 fuel frame (C35), has no separation gap (G0), and comprises four rows of fuel frames (4R).

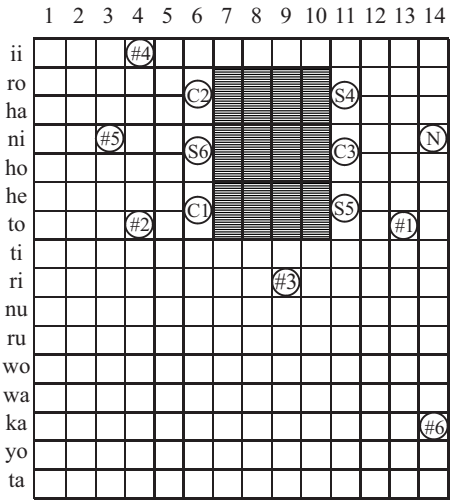

Fig. 12 Example of core configuration (C1−C3: control rods, S4−S6: safety rods, N: neutron source, #1−#3: fission chambers, #4−#6: uncompensated ionization chambers)

The light water stored in the dump tank is pumped up into the core tank during the startup of the reactor. Light water acts as a moderator and reflector. The water levels in the core tank corresponding to the fuel frame, fuel plate, and detectors are shown in Fig. 13 and also in Fig. 9. This relationship between the water levels in the core tank and the core structure is used to analyze several experiments.

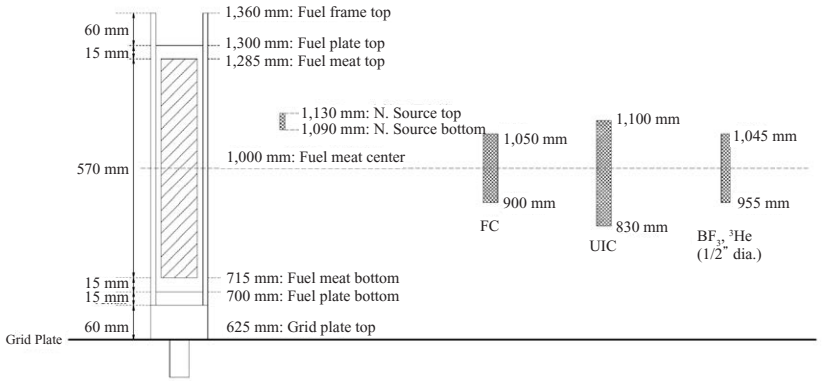

Fig. 13 Water level in the core tank and vertical positions of fuel frame, fuel plate, neutron source, and detectors

References

1. K. Nishina, "Experience of Joint Reactor Laboratory Course with KUCA," *J. the Atomic Energy Society of Japan*, **24**, 865 (1982).
2. H. Nishihara, S. Shiroya, and K. Kanda, "Reactor Laboratory Course for Students Majoring in Nuclear Engineering with the Kyoto University Critical Assembly (KUCA)," *Proc. 10th Pacific Basin Nucl. Conf.* (10PBNC), Kobe, Japan, Oct. 20−25, 984−993 (1996).
3. T. Misawa, K. Kobayashi, H. Unesaki, C. Ichihara, and S. Shiroya, "Reactor Laboratory Course for Students with the Kyoto University Critical Assembly (KUCA)," *Proc. Int. Conf. on New Frontiers of Nucl. Technol.: Reactor Physics, Safety and High-Performance Computing* (PHYSOR2002), Seoul, Korea, Oct. 7−10, **9E−28**, (2002).
4. C. H. Pyeon, T. Misawa, H. Unesaki, C. Ichihara, and S. Shiroya, "Korean Under-Graduate Students in Kyoto University Critical Assembly Program (KUGSiKUCA Program)," *Proc. 2004 Ann. Mtg. of the Atomic Energy Society of Japan*, Okayama, Japan, Mar. 29−31, **G26**,

(2004).
5. C. H. Pyeon, T. Misawa, H. Unesaki, C. Ichihara, and S. Shiroya, “Reactor Laboratory Course for Korean Under-Graduate Students in Kyoto University Critical Assembly,” *Proc*. *Int. Sympo. Research Reactor and Nucl. Sci.* (Hanaro 2005), Daejeon, Korea, Apr. 11−13, (2005).
6. C. H. Pyeon, T. Misawa, H. Unesaki, C. Ichihara, and S. Shiroya, “Reactor Physics Experiments by Korean Under-Graduate Students in Kyoto University Critical Assembly Program (KUGSiKUCA Program),” *Proc*. *Fall Mtg. of Korean Nuclear Society*, Gyeongju, Korea, Nov. 2−3, (2006).
7. T. Misawa, H. Unesaki, C. Ichihara, C. H. Pyeon, and S. Shiroya, “Reactor Laboratory Course for Students using Kyoto University Critical Assembly (KUCA),” *Proc. 16th Pacific Basin Nucl. Conf.* (16PBNC) - *Pacific Partnership toward a Sustainable Nuclear Future*-Aomori, Japan, Oct. 13−18, (2008).

Chapter 1 Approach to Criticality

1−1 Fission Chain Reaction, Neutron Multiplication, and Approach to Criticality

1−1−1 Fission Chain Reaction

Let us begin by examining the "life" of a neutron in a multiplying system. We assume that our system is a thermal reactor, where most of the fission process takes place within the thermal energy region.

The neutrons born due to fission have an average energy of 2 MeV and appear in the fast energy range. These fast neutrons collide with the nuclides in the media and lose their energy. After losing considerable energy, the neutrons reach the thermal energy range, where they are absorbed in the fuel and trigger the next fission process with a certain probability. We also consider the probability that a certain fraction of the fast neutrons trigger a fission process within the fast energy range. Some of the neutrons are lost due to leakage from the system and absorption by non-fuel materials. This process, together with other possible phenomena, is depicted in Fig. 1−1.

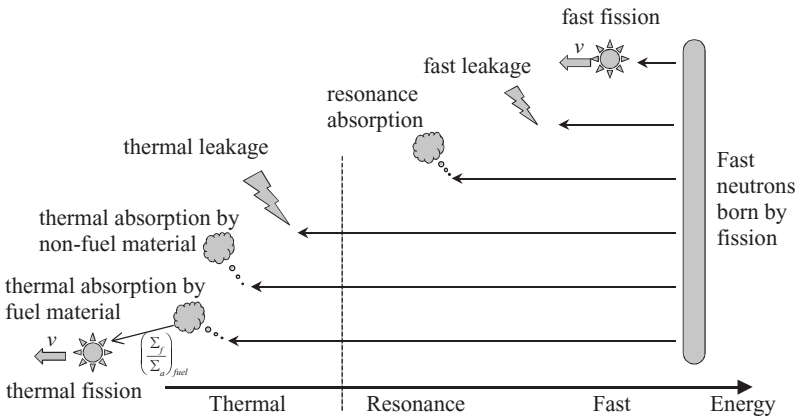

Fig. 1−1 Slowing down, loss and production of neutrons

Now let us assume that there are N_i initial fission neutrons in generation i. All of these neutrons will eventually be lost by the end of the generation, either by leakage or absorption (= capture + fission). We set the number of neutrons leaking out of the system as L and those absorbed as A, so that $N_i = A + L$. We set the total number of neutrons produced by fission as P, which form the initial group of neutrons for the next generation $i+1$, i.e., $N_{i+1} = P$. The ratio of N_i to N_{i+1} is a measure of the multiplication of neutrons through a fission chain reaction. We set this ratio as k_{eff} and designate it as the "effective multiplication factor":

$$k_{eff} = \frac{N_{i+1}}{N_i} = \frac{P}{A+L}. \qquad (1\text{−}1)$$

Let us assume that N_0 neutrons are injected into the system at $t = 0$. The time evolution of neutrons in the system is shown schematically in Fig. 1−2.

- If k_{eff} is less than unity, $N_{i+1} < N_i$, the neutron population will die out − this is designated as "subcritical."
- If $k_{eff} > 1$, $N_{i+1} > N_i$, the neutron population increases exponentially − this is designated as "supercritical."
- If $k_{eff} = 1$, $N_{i+1} = N_i$, the neutron population does not change with succeeding generations − this is designated as "critical."

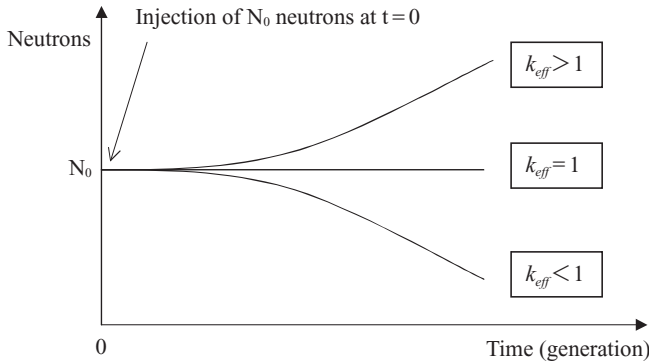

Fig. 1−2 Time evolution of neutrons

As shown in Fig. 1−1, absorption A comprises resonance absorption, absorption by non-fuel material, and non-fission absorption (capture) by the fuel material. Leakage L comprises fast leakage and thermal leakage. Production P comprises fast fission and thermal fission.

1−1−2 Neutron Multiplication

When the system is subcritical (i.e., $k_{eff} < 1$), the fission chain cannot be sustained without supplying neutrons from outside the system; this is because the neutron population within the media eventually becomes zero. However, when there is a sufficient supply of neutrons, a constant neutron population is maintained.

In the following discussion, we treat the time axis in a discrete manner and separate each neutron generation. We designate the number of externally supplied neutrons per generation as S.

The initial external neutrons S in the first generation undergo multiplication and become Sk_{eff} at the end of the generation. This Sk_{eff} group of neutrons multiply in the same manner in the next generation, and the resultant number of neutrons becomes Sk_{eff}^2 at the end of the second generation, Sk_{eff}^3 at the end of the third generation, and so on. Thus, the initial number of external neutrons S becomes Sk_{eff}^n after n generations.

Let us now consider the total number of neutrons in the system after considerable generations. Keep in mind that S neutrons are supplied in each generation. The neutrons that exist in the present generation originate from each and every preceding generation combined, each undergoing neutron multiplication. Therefore, the total number of neutrons existing in the present generation is a summation of neutrons originating from every preceding generation; this can be expressed as:

$$S + Sk_{eff} + Sk_{eff}^2 + Sk_{eff}^3 + \cdots = \frac{S}{1 - k_{eff}}. \tag{1−2}$$

In other words, the number of neutrons S from the neutron source becomes $S/(1 - k_{eff})$ with the multiplication rate of k_{eff} (< 1), that is, it becomes $1/(1 - k_{eff})$ times S.

This means that the neutron multiplication M in this media is given by:

$$M = \frac{S}{S(1 - k_{eff})} = \frac{1}{1 - k_{eff}}. \tag{1−3}$$

As the media approaches criticality, i.e., as $k_{eff} \rightarrow 1$, neutron multiplication M approaches infinity. In order to avoid the practical difficulties entailed with handling infinite neutron multiplication, we usually take the inverse of M, denoted as $1/M$, and refer to it as the inverse multiplication of M, which approaches zero as $k_{eff} \rightarrow 1$:

$$\frac{1}{M} = 1 - k_{eff}. \tag{1-4}$$

If we can measure neutron multiplication M, then we can predict the critical mass by plotting the $1/M$ value versus fuel mass (number of fuel plates, core size, etc.) and extrapolating the $1/M$ curve to $1/M = 0$, as shown in Fig. 1−3.

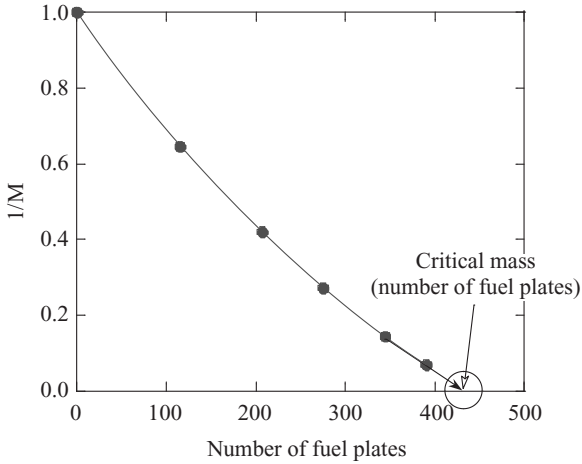

Fig. 1−3 Plot of $1/M$ versus fuel mass (number of fuel plates)

1−1−3 Inverse Count Rate and Approach to Criticality

In a practical reactor experiment, data on neutron density (or flux) at a certain location can be obtained by using a detector. Hereafter, we try to relate this detector response to the neutron multiplication M. Furthermore, we assume that our critical approach starts from a base core configuration (hereafter labeled with suffix 0) under the load of a certain amount of fuel. The i^{th} fuel loading is labeled with the suffix i.

The neutron flux for the base configuration and the i^{th} fuel loading are the results of neutron multiplication in the core and can be expressed as:

$$\phi_{T0} = \frac{S}{1 - k_{eff,0}} \quad \text{and} \quad \phi_{Ti} = \frac{S}{1 - k_{eff,i}}, \tag{1-5}$$

where $k_{eff,0}$ and $k_{eff,i}$ are the effective multiplication factors for base configuration and the i^{th} fuel loading, respectively. The ratio of this neutron flux ϕ_{Ti}/ϕ_{T0} can be expressed as:

$$\phi_{Ti}/\phi_{T0} = \frac{S}{1-k_{eff,i}} \Big/ \frac{S}{1-k_{eff,0}} = \frac{1-k_{eff,0}}{1-k_{eff,i}}. \quad (1\text{−}6)$$

As $1-k_{eff,0}$ is constant for every i^{th} loading, the flux ratio is inversely proportional to $1-k_{eff,i}$, and it can be expressed as:

$$\phi_{Ti}/\phi_{T0} \propto \frac{1}{1-k_{eff,i}}, \quad (1\text{−}7)$$

so that

$$\phi_{T0}/\phi_{Ti} \propto 1-k_{eff,i}. \quad (1\text{−}8)$$

As the relation between ϕ_{T0}/ϕ_{Ti} and $1-k_{eff,i}$ is exactly the same as that between ϕ_{T0}/ϕ_{Ti} and $1/M$, we can use ϕ_{T0}/ϕ_{Ti} for the critical approach. In actual experiments, neutron flux is measured on the basis of detector response such as the count rate of the neutron detectors placed in fission chambers, such as BF_3 counters and ^{3}He counters. We finally assume that the detector count rates A_0 and A_i are proportional to neutron flux, and use the detector count rates to obtain the neutron multiplication as follows:

$$A_0/A_i \propto \phi_{T0}/\phi_{Ti} \propto 1-k_{eff,i}. \quad (1\text{−}9)$$

The ratio A_0/A_i is hereafter designated as the inverse count rate.

$$\text{Inverse Count Rate} = A_0/A_i. \quad (1\text{−}10)$$

On the basis of the inverse count rate, the actual approach to criticality experiments for the KUCA core can be described as follows:

- Step 1. Measure the count rate of the detectors.
- Step 2. Calculate the inverse count rate. Plot it versus fuel mass (number of fuel plates used in KUCA experiments), as shown in Fig. 1−4.
- Step 3. Extrapolate the inverse count rate curve to $A_0/A_i = 0$ and predict the critical mass.
- Step 4. Determine the fuel loading for the next step and load the fuel.
- Repeat Steps 1 through 4.

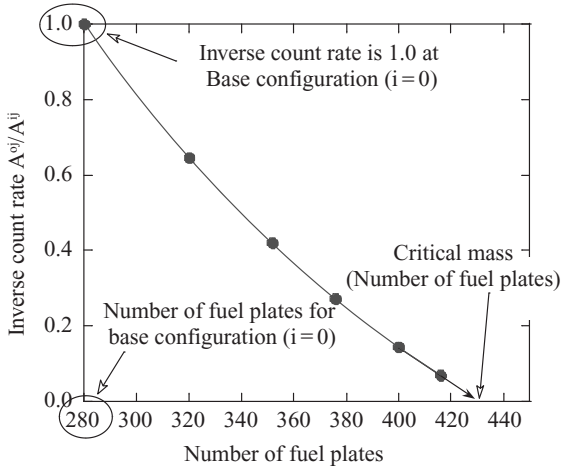

Fig. 1−4 Inverse count rate curve and critical approach

1−2 Experiments

1−2−1 Neutron Detectors

In this experiment, three fission chambers (FC #1−#3) and two uncompensated ionization chambers (UIC #4 : Log-N and UIC #5 : Lin-N) of the KUCA instrumentation system are used along with several experimental detectors such as BF_3 and ^3He.

1−2−2 Actual Procedure of Experiments

In this subsection, we denote the fuel loading pattern with suffix *i*, starting from $i = 0$ for the reference core. We also assume that an appropriate reference core has already been constructed.

(1) Reactor Start-up

The external neutron source is inserted into the reactor, followed by the withdrawal of three safety rods (S4−S6) and tank water feed up to a water level of 1,500 mm.

(2) Control Rod Pattern

Neutron count rate measurements are performed at three different control rod patterns, as shown in Table 1−1. We denote this pattern with suffix *j*.

(3) Neutron Count Rate Measurement

For each detector, the count rate measurement is conducted at each control

Table 1−1 Control rod patterns for approach to criticality experiment

Pattern \ Control rod	C1	C2	C3
$j = 1$	Lower limit: 0 mm	Lower limit: 0 mm	Lower limit: 0 mm
$j = 2$*	Two at upper limit (650 mm) / One at lower limit (0 mm)		
$j = 3$	Upper limit: 650 mm	Upper limit: 650 mm	Upper limit: 650 mm

*depends on the core

rod pattern j ranging from 1 to 3 for each fuel loading pattern i. Thus, the count rate data for each detector should be written using the suffixes i and j as:

Count rate at fuel loading i and control rod pattern j : A_{ij}

The actual measurement procedure is as follows:

$j = 1$: After reactor startup (neutron source insertion, safety rod withdrawal, and tank water feed), the control rod pattern is $j = 1$ (three control rods at the lower limit position). Conduct the measurements after ensuring that the reactor power is stabilized.

$j = 2$: Two control rods, depending on the core, will be withdrawn to the upper limit. Conduct the measurements after ensuring that the reactor power is stabilized.

$j = 3$: The remaining control rod will be withdrawn to the upper limit. If the reactor is still subcritical, Conduct the measurements after ensuring that the reactor power is stabilized. At the final step of approaching the critical state, criticality is achieved during control rod withdrawal from $j = 2$ to $j = 3$, so that the last control rod is partially inserted at the critical level.

(4) Inverse Count Rate Plot

After each measurement, calculate the inverse count rate A_{0j}/A_{ij} for $j = 1$ to 3 by using the count rate data for reference loading A_{0j} and current loading A_{ij}. Plot the inverse count rate versus the number of fuel plates. Note that three plots per detector, which correspond to the three control rod withdrawal patterns, are obtained.

(5) Prediction of Critical Mass (number of fuel plates)

Extrapolate the inverse multiplication curves and determine the number of fuel plates that have attained criticality. Calculate the linear extrapolation using the last two data points. Generally, the inverse multiplication curves exhibit various shapes (slopes) depending on the location of the detector; they could be convex or concave, as shown in Fig. 1−5. As a result, the actual critical mass can be lower or higher than that obtained by linear extrapolation.

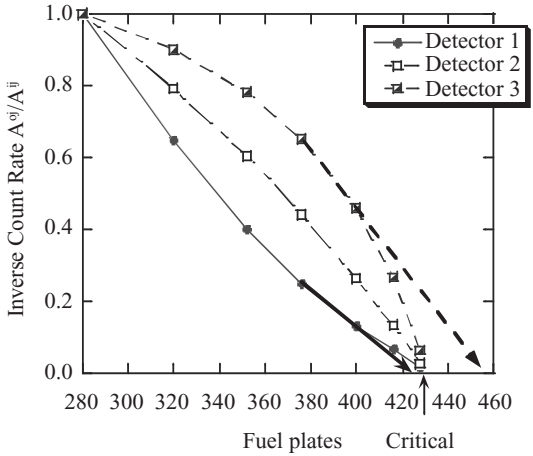

Fig. 1−5 Various shapes of inverse multiplication curves

(6) Fuel Loading

In the first several steps, the number of fuel plates to be assessed is determined prior to the experiment. In the final steps, the number of fuel plates to be added is determined from the predicted value. Fuel loading is performed in the fuel room.

Hereafter, steps (2) through (6) are repeated until criticality is achieved.

(7) Confirmation of Criticality

In this experiment, criticality is confirmed by examining the time evolution of the reactor power under the absence of a neutron source. After criticality is confirmed, the following data should be recorded:

- Number of fuel plates
- Control rod position (height); this will be used to determine the

excess reactivity of the core
- Tank water level
- Reactor power level by Lin-N and Log-N monitors
- γ-ray level
- Core temperature

(8) Determination of Excess Reactivity and Minimum Number of Critical Fuel Plates

In most cases, in the final step of the approach to criticality experiment, the reactor reaches the critical state with one control rod being partially inserted. This means that the number of fuel plates loaded are exceeding the "true" number of fuel plates required to achieve criticality, and the reactor is supercritical with $k_{eff} > 1$. Let us call this "true" number of fuel plates as the minimum number of critical fuel plates.

In order to determine the minimum number of critical fuel plates, we must first determine the extent by which the reactor deviates from criticality when all the control rods are withdrawn from the core. The deviation from the critical state is generally expressed as "reactivity," which is defined as:

$$\rho = \frac{k_{eff} - 1}{k_{eff}} = 1 - \frac{1}{k_{eff}}. \qquad (1\text{−}11)$$

It can be easily understood that the reactivity of the reactor is equivalent to the reactivity that the partially inserted control rod can adjust. In order to clarify these two, let us refer to the reactivity of the core as "excess reactivity (ρ_{ex})," as this reactivity is caused by an "excess" of fuel material in the core.

There are several methods to measure the excess reactivity. In this experiment, we make use of the control rod calibration curve, which is experimentally determined in Chapter 2 (Control Rod Calibration).

This procedure is as follows:

- After criticality is achieved, the control rod pattern is changed so that criticality is controlled with the control rod whose calibration curve is to be measured.
- Ensure that the reactor power is stabilized and then record the control rod position (height).
- At the end of Chapter 2 (Control Rod Calibration) (usually performed the next day), calculate the reactivity of the control rod, which corresponds to the control rod position. This reactivity is

equivalent to the excess reactivity.

The excess reactivity is now determined, but in order to determine the minimum number of critical fuel plates, we must convert this excess reactivity to the number of fuel plates. This can be achieved by determining the reactivity equivalent of one fuel plate.

Let us denote this reactivity equivalent to one single plate as α_{plate} ($\Delta k/k/plate$). Then, the number of fuel plates corresponding to the excess reactivity ρ_{ex} can be obtained by:

$$M_{ex} = \rho_{ex}/\alpha_{plate}, \tag{1−12}$$

so that the minimum number of critical fuel plates $M_{\min}$ can be obtained by subtracting M_{ex} from the actual number of fuel plates loaded in the critical state configuration M_{crit}:

$$M_{\min} = M_{crit} - M_{ex}. \tag{1−13}$$

In order to obtain α_{plate}, we make use of the excess reactivity of the core in the control rod calibration experiment. The requirements for this experiment entail the inclusion of additional fuel plates to the core in order to increase excess reactivity.

Let us denote the number of fuel plates loaded and excess reactivity in the control rod experiment as M_{rod} and $\rho_{ex,rod}$, respectively, and those in the approach to criticality experiment as M_{cri} and $\rho_{ex,cri}$, respectively. Then, α_{plate} can be obtained as:

$$\alpha_{plate} = \frac{\rho_{ex,rod} - \rho_{ex,cri}}{M_{rod} - M_{crit}}. \tag{1−14}$$

Note that the minimum number of critical fuel plates cannot be obtained until the end of the control rod calibration experiment.

1−2−3 Determination of Infinite Reflector Thickness

An additional experiment on the determination of infinite reflector thickness is carried out during the approach to criticality experiment.

In a reflected reactor, some of the neutrons leak out from the core and enter the reflector while the others are reflected back into the core and contribute to the multiplication process. When we change the thickness of the reflector, it is obvious that this effect depends on the reflector thickness,

as depicted in Fig. 1−6. Qualitatively speaking, one can say that this reflector effect

- Increases with reflector thickness up to a certain reflector thickness, and,
- Will not increase further and becomes saturated when the reflector is sufficiently thick such that the neutrons reaching the outer boundary of the reflector can be neglected and the reflected neutrons cannot reenter the core.

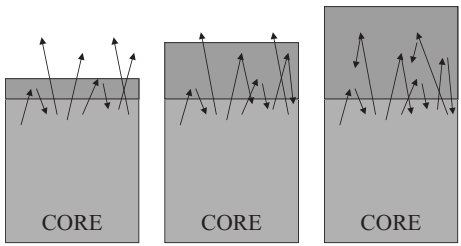

Fig. 1−6 Reflector thickness and behavior of neutrons inside the reflector

Beyond this thickness, the reflector can practically be considered to have infinite thickness. Let us consider a reactor having infinite reflector thickness.

In this experiment, the infinite reflector thickness for light water is measured by observing the reactor power behavior while the axial reflector thickness is varied. We use the detector response of Lin-N (UIC #4) detector as a measure of reactor power.

The experimental procedure is as follows:

- The core tank water level is decreased from 1,500 mm (full level) to 1,280 mm using the normal drainage lever.
- For every 10 mm decrease of water level, record the water level on the Lin-N (UIC #4) chart sheet.
- Continue the measurement until the water level reaches 1,280 mm.
- A copy of the Lin-N chart sheet with the recorded water level will be distributed after the experiment. Create a plot of Lin-N power versus water level, as shown in Fig. 1−7.
- Determine the water level at which the Lin-N power starts to apparently deviate from the constant value. This water level corresponds to the infinite reflector thickness of the reactor.

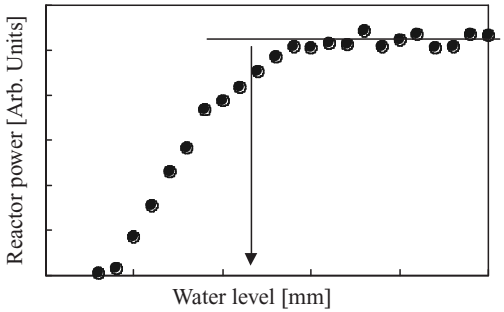

Fig. 1−7 Plot of Lin-N power versus water level

1−3 Discussion

The following information should be included and summarized in the report:

- Core configuration of the reference core (locations of fuel elements, control and safety rods, neutron detectors, and neutron source)
- Fuel loading for the reference core and afterwards
- Count rate measurement data and inverse count rate plots
- Change in predicted critical mass by fuel loading
- Explanation of the process for determining critical mass
- Excess reactivity and minimum number of critical fuel plates

Furthermore, discussions should be made for the following topics:

- Comparison between the inverse count rate curves obtained by each detector

  - Compare the shapes of the inverse count rate curves obtained from the different detectors. How can the differences, if any, be interpreted?
  - Can the measured data be successfully compared to the results obtained by simulation, as obtained in the preparatory report?
  - Can any quantitative information on the effect of the direct source be obtained from the measured count rate data?

- Discussion on the infinite reflector thickness:

- Describe the behavior of Lin-N versus water level plot. What was the thickness of the infinite reflector? How could the behavior below this water level be described?
- What are the relationships between the calculated two-energy-group flux distributions and between the experimental Au reaction rate distributions?

1−4 Preparatory Report

1−4−1 Numerical Simulation of Approach to Criticality Experiment

In this section, the approach to criticality experiment is numerically simulated by using the classical six-factor formula for determining the effective multiplication factor.

Based on the classical six-factor formula, the effective multiplication factor k_{eff} is given by:

$$k_{eff} = \frac{k_\infty e^{-B^2\tau_T}}{1 + L_T^2 B^2}, \tag{1−15}$$

where k_∞ is the infinite multiplication factor, τ_T is the Fermi age of thermal neutrons, L_T is the diffusion length, and B is the buckling.

k_∞ and L_T^2 are given as follows:

$$k_\infty = \eta \varepsilon p f, \tag{1−16}$$

$$L_T^2 = D/\Sigma_a. \tag{1−17}$$

The buckling B for a bare and homogeneous rectangular parallelepiped core with lengths in the x-, y-, and z-directions as a, b, and c, respectively, is given by:

$$B^2 = \left(\frac{\pi}{a + 2\delta}\right)^2 + \left(\frac{\pi}{b + 2\delta}\right)^2 + \left(\frac{\pi}{c + 2\delta}\right)^2, \tag{1−18}$$

where δ is the extrapolation length.

In the KUCA experiment, the critical approach is adopted by adding the fuel plates to the core, as shown schematically in Fig. 1−8. The lengths in the y- and z-directions are fixed at $b = y_0$ and $c = z_0$, and the length in the x-direction of the core increases with fuel loading. Therefore, in the approach to criticality experiment, buckling depends on the length in the

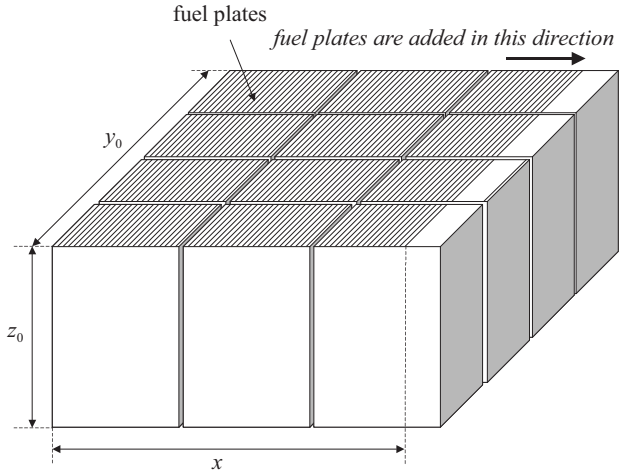

Fig. 1−8 Simplified right rectangular parallelepiped core of KUCA

x-direction, and the increase of k_{eff} due to fuel loading can be simulated by increasing x on the basis of the following formula:

$$k_{eff}(x) = \frac{k_\infty e^{-B^2(x)\tau_T}}{1 + L_T^2 B^2(x)}, \tag{1−19}$$

where:

$$B^2(x) = \left(\frac{\pi}{x + 2\delta}\right)^2 + \left(\frac{\pi}{y_0 + 2\delta}\right)^2 + \left(\frac{\pi}{z_0 + 2\delta}\right)^2, \tag{1−20}$$

and δ is the extrapolation length. In the following numerical simulation, we assume that $x_0 = 20$ cm for the base configuration ($i = 0$).

Simulation of the Inverse Count Rate Curve

- Calculate $k_{eff}(x)$ as a function of x using:

$$k_{eff}(x) = \frac{k_\infty e^{-B^2(x)\tau_T}}{1 + L_T^2 B^2(x)}, \tag{1−21}$$

by subsequently increasing the x value, starting from $x = x_0 = 20$ with $\Delta x = 1$ cm until k_{eff} reaches 1 (i.e., critical). Note that the x-dependence is taken into account via bucking, Eq. (1−20).

Calculate the inverse count rate:

$$\frac{A_0}{A(x)} = \frac{1 - k_{eff}(x)}{1 - k_{eff}(x_0)}, \tag{1−22}$$

and plot it versus x. The constants for the six-factor formula as well as the core size (y_0 and z_0) are given in Table 1−2.

- Examine the overall shape of the inverse count rate curve. What is the shape? Is it linear, convex, or any other?
- Choose any two appropriate points on the inverse count rate curve. Define the critical length in the x-direction of this core by linear extrapolation using the two points. How does the extrapolated critical x-length change with the choice of the two points on the curve? Examine two cases:
  1) two points chosen at the very early stage (i.e., small x) of the critical approach
  2) two points chosen at the very latest stage (i.e., large x) of the critical approach

The actual detector count rate can be separated into two components, namely neutrons multiplied in the core and direct neutrons from the neutron source. This is shown schematically in Fig. 1−9. Under this simple assumption, the detector count rate can be expressed as:

$$A(x) = A_{core}(x) + A_{source}. \tag{1−23}$$

Note that the multiplied component $A_{core}(x)$ is dependent on the core size x, whereas the direct source component A_{source} is independent of the core size.

Table 1−2 Constants for six-factor formula and core size

	C30	C35	C45
τ_T(cm^2)	64.1	56.2	48.4
k_∞	1.721	1.684	1.626
L_T^2(cm^2)	2.914	2.788	2.804
δ(cm)	9.4	8.2	7.8
y_0(cm)	7.1 x(number of rows)		
z_0(cm)	57.0		

The multiplied component for the base configuration $A_{core,0}$ and $A_{core}(x)$ is related to k_{eff} through the following equation:

$$\frac{1-k_{eff}(x)}{1-k_{eff}(x_0)}=\frac{A_{core,0}}{A_{core}(x)}. \tag{1−24}$$

The inverse multiplication is given by:

$$\frac{A_0}{A(x)}=\frac{A_{core,0}+A_{source}}{A_{core}(x)+A_{source}}. \tag{1−25}$$

Now, we set the ratio of A_{source} and $A_{core,0}$ as:

$$f_s=A_{source}/A_{core,0}. \tag{1−26}$$

Here, $f_s=0$ means that there is no direct source component in the count rate; f_s increases with the direct source component in the count rate.

- Calculate the inverse count rate for $f_s=0$, 1, 2, 3, 4 and 5 and plot each inverse count rate curve versus x.
- Qualitatively describe the f_s-dependence of the inverse count rate curves. What will the inverse count rate curves for detectors I, II, and III, shown in Fig. 1−9, look like?

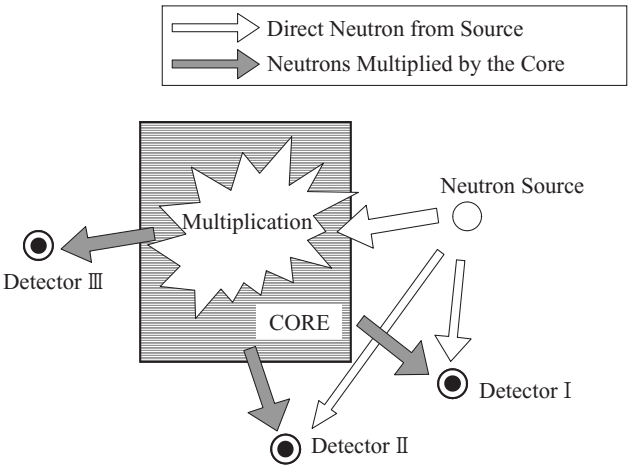

Fig. 1−9 Multiplied neutron and direct neutron components in detectors

1−4−2 Two-Energy-Group Diffusion Calculation of Reflected Reactor

We will not address the reflector surrounding the core since it is not explicitly considered in the six-factor formula. Further, the energy distribution of neutrons is separated into two-energy-group at a boundary around 1 eV. Let us designate the higher energy group as the "fast group" (group 1) and the lower energy group as the "thermal group" (group 2) and examine the behavior of the neutrons belonging to the two-energy-group.

In the diffusion theory (or diffusion approximation), the angular distribution of neutrons is treated as isotropic. Furthermore, the neutron current is expressed using Fick's law as $-D\nabla^2\phi$, where D is the diffusion coefficient and ϕ is the neutron flux.

As shown in Fig. 1−8, we approximate the reactor as a two-region reactor with a homogeneous rectangular parallelepiped core surrounded by a light-water reactor. We denote the core and the reflector regions with suffixes c and r. As described above, the two-energy-group is considered; the fast and thermal groups are denoted with suffixes 1 and 2.

Let us derive the balance equations in the core and reflector regions. We assume that the system is critical, i.e., $k_{eff} = 1$.

1) Core region, Group 1 (Fast group)

Neutrons of Group 1 (Fast group) are produced by fission. In a thermal reactor, most of the fission process takes place within the thermal energy range; however, a certain fraction of fission also occurs in the fast energy range. The contribution of this fast fission is usually determined by multiplying the thermal fission rate with a fast fission factor ε ($\varepsilon > 1$).

The neutron production rate at the core for Group 1 can be written as $\varepsilon\nu\Sigma_{2fc}\phi_{2c}$, where ν is the number of (fast) neutrons born per fission, Σ_{2fc} is the fission cross-section of the core Group 2, and ε is the fast fission factor. The leakage rate and absorption rate of neutrons from the core for Group 1 are $-D_{1c}\nabla^2\phi_{1c}$ and $\Sigma_{1ac}\phi_{1c}$, respectively; the removal rate from Group 1 to Group 2 by scattering and slowing down is $\Sigma_{1\to 2c}\phi_{1c}$. In a critical system, neutron production and loss are in balance, that is, the balance equation becomes:

$$D_{1c}\nabla^2\phi_{1c} - (\Sigma_{1ac} + \Sigma_{1\to 2c})\,\phi_{1c} + \varepsilon\nu\Sigma_{2fc}\phi_{2c} = 0. \qquad (1-27)$$

2) Core region, Group 2 (Thermal group)

For the thermal group, the source term is the neutrons removed from the Fast Group. Absorption and leakage terms are similar to Eq. (1−27), and

the balance equation is:

$$D_{2c}\nabla^2\phi_{2c} - \Sigma_{2ac}\phi_{2c} + \Sigma_{1\to 2c}\phi_{1c} = 0. \tag{1-28}$$

3) Reflector region, Group 1 (Fast group)
The balance equation is similar to Eq. (1−27), except that the fission term does not exist:

$$D_{1r}\nabla^2\phi_{1r} - (\Sigma_{1ar} + \Sigma_{1\to 2c})\,\phi_{1r} = 0. \tag{1-29}$$

4) Reflector region, Group 2 (Thermal group)
The source term is the neutrons removed from the Fast group; hence, the balance equation becomes:

$$D_{2r}\nabla^2\phi_{2r} - \Sigma_{2ar}\phi_{2r} + \Sigma_{1\to 2r}\phi_{1r} = 0. \tag{1-30}$$

The four abovementioned equations are collectively known as the two-energy-group diffusion equation of the system. It can easily be found that these equations are based on a simple balance between neutron production and loss. Note that we have assumed the group constants D and Σ to be constant within a region and also that neutron flux has three spatial variables, x, y, and z.

Eqs. (1−27) through (1−30) can be solved analytically by reducing the spatial variables to one by using appropriate approximations. For this purpose, we approximate the flux distribution in the y- and z-directions with a cosine function, and treat the neutron leakage in the two directions on the basis of the buckling value. Detailed procedures for this approximation and further algebra are summarized in Appendix 1 and also may be found in various reactor physics textbooks. After this approximation, we obtain a set of four equations with a single variable x.

Finally, we derive a 4×4 matrix using the boundary conditions for neutron flux and neutron current at the core-reflector interface. The size of the critical core can be determined by setting the determinant of the 4×4 matrix. If we set the length in the x-direction of the critical core as $2a$ for simplicity:

$$a = \frac{1}{\mu}\arctan\left[\frac{1}{\mu}\cdot\right.$$

$$\left.\frac{[-D_{1r}D_{2c}S_2\kappa_{1r}+D_{1c}D_{2r}\{\kappa_{2r}(S_1-S_3)+\kappa_{1r}S_3\}]\lambda+D_{1r}D_{2r}(S_1-S_2)\kappa_{1r}\kappa_{2r}}{D_{1c}D_{2c}(S_1-S_2)\lambda+D_{1r}D_{2c}S_1\kappa_{1r}+D_{1c}D_{2r}\{S_3(\kappa_{2r}-\kappa_{1r})-S_2\kappa_{2r}\}}\right], \tag{1−31}$$

where the parameters in Eq. (1−31) are defined as follows:

$$B_\perp^2=\pi^2\left\{\frac{1}{(y_0+2\delta)^2}+\frac{1}{(z_0+2\delta)^2}\right\}: y\text{- and } z\text{-direction buckling (transverse buckling)}, \tag{1−32}$$

$\Sigma_{1c}=\Sigma_{1ac}+\Sigma_{1\to 2c}+D_{1c}B_\perp^2$: cross-section removal for core region, Group 1

(absorption + scattering to group 2 + transverse leakage), (1−33)

$\Sigma_{2c}=\Sigma_{2ac}+D_{2c}B_\perp^2$: cross-section removal for core region, Group 2

(absorption + transverse leakage), (1−34)

$$\mu^2=\frac{1}{2D_{1c}D_{2c}}\left\{-(D_{1c}\Sigma_{2c}+D_{2c}\Sigma_{1c})\right.$$
$$\left.+\sqrt{(D_{1c}\Sigma_{2c}+D_{2c}\Sigma_{1c})^2-4D_{1c}D_{2c}(\Sigma_{1c}\Sigma_{2c}-\varepsilon v\Sigma_{2fc}\Sigma_{1\to 2c})}\right\}, \tag{1−35}$$

$$\lambda^2=-\frac{1}{2D_{1c}D_{2c}}\left\{-(D_{1c}\Sigma_{2c}+D_{2c}\Sigma_{1c})\right.$$
$$\left.-\sqrt{(D_{1c}\Sigma_{2c}+D_{2c}\Sigma_{1c})^2-4D_{1c}D_{2c}(\Sigma_{1c}\Sigma_{2c}-\varepsilon v\Sigma_{2fc}\Sigma_{1\to 2c})}\right\}, \tag{1−36}$$

$\Sigma_{1r}=\Sigma_{1ar}+\Sigma_{1\to 2r}+D_{1r}B_\perp^2$: cross-section removal for reflector region, Group 1

(absorption + scattering to Group 2 + transverse leakage), (1−37)

$\Sigma_{2r}=\Sigma_{2ar}+D_{2r}B_\perp^2$: cross-section removal for reflector region, Group 2

(absorption + transverse leakage), (1−38)

$$\kappa_{1r}^2\equiv\Sigma_{1r}/D_{1r}, \tag{1−39}$$

$$\kappa_{2r}^2\equiv\Sigma_{2r}/D_{2r}, \tag{1−40}$$

$S_1=\dfrac{\Sigma_{1\to 2c}}{D_{2c}\mu^2+\Sigma_{2c}}$: coupling coefficient for core region, (1−41)

$S_2=\dfrac{\Sigma_{1\to 2c}}{-D_{2c}\lambda^2+\Sigma_{2c}}$: coupling coefficient for core region, (1−42)

Table 1−3 Two-energy-group constants of the KUCA C-core

		Group 1 (Fast group)			Group 2 (Thermal group)				
		D_1(cm)	Σ_{1a}(1/cm)	$\Sigma_{1\to 2}$ (1/cm)	D_2(cm)	Σ_{2a}(1/cm)	$\nu\Sigma_{2f}$ (1/cm)*	ε	δ(cm)
Core	C30	1.58	0.00320	0.0178	0.271	0.0930	0.168	1.121	9.4
	C35	1.54	0.00286	0.0212	0.237	0.0850	0.149	1.092	8.2
	C45	1.50	0.00237	0.0254	0.203	0.0724	0.121	1.064	7.8
Light-Water Reflector		1.41	0.0	0.0476	0.117	0.0191	0.0	---	---

*$\nu = 2.44$

Table 1−4 Number density of ^{235}U for the homogenized core region

Fuel Lattice (Frame Type)	C30	C35	C45
Number Density of ^{235}U (atoms/cm^3)	1.867×10^{20}	1.589×10^{20}	1.231×10^{20}

$S_3 = \dfrac{\Sigma_{1\to 2r}/D_{2r}}{\kappa_{2r}^2 - \kappa_{1r}^2}$: coupling coefficient for reflector region. (1−43)

The two-energy-group constants are listed in Table 1−3. Note that the constants depend on the fuel lattice (fuel frame) used in the experiment.

- Calculate the length in the x-direction $2a$ of the critical core using Eq. (1−31).

- Calculate the number of ^{235}U atoms in the core region (core volume $V = xy_0z_0$ (cm^3)) using the homogenized number density of Table 1−4. Convert it to the critical mass of ^{235}U, that is, the mass of ^{235}U contained in the core region.
- Calculate the number of fuel plates in the critical core by dividing the critical mass of ^{235}U by 8.89 (g ^{235}U/fuel plates).

After the critical core size is obtained, one can determine the neutron flux distribution according to Sec. 1E of Appendix 1. This determination of neutron flux distribution, together with other related topics, is required in the preparatory report of Chapter 3 (Measurement of Reaction Rate).

Appendix 1

1A. Analytical Solution of Two-Energy-Group Diffusion Equation

The mathematical procedures for solving the two-energy-group diffusion equation are described below. We assume that the reactor consists of a homogeneous, rectangular parallelepiped core, surrounded by a light-water reflector.

As already described, the four equations that we are going to solve are as follows:

Core, Group 1: $$D_{1c}\nabla^2\phi_{1c} - (\Sigma_{1ac} + \Sigma_{1\to 2c})\,\phi_{1c} + \varepsilon v\Sigma_{2f}\phi_{2c} = 0, \quad (1A{-}1)$$

Core, Group 2: $$D_{2c}\nabla^2\phi_{2c} - \Sigma_{2ac}\phi_{2c} + \Sigma_{1\to 2c}\phi_{1c} = 0, \quad (1A{-}2)$$

Reflector, Group 1: $$D_{1r}\nabla^2\phi_{1r} - (\Sigma_{1ar} + \Sigma_{1\to 2r})\,\phi_{1r} = 0, \quad (1A{-}3)$$

Reflector, Group 2: $$D_{2r}\nabla^2\phi_{2r} - \Sigma_{2ar}\phi_{2r} + \Sigma_{1\to 2r}\phi_{1r} = 0. \quad (1A{-}4)$$

Reduction of Space Variables using Buckling

We assume that,

- neutron flux $\phi(x, y, z)$ can be written as $\phi(x, y, z) = \phi(x)\phi(y)\phi(z)$,
- y- and z-direction neutron flux can be expressed as a cosine function, so $\phi(x, y, z)$ becomes:

$$\phi(x, y, z) = \phi(x)\cos\left(\frac{\pi}{b}y\right)\cos\left(\frac{\pi}{c}z\right), \quad (1A{-}5)$$

where b and c are the extrapolated lengths in the y- and z-directions of the critical core given by:

$$b = y_0 + 2\delta, \quad (1A{-}6)$$

$$c = z_0 + 2\delta, \quad (1A{-}7)$$

where δ is the extrapolation length.

Then, $\nabla^2\phi = \nabla^2\phi(x, y, z)$ appearing in the leakage term becomes:

$$\nabla^2\phi = \left[\frac{d^2\phi(x)}{dx^2} - \pi^2\left\{\frac{1}{(y_0+2\delta)^2} + \frac{1}{(z_0+2\delta)^2}\right\}\phi(x)\right]\cos\left(\frac{\pi}{y_0+2\delta}y\right)\cos\left(\frac{\pi}{z_0+2\delta}z\right). \quad (1A{-}8)$$

We define the transverse buckling, i.e., buckling in *y*- and *z*-directions, as:

$$B_{\perp}^2 = \pi^2 \left\{ \frac{1}{(y_0 + 2\delta)^2} + \frac{1}{(z_0 + 2\delta)^2} \right\}. \tag{1A−9}$$

Then, Eq. (1A−8) could be expressed as:

$$\nabla^2 \phi = \left[\frac{d^2 \phi(x)}{dx^2} - B_{\perp}^2 \phi(x) \right] \cos\left(\frac{\pi}{y_0 + 2\delta} y \right) \cos\left(\frac{\pi}{z_0 + 2\delta} z \right). \tag{1A−10}$$

Using Eq. (1A−10) for the leakage terms of the two-energy-group diffusion equations (1A−1) through (1A−4), we obtain the set of equations with only one space variable, *x*:

$$D_{1c} \frac{d^2 \phi_{1c}(x)}{dx^2} - (\Sigma_{1ac} + \Sigma_{1\to 2c} + D_{1c} B_{\perp}^2) \phi_{1c}(x) + \varepsilon v \Sigma_{2f} \phi_{2c}(x) = 0, \tag{1A−11}$$

$$D_{2c} \frac{d^2 \phi_{2c}(x)}{dx^2} - (\Sigma_{2ac} + D_{2c} B_{\perp}^2) \phi_{2c}(x) + \Sigma_{1\to 2c} \phi_{1c}(x) = 0, \tag{1A−12}$$

$$D_{1r} \frac{d^2 \phi_{1r}(x)}{dx^2} - (\Sigma_{1ar} + \Sigma_{1\to 2r} + D_{1r} B_{\perp}^2) \phi_{1r}(x) = 0, \tag{1A−13}$$

$$D_{2r} \frac{d^2 \phi_{2r}(x)}{dx^2} - (\Sigma_{2ar} + D_{2r} B_{\perp}^2) \phi_{2r}(x) + \Sigma_{1\to 2r} \phi_{1r}(x) = 0. \tag{1A−14}$$

Note that the second terms on the LHS of these equations contain $DB_{\perp}^2$, which corresponds to the leakage in *y*- and *z*-directions. This means that these leakages are treated as absorption in Eqs. (1A−11) through (1A−14).

1B. Solution for Core Region

For simplicity, we set:

$$\Sigma_{1c} = \Sigma_{1ac} + \Sigma_{1\to 2c} + D_{1c} B_{\perp}^2, \tag{1A−15}$$

$$\Sigma_{2c} = \Sigma_{2ac} + D_{2c} B_{\perp}^2. \tag{1A−16}$$

We assume that $\phi_{1c}(x)$ and $\phi_{2c}(x)$ can be expressed using the *x*-direction buckling as follows:

$$\frac{d^2 \phi_{1c}(x)}{dx^2} + B_x^2 \phi_{1c}(x) = 0, \tag{1A−17}$$

$$\frac{d^2\phi_{2c}(x)}{dx^2} + B_x^2\phi_{2c}(x) = 0, \tag{1A−18}$$

Then Eqs. (1A−11) and (1A−12) become:

$$-D_{1c}B_x^2\phi_{1c}(x) - \Sigma_{1c}\phi_{1c}(x) + \varepsilon v\Sigma_{2fc}\phi_{2c}(x) = 0, \tag{1A−19}$$

$$-D_{2c}B_x^2\phi_{2c}(x) - \Sigma_{2c}\phi_{2c}(x) + \Sigma_{1\to 2c}\phi_{1c}(x) = 0. \tag{1A−20}$$

This can be expressed as:

$$\begin{pmatrix} -D_{1c}B_x^2 - \Sigma_{1c} & \varepsilon v\Sigma_{2fc} \\ \Sigma_{1\to 2c} & -D_{2c}B_x^2 - \Sigma_{2c} \end{pmatrix} \begin{pmatrix} \phi_{1c}(x) \\ \phi_{2c}(x) \end{pmatrix} = \begin{pmatrix} 0 \\ 0 \end{pmatrix}. \tag{1A−21}$$

The condition for this equation to have a solution other than $\phi_{1c}(x) = \phi_{2c}(x) = 0$ is that the determinant of the first matrix is zero, that is:

$$(-D_{1c}B_x^2 - \Sigma_{1c})(-D_{2c}B_x^2 - \Sigma_{2c}) - \varepsilon v\Sigma_{2fc}\Sigma_{1\to 2c} = 0. \tag{1A−22}$$

This is a second-order polynomial equation of B_x^2:

$$D_{1c}D_{2c}(B_x^2)^2 + (D_{1c}\Sigma_{2c} + D_{2c}\Sigma_{1c})B_x^2 + (\Sigma_{1c}\Sigma_{2c} - \varepsilon v\Sigma_{2fc}\Sigma_{1\to 2c}) = 0. \tag{1A−23}$$

We set the two solutions of B_x^2 as μ^2 and $-\lambda^2$, which can be expressed as:

$$\mu^2 = \frac{1}{2D_{1c}D_{2c}}\left\{-(D_{1c}\Sigma_{2c} + D_{2c}\Sigma_{1c}) + \sqrt{(D_{1c}\Sigma_{2c} + D_{2c}\Sigma_{1c})^2 - 4D_{1c}D_{2c}(\Sigma_{1c}\Sigma_{2c} - \varepsilon v\Sigma_{2fc}\Sigma_{1\to 2c})}\right\}, \tag{1A−24}$$

$$-\lambda^2 = \frac{1}{2D_{1c}D_{2c}}\left\{-(D_{1c}\Sigma_{2c} + D_{2c}\Sigma_{1c}) - \sqrt{(D_{1c}\Sigma_{2c} + D_{2c}\Sigma_{1c})^2 - 4D_{1c}D_{2c}(\Sigma_{1c}\Sigma_{2c} - \varepsilon v\Sigma_{2fc}\Sigma_{1\to 2c})}\right\}. \tag{1A−25}$$

Therefore, $\phi_{1c}(x)$ can be expressed as a linear combination of $X(x)$ and $Y(x)$:

$$\phi_{1c}(x) = AX(x) + CY(x), \tag{1A−28}$$

where A and C are constants and $X(x)$ and $Y(x)$ satisfy the following equations:

$$\frac{d^2X(x)}{dx^2} + \mu^2 X(x) = 0, \tag{1A−26}$$

$$\frac{d^2Y(x)}{dx^2} - \lambda^2 Y(x) = 0. \tag{1A−27}$$

Similarly, $\phi_{2c}(x)$ can be expressed as:

$$\phi_{2c}(x) = A'X(x) + C'Y(x). \tag{1A−29}$$

As $X(x)$ and $Y(x)$ should be symmetrical to $x = 0$, the solutions for Eqs. (1A−26) and (1A−27) are:

$$X(x) = \cos(\mu x), \tag{1A−30}$$

$$Y(x) = \cosh(\lambda x), \tag{1A−31}$$

so that:

$$\phi_{1c}(x) = A\cos(\mu x) + C\cosh(\lambda x), \tag{1A−32}$$

$$\phi_{2c}(x) = A'\cos(\mu x) + C'\cosh(\lambda x). \tag{1A−33}$$

In order to relate A to A' and C to C', we use Eqs. (1A−32) and (1A−33) with Eq. (1A−20) and get:

$$S_1 \equiv \frac{A'}{A} = \frac{\Sigma_{1\to 2c}}{D_{2c}\mu^2 + \Sigma_{2c}}, \tag{1A−34}$$

$$S_2 \equiv \frac{C'}{C} = \frac{\Sigma_{1\to 2c}}{-D_{2c}\lambda^2 + \Sigma_{2c}}. \tag{1A−35}$$

These two parameters S_1 and S_2 are designated as coupling coefficients, which describes the relation between the Fast-group flux and the Thermal-group flux in the core.

1C. Solution for Reflector Region

In the reflector region, we set for simplicity:

$$\Sigma_{1r} = \Sigma_{1ar} + \Sigma_{1\to 2r} + D_{1r}B_\perp^2, \tag{1A−36}$$

$$\Sigma_{2r} = \Sigma_{2ar} + D_{2r}B_\perp^2. \tag{1A−37}$$

We express Eq. (1A−13):

$$D_{1r}\frac{d^2\phi_{1r}(x)}{dx^2}-\Sigma_{1r}\phi_{1r}(x)=0, \tag{1A−38}$$

as:

$$\frac{d^2\phi_{1r}(x)}{dx^2}-\kappa_{1r}^2\phi_{1r}(x)=0, \tag{1A−39}$$

where:

$$\kappa_{1r}^2\equiv\Sigma_{1r}/D_{1r}. \tag{1A−40}$$

Under the boundary condition in which the flux becomes zero at $x =$ infinity, the solution for Eq. (1A−39) is:

$$\phi_{1r}(x)=Fe^{-\kappa_{1r}|x|}, \tag{1A−41}$$

where F is a constant.

Next, we set Eq. (1A−14):

$$D_{2r}\frac{d^2\phi_{2r}(x)}{dx^2}-\Sigma_{2r}\phi_{2r}(x)+\Sigma_{1\to 2r}\phi_{1r}(x)=0, \tag{1A−42}$$

as:

$$\frac{d^2\phi_{2r}(x)}{dx^2}-\kappa_{2r}\phi_{2r}(x)+\frac{\Sigma_{1\to 2r}}{D_{2r}}\phi_{1r}(x)=0, \tag{1A−43}$$

where:

$$\kappa_{2r}^2\equiv\Sigma_{2r}/D_{2r}. \tag{1A−44}$$

We assume that the Group 2 flux can be expressed as:

$$\phi_{2r}(x)=F'e^{-\kappa_{1r}|x|}+Ge^{-\kappa_{2r}|x|}. \tag{1A−45}$$

Then, Eq. (1A−43) becomes:

$$\left(\kappa_{1r}^2 F' - \kappa_{2r}^2 F' + \frac{\Sigma_{1\to 2r}}{D_{2r}} F\right) e^{-\kappa_{1r}|x|} = 0. \tag{1A−46}$$

In order for Eq. (1A−46) to be valid for any value of x, it is necessary that:

$$\kappa_{1r}^2 F' - \kappa_{2r}^2 F' + \frac{\Sigma_{1\to 2r}}{D_{2r}} F = 0. \tag{1A−47}$$

or:

$$S_3 \equiv \frac{F'}{F} = \frac{\Sigma_{1\to 2r}/D_{2r}}{\kappa_{2r}^2 - \kappa_{1r}^2}. \tag{1A−48}$$

This parameter S_3 is also designated as a coupling coefficient, which relates the Fast-group flux to Thermal-group flux in the reflector region.

1D. Determination of Critical Core Size

We have now obtained the following set of equations for neutron flux:

$$\phi_{1c}(x) = A\cos(\mu x) + C\cosh(\lambda x), \tag{1A−49}$$

$$\phi_{2c}(x) = S_1 A\cos(\mu x) + S_2 C\cosh(\lambda x), \tag{1A−50}$$

$$\phi_{1r}(x) = Fe^{-\kappa_{1r}|x|}, \tag{1A−51}$$

$$\phi_{2r}(x) = S_3 Fe^{-\kappa_{1r}|x|} + Ge^{-\kappa_{2r}|x|}. \tag{1A−52}$$

The boundary conditions for Eqs. (1A−49) through (1A−52) are that the neutron flux and neutron current $J = Dd\phi/dx$ is continuous at the core/reflector boundary. We set the length in the x-direction of the core as $2a$ for simplicity, so that the core/reflector boundary is $x = a$. Expressing the derivatives of neutron flux as ϕ', the boundary conditions will be:

$$\phi_{1c}(a) = \phi_{1r}(a), \tag{1A−53}$$

$$D_{1c}\phi'_{1c}(a) = D_{1r}\phi'_{1r}(a), \tag{1A−54}$$

$$\phi_{2c}(a) = \phi_{2r}(a), \tag{1A−55}$$

$$D_{2c}\phi'_{2c}(a) = D_{2r}\phi'_{2r}(a). \tag{1A−56}$$

After some algebra, we obtain:

$$A\cos(\mu a) + C\cosh(\lambda a) = Fe^{-\kappa_{1r}a}, \tag{1A−57}$$

$$-AD_{1c}\mu\sin(\mu a) + CD_{1c}\lambda\sinh(\lambda a) = -FD_{1r}\kappa_{1r}e^{-\kappa_{1r}a}, \tag{1A−58}$$

$$S_1A\cos(\mu a) + S_2C\cosh(\lambda a) = S_3Fe^{-\kappa_{1r}a} + Ge^{-\kappa_{2r}a}, \tag{1A−59}$$

$$-S_1AD_{2c}\mu\sin(\mu a) + S_2CD_{2c}\lambda\sinh(\lambda a) = -S_3FD_{2r}\kappa_{1r}e^{-\kappa_{1r}a} - GD_{2r}\kappa_{2r}e^{-\kappa_{2r}a}, \tag{1A−60}$$

This set of equations can be expressed in matrix form with unknowns A, C, F, and G:

$$\begin{pmatrix} \cos(\mu a) & \cosh(\lambda a) & -e^{-\kappa_{1r}a} & 0 \\ -D_{1c}\,\mu\sin(\mu a) & D_{1c}\lambda\sinh(\lambda a) & D_{1r}\kappa_{1r}e^{-\kappa_{1r}a} & 0 \\ S_1\cos(\mu a) & S_2\cosh(\lambda a) & -S_3e^{-\kappa_{1r}a} & -e^{-\kappa_{2r}a} \\ -S_1D_{2c}\mu\sin(\mu a) & S_2D_{2c}\lambda\sinh(\lambda a) & S_3D_{2r}\kappa_{1r}e^{-\kappa_{1r}a} & D_{2r}\kappa_{2r}e^{-\kappa_{2r}a} \end{pmatrix} \begin{pmatrix} A \\ C \\ F \\ G \end{pmatrix} = 0. \tag{1A−61}$$

In order for Eq. (1A−61) to have a solution set other than $A = C = F = G = 0$, the determinant of the first matrix should be zero. That is:

$$\begin{vmatrix} \cos(\mu a) & \cosh(\lambda a) & -e^{-\kappa_{1r}a} & 0 \\ -D_{1c}\mu\sin(\mu a) & D_{1c}\lambda\sinh(\lambda a) & D_{1r}\kappa_{1r}e^{-\kappa_{1r}a} & 0 \\ S_1\cos(\mu a) & S_2\cosh(\lambda a) & -S_3e^{-\kappa_{1r}a} & -e^{-\kappa_{2r}a} \\ -S_1D_{2c}\mu\sin(\mu a) & S_2D_{2c}\lambda\sinh(\lambda a) & S_3D_{2r}\kappa_{1r}e^{-\kappa_{1r}a} & D_{2r}\kappa_{2r}e^{-\kappa_{2r}a} \end{vmatrix} = 0. \tag{1A−62}$$

Eq. (1A−62) can be simplified as:

$$\begin{vmatrix} 1 & 1 & 1 & 0 \\ -D_{1c}\mu\tan(\mu a) & D_{1c}\lambda\tanh(\lambda a) & -D_{1r}\kappa_{1r} & 0 \\ S_1 & S_2 & S_3 & 1 \\ -S_1D_{2c}\mu\tan(\mu a) & S_2D_{2c}\lambda\tanh(\lambda a) & -S_3D_{2r}\kappa_{1r} & -D_{2r}\kappa_{2r} \end{vmatrix} = 0, \tag{1A−63}$$

and we finally obtain the equation for determining a:

$\mu\tan(\mu a)$

$$= \frac{[-D_{1r}D_{2c}S_2\kappa_{1r} + D_{1c}D_{2r}\{\kappa_{2r}(S_1 - S_3) + \kappa_{1r}S_3\}]\lambda \tanh(\lambda a) + D_{1r}D_{2r}(S_1 - S_2)\kappa_{1r}\kappa_{2r}}{D_{1c}D_{2c}(S_1 - S_2)\lambda \tanh(\lambda a) + D_{1r}D_{2c}S_1\kappa_{1r} + D_{1c}D_{2r}\{S_3(\kappa_{2r} - \kappa_{1r}) - S_2\kappa_{2r}\}}. \quad \text{(1A−64)}$$

As Eq. (1A−64) cannot be further solved analytically, we must obtain a with the aid of a numerical solution and finally obtain the length in the x-direction of the core $2a$.

However, we can use some valid approximations to further simplify Eq. (1A−64). Using the two-group constants of Table 1−3, one can find from Eq. (1A−25) that λ is around 0.6. In most of the KUCA C-cores, a is approximately 20 to 30 cm; hence, we can assume that $\tanh(\lambda a) = 1$ (caution: check that this is valid!). Then, Eq. (1A−64) becomes:

$$\mu \tan(\mu a) = \frac{[-D_{1r}D_{2c}S_2\kappa_{1r} + D_{1c}D_{2r}\{\kappa_{2r}(S_1 - S_3) + \kappa_{1r}S_3\}]\lambda + D_{1r}D_{2r}(S_1 - S_2)\kappa_{1r}\kappa_{2r}}{D_{1c}D_{2c}(S_1 - S_2)\lambda + D_{1r}D_{2c}S_1\kappa_{1r} + D_{1c}D_{2r}\{S_3(\kappa_{2r} - \kappa_{1r}) - S_2\kappa_{2r}\}}, \quad \text{(1A−65)}$$

and a can be obtained as:

$$a = \frac{1}{\mu} \arctan\left[\frac{1}{\mu} \cdot \frac{[-D_{1r}D_{2c}S_2\kappa_{1r} + D_{1c}D_{2r}\{\kappa_{2r}(S_1 - S_3) + \kappa_{1r}S_3\}]\lambda + D_{1r}D_{2r}(S_1 - S_2)\kappa_{1r}\kappa_{2r}}{D_{1c}D_{2c}(S_1 - S_2)\lambda + D_{1r}D_{2c}S_1\kappa_{1r} + D_{1c}D_{2r}\{S_3(\kappa_{2r} - \kappa_{1r}) - S_2\kappa_{2r}\}}\right]. \quad \text{(1A−66)}$$

1E. Neutron Flux Distribution

We need to obtain the four constants A, C, F, and G that appear in Eqs. (1A−49) through (1A−52) to determine the neutron flux distribution. However, in a critical reactor, Eqs. (1A−57) through (1A−60) are not independent; hence, we cannot uniquely define the non-trivial solutions for A, C, F, and G. We must choose one of the constants as an arbitrary constant and express the others with this arbitrary constant. Hereafter, we select A as the arbitrary constant and express the remainder using A.

Starting from Eqs. (1A−57) and (1A−58):

$$-C\cosh(\lambda a) + Fe^{-\kappa_{1r}a} = A\cos(\mu a), \quad \text{(1A−67)}$$

$$CD_{1c}\lambda \sinh(\lambda a) + FD_{1r}\kappa_{1r}e^{-\kappa_{1r}a} = AD_{1c}\mu \sin(\mu a), \tag{1A−68}$$

we cancel out F and obtain:

$$C = -A\frac{D_{1r}\kappa_{1r}\cos(\mu a) - D_{1c}\mu \sin(\mu a)}{D_{1r}\kappa_{1r}\cosh(\lambda a) + D_{1c}\lambda \sinh(\lambda a)}. \tag{1A−69}$$

We can combine Eqs. (1A−57) through (1A−60) in a similar manner and express F and G using A.

When plotting the neutron flux distribution, it might be necessary to make an appropriate normalization to Eqs. (1A−49) through (1A−52), such as $\phi_{1c}(x = 0) = 1$.

Chapter 2 Control Rod Calibration

2−1 Purpose

Control rods are installed in a reactor to control nuclear fission chain reactions. Primarily, they are used to adjust criticality, control reactor power level, and shut down the reactor. Materials with large neutron absorption cross sections, such as boron (B), cadmium (Cd), and hafnium (Hf) are used as control rods. When a control rod is withdrawn from a reactor, the amount of fission reactions increases; inversely, inserting the control rod into the core causes a decrease in the amount of fission reactions.[1] This means that control rods can change the effective multiplication factor (k_{eff}) of the core.

To explain the ability of control rod to adjust k_{eff} quantitatively, the technical term "reactivity" is introduced. Reactivity, which is often represented as ρ, is a measure of the departure from the critical state of a reactor and is written as follows:

$$\rho = \frac{k_{eff} - 1}{k_{eff}}. \tag{2−1}$$

Reactivity ρ is a non-dimensional quantity, however, its unit is usually represented as $\Delta k/k$ ($10^{-2}\Delta k/k$ is $1\%\Delta k/k$, and $10^{-5}\Delta k/k$ is equal to 1 pcm).[2] Reactivity ρ divided by β_{eff} (effective delayed neutron fraction) is known as "reactivity in dollar units," namely, the reactivity of one dollar corresponds to a prompt critical state.

In order to ensure the safety of a reactor, the total reactivity of each

[1] There is a special research reactor where fuel elements are used for control rods, for example, the Fast Critical Assembly (FCA) at the Japan Atomic Energy Agency (JAEA). In this case, positive reactivity is added to the core by the insertion of the control rods. At a certain critical assembly, including KUCA, the water level in the core can be used for controlling its reactivity. In the Pressurized-Water Reactor (PWR) core, boron oxide (B_2O_3) is dissolved into water to adjust the criticality.

[2] Sometimes, the units of reactivity are represented as $\Delta k/k/k'$, which is the same as $\Delta k/k$.

control rod should be determined; this corresponds to the amount of reactivity measured when moving a control rod from its lower limit to the upper limit. Further, the reactivity insertion rate as a function of the position of the control rod, which is designated by the "control rod calibration curve," is also an important parameter of the control rod. Measurement of the total reactivity value (which is often called the total reactivity worth), or calibration curve, is known as the control rod calibration experiment. For safety reasons, when a new reactor core is constructed, the control rod calibration experiment is conducted immediately after conducting the approach to criticality experiment.

Control rod calibration is important not only for safe operation but also for carrying out other reactivity measurement experiments. For example, the amount of sample reactivity caused by introducing a material into the core can be determined on the basis of the difference between the positions of a calibrated control rod before and after the introduction of the sample material.

There are several methods for measuring control rod reactivity: (1) period method, (2) compensation method, (3) rod drop method, (4) subcriticality measurement method (i.e., neutron source multiplication method or pulsed neutron method), (5) inverse kinetic method, etc. In the present experiments, the period method and compensation method are used for control rod calibration, and the rod drop method is adopted for measuring large negative reactivity.

2−2 Principle

2−2−1 Reactor Kinetic Equation

The reactor kinetic equations based on one-point reactor approximation with one-energy-group theory, which are the basis for reactivity measurement, are as follows:

$$\frac{dn}{dt} = \frac{\rho - \beta_{eff}}{\Lambda} n + \sum_{i}^{6} \lambda_i C_i, \tag{2−2}$$

$$\frac{dC_i}{dt} = \frac{\beta_{i,eff}}{\Lambda} n - \lambda_i C_i, \tag{2−3}$$

where $n(t)$ is neutron density; C_i is the i^{th} group delayed neutron precursor density; λ_i is the decay constant of the i^{th} group delayed neutron precursor; Λ is the neutron generation time, which is the neutron life time ℓ divided

by k_{eff}; β_{eff} is the effective delayed neutron fraction; and $\beta_{i,eff}$ is the i^{th} group delayed neutron fraction. The derivation of these kinetic equations is not included in this text (please refer to the textbooks[1−5] on reactor physics); however, the meaning of these equations is noted here. Eq. (2−2) implies the following:

(A rate of change of the number of neutrons)
= (the number of increasing neutrons caused by neutron production by prompt fission reaction)
− (the number of decreasing neutrons caused by neutron absorption and neutron leakage)
+ (the number of increasing neutrons generated by the decay of a delayed neutron precursor).

Eq. (2−3) indicates the neutron balance for the i^{th} group delayed neutron precursor as follows:

(A rate of the i^{th} group delayed neutron precursor)
= (the number of the i^{th} group delayed neutron precursors produced by fission reaction)
− (the number of the i^{th} group delayed neutron precursors decreased by decay).

Usually, delayed neutron precursors are treated in groups of six, therefore, kinetic equations in Eqs. (2−2) and (2−3) are simultaneous differential equations of seven unknowns (n, C_1 to C_6).

2−2−2 Positive Period Method

When step-wise reactivity ρ is inserted into a reactor in the critical state, the neutron flux $\phi(t)$ after the insertion of the reactivity is expressed as a summation of exponential functions as follows:

$$\phi(t) = \sum_{j=1}^{7} A_j e^{\omega_j t}, \tag{2−4}$$

where A_j and ω_j are constant. Substituting $\phi(t)$ of Eq. (2−4) in Eqs. (2−2) and (2−3),[3] the equation where ω_j should be satisfied is written as follows:

[3] The reactor kinetic equation is usually represented with $n(t)$. Since Eqs. (2−2) and (2−3) are based on the one-group theory, $\phi(t)$ is proportional to $n(t)$ as $\phi(t) = \upsilon n(t)$,

$$\rho = \frac{\omega \ell}{1+\omega \ell} + \frac{\omega}{1+\omega \ell} \sum_{i=1}^{6} \frac{\beta_{i,eff}}{\omega + \lambda_i}. \tag{2-5}$$

This means that ω_j in Eq. (2−4) are the roots of Eq. (2−5). Fig. 2−1 illustrates the relation between ω and ρ according to Eq. (2−5). From this figure, when positive reactivity ρ ($0 < \rho < 1$) is inserted into the core, only one positive ω_j is obtained and the rest of six ω_j are negative values; this means that after the terms with negative ω_j components in Eq. (2−4) vanish, the reactor power increases as:

$$\phi(t) \simeq A_1 e^{\omega_1 t}, \tag{2-6}$$

where A_1 is constant. The inverse value of ω_1, T, is written as follows:

$$T = \frac{1}{\omega_1}. \tag{2-7}$$

T is known as the stable reactor period (or, merely, the period), which satisfies the following equation:

$$\rho = \frac{\ell}{T+\ell} + \frac{T}{T+\ell} \sum_{i=1}^{6} \frac{\beta_{i,eff}}{1+\lambda_i T}. \tag{2-8}$$

According to Eq. (2−8), for measuring positive reactivity, the positive period T should be measured and the reactivity ρ is calculated using Eq. (2−8).

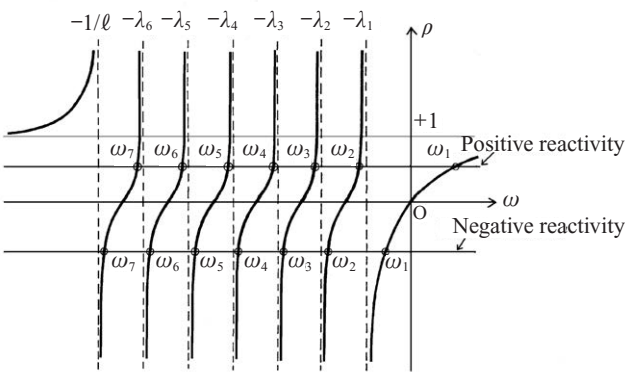

Fig. 2−1 Relation between reactivity ρ and ω

where v is the neutron velocity.

This method is called the positive period method.

In a thermal reactor, neutron lifetime is approximately less than 10^{-3}s (see Sec. 2A of Appendix 2) and the period T that is measured in the experiment is more than 10 s; therefore, the first term on the right-hand side of Eq. (2−8) can be neglected, and the reactivity can be expressed as follows:

$$\rho = \sum_{i=1}^{6} \frac{\beta_{i,eff}}{1+\lambda_i T}. \tag{2−9}$$

If it is assumed that the i^{th} group effective delayed neutron fraction $\beta_{i,eff}$ is proportional to β_i (the i^{th} group delayed neutron fraction, which is obtained from the nuclear data of the fissile nuclide and is independent of the reactor type) as:

$$\beta_{i,eff} = \gamma_i \beta_i, \tag{2−10}$$

and, if γ_i is independent of the delayed neutron group as follows:

$$\beta_{i,eff} = \gamma \beta_i, \tag{2−11}$$

then, the effective delayed neutron fraction can be written as follows:

$$\beta_{eff} \equiv \sum_i \beta_{i,eff} = \gamma \sum_i \beta_i = \gamma\beta. \tag{2−12}$$

From Eqs. (2−11) and (2−12), the following equation can be derived:

$$\frac{\beta_{i,eff}}{\beta_{eff}} = \frac{\beta_i}{\beta} \equiv \alpha_i. \tag{2−13}$$

This means that $\beta_{i,eff}/\beta_{eff}$ is approximated by β_i/β which is obtained from the nuclear data and is independent of the reactor characteristics.

From Eqs. (2−9) and (2−13), the following equation is derived:

$$\frac{\rho}{\beta_{eff}} = \sum_{i=1}^{6} \frac{\alpha_i}{1+\lambda_i T}. \tag{2−14}$$

The parameters appearing in this equation are listed in Sec. 2B of Appendix 2.

2−2−3 Control Rod Drop Method

(1) Extrapolation Method

When the reactor power is maintained at a constant value for a certain period of time, the neutron density and delayed neutron precursor density, n_0 and C_{i0}, respectively, are constant, and the left-hand sides of Eqs. (2−2) and (2−3) are zero; then, the following relation is obtained from Eq. (2−3):

$$\sum_i \lambda_i C_{i0} = \sum_i \frac{\beta_{i,eff}}{\Lambda} n_0 = \frac{\beta_{eff}}{\Lambda} n_0, \tag{2−15}$$

where Λ ($\ell = \Lambda \times k_{eff}$) is the neutron generation time.

If a control rod whose reactivity is ρ is suddenly inserted into the core, Eq. (2−2) can be written as follows:

$$\frac{dn}{dt} = \frac{\rho - \beta_{eff}}{\Lambda} n + \frac{\beta_{eff}}{\Lambda} n_0. \tag{2−16}$$

This is because the delayed neutron precursor densities are constant as in Eq. (2−15). One can easily solve Eq. (2−16) under the initial condition that $n = n_0$ at $t = 0$ and express n (t) as:

$$n(t) = \frac{\beta_{eff} n_0}{\beta_{eff} - \rho} - \frac{\rho n_0}{\beta_{eff} - \rho} e^{-\frac{\beta_{eff} - \rho}{\Lambda} t}. \tag{2−17}$$

When $\rho < 0$, the second term on the right-hand side decreases immediately, and n (t) immediately approaches the following value:

$$n_1 = \frac{\beta_{eff}}{\beta_{eff} - \rho} n_0. \tag{2−18}$$

Therefore, reactivity can be obtained by the following equation:

$$\rho = \frac{n_1 - n_0}{n_1} \beta_{eff}. \tag{2−19}$$

This method is known as the extrapolation method in the control rod drop experiment.

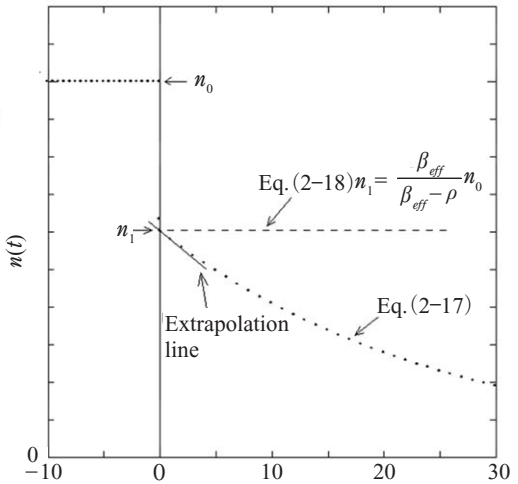

Fig. 2−2 Reactor power change after insertion of a control rod

(2) Integral Counting Method

If one solves Eqs. (2−2) and (2−3) by the Laplace transformation method, the following equation is obtained:

$$\overline{n}(s) = n_0 \frac{\Lambda + \sum_i \frac{\beta_{i,eff}}{s + \lambda_i}}{s\Lambda + s\sum_i \frac{\beta_{i,eff}}{s + \lambda_i} - \rho}. \tag{2−20}$$

By using the following well-known relation in the Laplace transformation method:

$$\lim_{s \to 0} \overline{n}(s) = \lim_{s \to 0} \int_0^\infty e^{-st} n(t)\, dt = \int_0^\infty n(t)\, dt, \tag{2−21}$$

Eq. (2−20) can be transformed as follows if the limit of s approaches zero:

$$n_0 \frac{\Lambda + \sum_i \frac{\beta_{i,eff}}{\lambda_i}}{-\rho} = n_0 \frac{\Lambda + \beta_{eff} \sum_i \frac{a_i}{\lambda_i}}{-\rho} = \int_0^\infty n(t)\, dt. \tag{2−22}$$

When compared to the value of $\beta_{eff}\sum_i \frac{a_i}{\lambda_i}$ in the numerator, the neutron generation time Λ in this equation can be neglected. Reactivity is obtained as follows:

$$-\frac{\rho}{\beta_{eff}} = \frac{n_0 \sum_i \frac{a_i}{\lambda_i}}{\int_0^\infty n(t)\,dt} = \frac{13.04 \times n_0}{\int_0^\infty n(t)\,dt}. \qquad (2\text{−}23)$$

By determining both n_0, which is the count rate before the control rod drop, and $\int_0^\infty n(t)dt$, which is the total count after the control rod drop is measured, the reactivity of the control rod can be obtained easily, as shown in Eq. (2−23). This method is known as the integral counting method in the control rod drop experiment.

2−2−4 Compensation Method

In the positive period experiments, a control rod (for example: C1 rod) is withdrawn to a certain length to add a positive reactivity, and after measuring the positive period, another control rod (for example: C2 rod) is inserted into the core to achieve a critical state. In this case, the absolute value of negative reactivity by the C2 rod is the same as the absolute value of the positive reactivity by the C1 rod measured by the positive period method. This means that the calibration of the C1 and C2 rods can be carried out simultaneously by using the positive period method, which is also known as the compensation method for C2 rod calibration.

2−3 Experiments

2−3−1 Core Configuration

An example of the core configuration of the KUCA C-core is shown in Fig. 2−3. As mentioned in Chapter 1 (Approach to Criticality), the KUCA core comprises six identical control rods; however, three (C1 to C3) out of six rods are used for adjusting criticality, and the remaining three rods (S4 to S6) are used as safety rods. They are used as a backup system for emergency shutdown of the reactor, which is achieved by withdrawing them from the core. As shown in Fig. 2−3, since safety rods and control rods are located in a symmetrical position with respect to the core centerline, the reactivity value of the safety rods is supposed to be the same as that of the control rods.

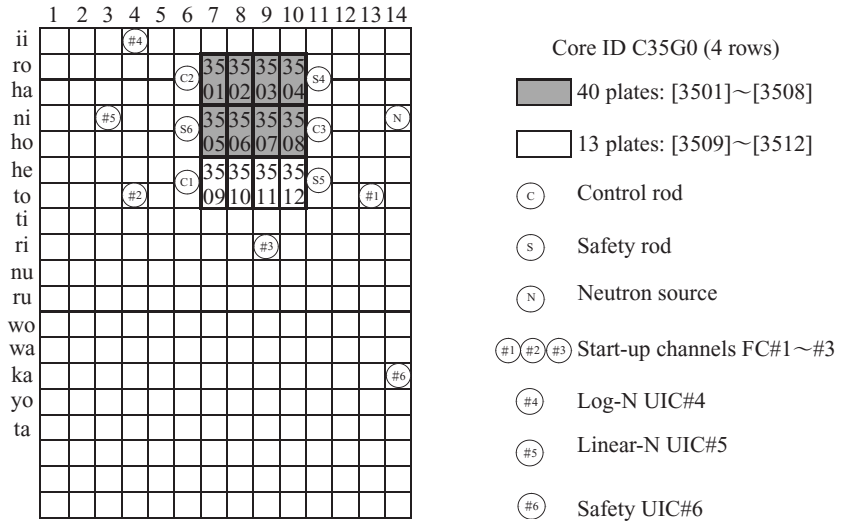

Fig. 2−3 Core configuration of the KUCA core (horizontal view)

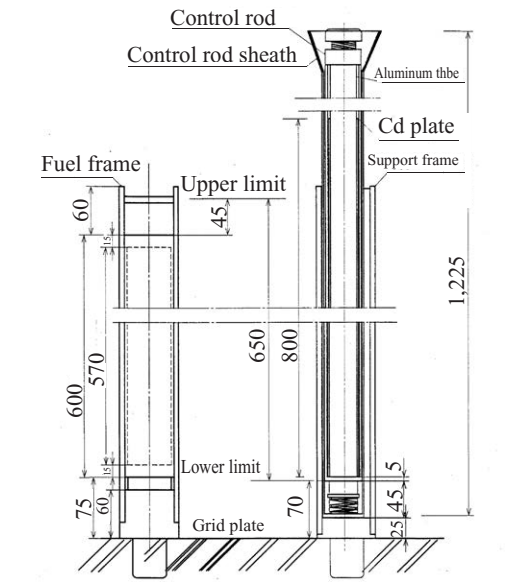

Fig. 2−4 Vertical position of fuel assembly and control rod in KUCA C core (unit: mm)

Note that before carrying out the control rod calibration experiment, some fuel plates are inserted into the core that was constructed in the approach to criticality experiment; this is because criticality should be attained with one control rod in a lower limit position in order to measure the control rod calibration curve of the total stroke of the rod.

2−3−2 Period Method Experiment

The experimental procedure for the positive period method is as follows:

(1) Adjust criticality
(2) Withdraw a designated control rod to a pre-designated distance
(3) Wait for a prescribed time period for the disappearance of the higher-order terms in Eq. (2−4)
(4) Measure the doubling time T_d (time to double the power level) with a stop watch
(5) Obtain period T by $T = T_d/\ln 2$ relationship
(6) Obtain ρ through Eq. (2−8)
(7) Insert another control rod to a specified length to reestablish criticality
(8) Repeat procedures (1) through (7) until the first rod is in the upper limit position, namely, fully withdrawn from the core.

2−3−3 Rod Drop Method Experiment

The experimental procedure for the rod drop method is as follows:

(1) Adjust criticality
(2) Measure the n_0 count several times to confirm criticality
(3) Start the MCS (Multi-channel Scalar)
(4) Stop the supply of electric current to the control rod that is in the upper limit position and start measuring the integral count required in Eq. (2−23)
(5) Stop the counting when the neutron flux level decreases considerably

2−4 Discussion

The following quantities should be summarized:

(1) Control rod reactivity of each rod (C1, C2, and C3)
(2) Integrated and differential calibration curves of measured rods
(3) Excess reactivity of the core
(4) Mass reactivity of each fuel plate

(5) Shutdown margin of the core

The following items should be discussed:

(1) Is there a difference between the control rod values of the rods (C1, C2, C3)? If yes, what is the reason behind it?
(2) The control rod worth of one particular rod is measured by using different techniques. Are there any differences between the results obtained by the different techniques? If yes, what is the reason behind these differences?
(3) Is the integrated calibration curve the same as the theoretically obtained curve? If there is a difference, what is the reason behind it?

2−5 Preparatory Report

(1) According to the one-group first-order perturbation theory, when a control rod is inserted into the core whose total length is H, the inserted reactivity $\rho(x)$ can be expressed using the following equation (see Sec. 2D of Appendix 2):

$$\rho(x) = \rho(H)\left\{\frac{x}{H} - \frac{1}{2\pi}\sin\left(\frac{2\pi x}{H}\right)\right\}, \tag{2−24}$$

where the total reactivity value is $\rho(H)$.

Plot the control rod calibration curve by using the above equation. This curve is called the integral control rod calibration curve. Plot the differential control rod calibration curve, which is defined as $d\rho(H)/dx$. Note that the total stroke of the KUCA C-core is 650 mm, and $\rho(H)$ is assumed to be unity ($\rho(H) = 1$).

(2) Assuming that C2 is at the lower limit and C3 is at the upper limit, C1 is used to adjust criticality, as shown in Fig. 2−5. Subsequently, C2 is withdrawn to a certain length and C3 is inserted to attain criticality. Assuming that C2 rod is withdrawn three times until C2 is fully withdrawn from the core, follow the procedure shown in the diagram.

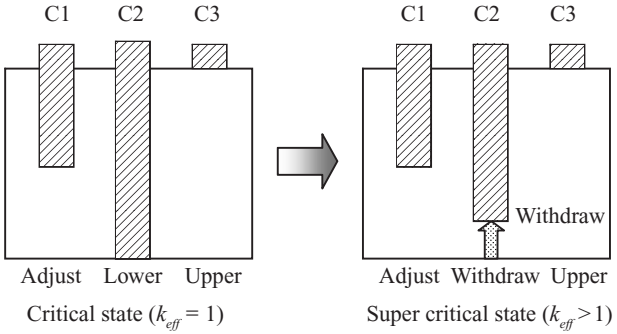

Fig. 2−5 Procedure for control rod calibration by the positive period method

References

1. J. R. Lamarsh, *Introduction to Nuclear Reactor Theory*, Addison-Wesley Pub. Co., (1966).
2. G. I. Bell and S. Glasstone, *Nuclear Reactor Theory*, Krieger Publishing Company, (1970).
3. J. J. Duderstadt and L. J. Hamilton, *Nuclear Reactor Analysis*, John Wiley & Sons, Inc., (1976).
4. K. O. Ott and W. A. Bezella, *Introductory Nuclear Reactor Statics*, American Nuclear Society, (1983).
5. K. O. Ott and W. A. Bezella, *Introductory Nuclear Reactor Dynamics*, American Nuclear Society, (1985).

Appendix 2

2A. Neutron Lifetime

The neutron lifetime of several reactors is listed in Table 2−1.

Table 2−1 Prompt neutron lifetime of several reactors

Reactor type	Thermal reactor moderator	Reactor name	Lifetime (s)
Thermal reactor	Graphite	Calder Hall	1×10^{-3}
	Heavy water	Douglas Point−1	6.5×10^{-4}
	Heavy water	JRR−2 (JAERI)	2.1×10^{-4}
	Light water	KUR (KURRI)	6.7×10^{-5}
	Light water	KUCA C45G0 core	5.5×10^{-5}
Fast reactor		Enrico Fermi (USA)	1.4×10^{-7}
		EBR−2 (USA)	8×10^{-8}
		Yayoi (U. of Tokyo)	2.9×10^{-8}

2B. Delayed Neutron Data and Basic Parameters of KUCA

Delayed neutron lifetime data, as obtained from Eqs. (2−8) and (2−13), are listed in Table 2−2. Prompt neutron lifetime and effective delayed neutron fraction of the KUCA cores are summarized in Table 2−3.

Table 2−2 Thermal fission delayed neutron data

Delayed neutron group	^{235}U Fission	
	Decay constant λ_i (1/s)	Fraction ($a_i=\beta_i/\beta$)
1	0.0124 ± 0.0003	0.033 ± 0.003
2	0.0305 ± 0.0010	0.219 ± 0.009
3	0.111 ± 0.004	0.196 ± 0.022
4	0.301 ± 0.011	0.395 ± 0.011
5	1.14 ± 0.15	0.115 ± 0.009
6	3.01 ± 0.29	0.042 ± 0.008

$\beta=\sum_i \beta_i=(0.640\pm0.032)\times10^{-2}$

Table 2−3 Constants of KUCA

Core name	Prompt neutron life time (s)	Effective delayed neutron fraction β_{eff}	γ
C45G0	5.52×10^{-5}	7.537×10^{-3}	1.178
C35G0	4.92×10^{-5}	7.611×10^{-3}	1.189
C30G0	4.79×10^{-5}	7.673×10^{-3}	1.199

2C. First-Order Perturbation Theory

The effect of a small change in the core parameters on reactivity, such as a change in material or core structure, can be expressed by the first-order perturbation theory.

The eigenvalue equation (namely, the neutron balance equation) can be written as follows:

$$M\phi=\frac{1}{k}F\phi\,, \tag{2A−1}$$

where M is the destruction operator including leakage and absorption reactions, F is the production operator including fission reactions, k is the effective multiplication factor, and ϕ is the neutron flux. In the one-group diffusion theory, M and F can be written as follows:

$$M=-\nabla D(\vec{r})\nabla+\sum_{\alpha}(\vec{r}),\quad \mathrm{F}=\nu\sum_{f}(\vec{r})\,. \tag{2A−2}$$

It is assumed that a small absorbing material is inserted into the core and the absorption cross-section changes according to the following equation:

$$\sum\nolimits'_{\alpha}(\vec{r})=\sum_{\alpha}(\vec{r})+\delta\sum_{\alpha}(\vec{r})\,. \tag{2A−3}$$

The eigenvalue equation of Eq. (2A−1) can be modified as follows:

$$M'\phi'=\frac{1}{k'}F\phi', \tag{2A−4}$$

$$M'=M+\delta\sum_{\alpha}, \tag{2A−5}$$

where prime (‘) indicates modified values.

Here, adjoint flux ϕ^{+} and adjoint operators M^{+} and F^{+} are introduced; these are defined as follows:

$$M^{+}\phi^{+}=\frac{1}{k}F^{+}\phi^{+}, \tag{2A−6}$$

$$\left\langle M^{+}f, g\right\rangle = \left\langle f, Mg\right\rangle, \tag{2A−7}$$

where < > indicates integration over the entire space and energy, and f and g are arbitrary functions. By making the inner product of Eq. (2A−7) and ϕ^{+}, the following equation can be obtained:

$$\left\langle \phi^{+}, M\phi'\right\rangle + \left\langle \phi^{+}, \delta\Sigma_{a}\phi'\right\rangle = \frac{1}{k'}\left\langle \phi^{+}, F\phi'\right\rangle. \tag{2A−8}$$

Using Eqs. (2A−6) and (2A−7), the first term on the left-hand side of the above equation is modified as:

$$\begin{aligned}\left\langle \phi^{+}, M\phi'\right\rangle = \left\langle M^{+}\phi^{+},\ \phi'\right\rangle &= \frac{1}{k}\left\langle F^{+}\phi^{+},\ \phi'\right\rangle \\ &= \frac{1}{k}\left\langle \phi^{+}, F\phi'\right\rangle.\end{aligned} \tag{2A−9}$$

Therefore, reactivity change $\Delta\rho$ can be expressed as follows:

$$\Delta\rho=\frac{1}{k}-\frac{1}{k'}=-\frac{\left\langle \phi^{+}, \delta\Sigma_{a}\phi'\right\rangle}{\left\langle \phi^{+}, F\phi'\right\rangle}. \tag{2A−10}$$

Note that no assumptions are made in the above procedures. However, Eq. (2A−10) can be written to accommodate the assumption that the change in neutron flux is very small, namely, $\phi' \doteqdot \phi$. The formula for this case is:

$$\Delta\rho=-\frac{\left\langle \phi^{+}, \delta\Sigma_{a}\phi\right\rangle}{\left\langle \phi^{+}, F\phi\right\rangle}. \tag{2A−11}$$

This equation does not include neutron flux or adjoint flux after perturbation, and is known as the first-order perturbation theory.

In the one-energy-group theory, the adjoint flux is the same as the neutron flux. Eq. (2A−11) can be written as follows:

$$\Delta\rho = -\frac{\int_{\Delta V}\phi(\vec{r})\,\delta\Sigma_{\alpha}(\vec{r})\,\phi(\vec{r})\,d\vec{r}}{\int_{V}\phi(\vec{r})\,\nu\Sigma_{f}(\vec{r})\,\phi(\vec{r})\,d\vec{r}}. \tag{2A−12}$$

For simplicity, it is assumed that uniform perturbation is introduced in region ΔV. Reactivity can be written as:

$$\Delta\rho = -\frac{\delta\Sigma_{\alpha}}{\nu\Sigma_{f}\int_{V}\{\phi(\vec{r})\}^{2}d\vec{r}}\int_{\Delta V}\{\phi(\vec{r})\}^{2}d\vec{r}\,. \tag{2A−13}$$

2D. Control Rod Calibration Curve

For an application of the first-order perturbation theory, a control rod calibration curve is derived.

It is assumed that a control rod is partially inserted ($0 \leqq x \leqq h$) into an infinite homogeneous slab core of thickness H without a reflector. Neutron flux distribution can be written as follows:

$$\phi(x) = A\sin\frac{\pi x}{H}, \quad (A\text{: const}). \tag{2A−14}$$

Perturbation shown in Eq. (2A−5) is expressed as follows:

$$\delta\Sigma_{\alpha}(x) = \begin{cases}\delta\Sigma_{\alpha} & (0 \leq x \leq h)\\ 0 & (h < x \leq H)\end{cases}. \tag{2A−15}$$

By substituting Eqs. (2A−14) and (2A−15) in Eq. (2A−12), the following equation can be obtained:

$$\Delta\rho(h) = -\frac{\delta\Sigma_{\alpha}\int_{0}^{h}\sin^{2}\frac{\pi x}{H}dx}{\nu\Sigma_{f}\int_{0}^{H}\sin^{2}\frac{\pi x}{H}dx} = -\frac{\delta\Sigma_{\alpha}}{\nu\Sigma_{f}}\left(\frac{h}{H}-\frac{1}{2\pi}\sin\frac{2\pi h}{H}\right). \tag{2A−16}$$

The total reactivity $\Delta\rho(H)$ can be written by $h = H$ in Eq. (2A−16) as follows:

$$\Delta\rho(H) = -\frac{\delta\Sigma_{\alpha}}{\nu\Sigma_{f}}. \tag{2A−17}$$

Using Eqs. (2A−16) and (2A−17), reactivity can be obtained as follows:

$$\Delta\rho(h) = \Delta\rho(H)\left(\frac{h}{H} - \frac{1}{2\pi}\sin\frac{2\pi h}{H}\right). \qquad (2A-18)$$

Chapter 3 Measurement of Reaction Rate

3−1 Purpose

Generally, the reactor core is in a critical state and the neutron flux distribution depends upon the spatial distribution, which is determined by the type and structure of the reactor, the composition and size of the fuel, and positioning of the control rods.

Currently, almost all nuclear power plants around the world are light-water reactors (LWRs). The spatial distribution of the fission reaction rate in LWRs, which are mostly thermal reactors, is proportional to that of the thermal neutron distribution because almost all the reactions are caused by thermal neutrons. It can then be said that the power distribution is proportional to the spatial distribution of the thermal neutrons. Therefore, it is possible to obtain the value of reactor power by measuring the relative spatial distribution of the thermal neutrons and the absolute value of thermal neutrons in suitable positions of the reactor.

Thermal neutron flux can be measured by using activation detectors, ionization chambers, fission counter tubes, and scintillation counters. Among these, activation detectors are more convenient to use and they measure the thermal neutron flux to a high degree of precision and spatial resolution. The activation detectors are also indispensable for measuring the absolute value of thermal neutron flux.

It should be noted that it is impossible to directly measure the neutron flux by any detector, even though the physical value of neutron flux is very important for theoretical and experimental studies on reactor physics. The only physical value that can be measured is the “reaction rate,” which is the value of the reaction with materials composed of detectors. It is necessary to know the cross sections of the materials composing the detectors, and to examine the interaction with the material in neutron yield from the theoretical point of reactor physics in order to obtain the neutron flux from the reaction rate measured. In this measurement of reaction rate distribution, the best use of both radiation instrumentation techniques and

reactor physics theory should be made.

In this experiment, the following measurements of the water-moderated and -reflected core (C-core) of KUCA are carried out by using a gold (Au) wire (which is a good activation detector for thermal neutrons):

1) Measurement of reaction rate distribution by using Au in the reactor core on the basis of the activation method of gold wire
2) Measurement of the absolute value of thermal neutrons in the reactor core on the basis of the activation method of gold foil

The purposes of this experiment are to:

1) Learn experimentally the basic techniques of the activation method.
2) Study the effect of control rods, reflectors, and structural materials in the reactor core on the neutron flux distribution.
3) Obtain knowledge about the neutron spectrum in the reactor core by using both gold wire and foil with and without Cd covering, each of which can be considered to be an activation detector and spectral index.

3−2 Principle

3−2−1 Features of Neutron Activation Detector

The activation detector is presented in this section. It can generally be utilized as a foil or a wire. The neutron activation foil can measure neutrons on the basis of the radiation induced in the foil by interaction with the neutrons. This foil has the following advantages and disadvantages:

Advantages:

1) The neutron field in the object of measurement is not disturbed and the resolution for measuring neutron flux is high, since the quantity and size of the foil are small in comparison with the quantity and size of other detectors.
2) The precision of measurement is high, when the fission reaction with the neutrons and foil is smooth.
3) Measurements on the neutrons can be carried out without the requirement of γ-ray.
4) The equipment used for the measurement of induced radioactivity is simple and cost effective.
5) The neutrons over a wide range of detector sensitivity can be easily

dealt with, regardless of the value of neutrons.

Disadvantages:

1) The resolution of neutron energy is not high, since the activation reaction is caused by the neutrons whose energy lies within a specific energy range.
2) The handling and interpretation of experimental data are complicated, since some corrections and calibrations are necessary.
3) Online measurement is difficult, since a considerable time is consumed to obtain the results after the irradiation.
4) The precision of measurement is low when the nuclides used are those whose activation cross-section data are not fully known.

The nuclear characteristics of foil materials that are often utilized for the measurement of thermal neutrons are shown in Table 3−1:

Table 3−1 Activation materials and nuclear characteristics of a thermal neutron detector

Element	Absorption [barn **]	Elastic [barn]	Isotope [%]	Number density [10^{22}/g]	Activation * [barn]	Radioisotope [Half-life]
$_{25}$Mn	13.2 ± 0.1	2.3 ± 0.3	^{55}Mn [100]	1.097	13.2 ± 0.1	^{56}Mn (2.58 h)
$_{29}$Cu	3.81 ± 0.3	7.2 ± 0.6	^{63}Cu [69.1] ^{65}Cu [30.9]	0.948	4.41 ± 0.20 1.8 ± 0.4	^{64}Cu (12.87 days) ^{66}Cu (5.14 min)
$_{66}$Dy	940 ± 20	100 ± 20	^{164}Dy [28.18]	0.1034	2,000 ± 200 800 ± 100	^{165m}Dy (1.3 min) ^{165}Dy (140 min)
$_{79}$Au	98.5 ± 0.4	9.3 ± 1.0	^{197}Au [100]	0.3055	98.5 ± 0.4	^{198}Au (2.698 days)

*: Neutron velocity 2,200 m/s (for a neutron energy of 0.0253 eV)
**: 1 barn = 10^{-24} cm^2

3−2−2 Measurement of Neutron Flux Using Activation Detector

Assuming that a material of mass M [g] exists in the reactor core, the number of atoms N_{Ia} of isotope Ia with weight W [wt%] and atomic weight A is expressed by using the Avogadro's number N_0 [1/mol] as follows:

$$N_{Ia} = \left(\frac{MW}{100A}\right) N_0 . \tag{3−1}$$

The isotope Ia is considered as the activation foil when Ia is activated by

the neutrons in the reactor core and the radioisotope *Ib* is generated.

(1) Activation Reaction Rate

For neutrons with energy in the range of E to $E+\Delta E$ [MeV], the number of activation reactions from *Ia* to *Ib* per unit time, that is, the activation reaction rate $R(E)dE$ [1/s] under the condition that there is no distortion of neutron flux in the activation foil is expressed as:

$$R(E)\,dE = N_{Ia}\sigma_{Ia}(E)\phi(E)\,dE, \tag{3−2}$$

where $\sigma_{Ia}(E)$ [cm^2] indicates the microscopic cross-section of *Ia*, and $\phi(E)\,dE$ [1/cm^2/s] indicates the neutron flux in the position of the activation foil.

The entire activation reaction rate R_{act} [1/s] is given as follows:

$$R_{act} = \int_0^{E\max} R(E)\,dE = \int_0^{E\max} N_{Ia}\sigma_{Ia}(E)\phi(E)\,dE. \tag{3−3}$$

Then, the entire neutron flux Φ [1/cm^2/s] and effective microscopic cross-section $\sigma_{eff,\,Ia}(E)$ [cm^2] in the position of the activation foil are defined as follows:

$$\Phi = \int_0^{E\max} \phi(E)\,dE, \tag{3−4}$$

$$\sigma_{eff,\,Ia} = \int_0^{E\max} \frac{\sigma_{Ia}(E)\phi(E)\,dE}{\Phi}. \tag{3−5}$$

By using Eqs. (3−4) and (3−5), Eq. (3−3) can be expressed as follows:

$$R_{act} = N_{Ia}\,\sigma_{eff,Ia}\,\Phi. \tag{3−6}$$

Therefore, during the principle measurement of neutron flux, Φ can be obtained, when R_{act} can be fixed by measuring the radioactivity (disintegration rate) of isotope *Ib*, since the value of $N_{Ia}\sigma_{eff,Ia}$ in Eq. (3−6) is specifically given to the activation foil if the configuration of neutron flux $\phi(E)$ is fixed in the reactor core, regardless of the absolute value of the neutron spectrum $\phi(E)$ [1/cm^2/s/MeV].

(2) Saturation Activity

It should be considered that the isotope *Ib* can not only be generated but

also undergo radioactive decay in the activation coil. By considering the production and decay in the foil, the atomic number of isotope *Ib* in microscopic time *dt* [s] is given as follows:

$$dN_{Ib}(t) = N_{Ia}\sigma_{eff,Ia}\Phi\, dt - \lambda_{Ib} N_{Ib}(t)\, dt, \tag{3−7}$$

where λ_{Ib} [1/s] indicates the decay constant, $N_{Ib}(t)$ is the number of atoms per time t [s], and $\lambda_{Ib} N_{Ib}(t)$ is the amount of decay per unit time.

By using Eq. (3−7), the N_{iIb} of isotope *Ib* after irradiation for T_i [s] under the condition that the isotope *Ib* never existed prior to irradiation can be obtained as follows:

$$N_{iIb} = \frac{N_{Ia}\sigma_{eff,Ia}\Phi\,(1 - e^{-\lambda_{Ib}T_i})}{\lambda_{Ib}}. \tag{3−8}$$

The radioactivity D_{iIb} [1/s] of isotope *Ib* after irradiation for T_i [s] can be obtained as follows:

$$D_{iIb} = \lambda_{Ib} N_{iIb} = N_{Ia}\sigma_{eff,Ia}\Phi\,(1 - e^{-\lambda_{Ib}T_i}). \tag{3−9}$$

The saturation activity D_∞[1/s], which refers to the radioactivity of isotope *Ib* generated by irradiation for infinite duration ($T_i \to \infty$), can be expressed as follows:

$$D_\infty = N_{Ia}\sigma_{eff,Ia}\Phi. \tag{3−10}$$

From Eqs. (3−6) and (3−10), the following equation can be obtained:

$$D_\infty = R_{act}. \tag{3−11}$$

Eq. (3−11) shows that the saturation activity is equal to the entire activation reaction rate. Namely, the entire activation reaction rate R_{act} can be obtained by measuring the saturation activity D_∞.

(3) Measurement of Saturation Activity and Time Correction for Decay

The isotope *Ib* generated by the irradiation dies out with time after irradiation, and its radioactivity D_{iIb} also decays and decreases. The radioactivity D_{wIb} can be expressed as follows (for the waiting time T_w [s], starting from the end of the irradiation till the start of measurement of radioactivity):

$$D_{wIb} = D_{iIb}\, e^{-\lambda_{Ib} T_w}. \tag{3−12}$$

By considering the decay of *Ib* in the measurement, when radioactivity D_{wIb} is measured by a radiation detector with a detection efficiency of ε for the measurement time of T_c [s], the count C_{total} during the measurement can be obtained as follows:

$$C_{total} = \int_0^{T_c} \varepsilon D_{wIb}\, e^{-\lambda_{Ib} t}\, dt = \frac{\varepsilon D_{wIb}(1 - e^{-\lambda_{Ib} T_c})}{\lambda_{Ib}}. \tag{3−13}$$

From Eq. (3−12), the average counting rate C_{av} [1/s] can be obtained in the measurement time of T_c as follows:

$$C_{av} = \frac{C_{total}}{T_c} = \frac{\varepsilon D_{wIb}\,(1 - e^{-\lambda_{Ib} T_c})}{\lambda_{Ib}\, T_c}. \tag{3−14}$$

By measuring C_{av}, the saturation activity D_∞ for T_i [s] of irradiation can be obtained from Eqs. (3−9), (3−10), (3−12), and (3−14) as follows:

$$D_\infty = \frac{\lambda_{Ib}\, T_c\, C_{av}(1 + \alpha)}{\varepsilon(1 - e^{-\lambda_{Ib} T_i})\, e^{-\lambda_{Ib} T_w}(1 - e^{-\lambda_{Ib} T_c})}, \tag{3−15}$$

where α indicates the internal conversion coefficient.

Finally, since the saturation activity is equal to the entire activation reaction rate, as shown in Eq. (3−11), the entire neutron flux can be obtained as follows:

$$\Phi = \frac{R_{act}}{N_{Ia}\, \sigma_{eff,Ia}} = \frac{D_\infty}{N_{Ia}\, \sigma_{eff,Ia}}. \tag{3−16}$$

It is observed that the neutron flux or the entire activation reaction rate in the activation foil can be obtained by measuring the saturation activity D_∞. Moreover, it is found that saturation activity D_∞ can be obtained by measuring the average counting rate C_{av} of radioactivity in the activation foil.

Subsequently, it is not necessary to obtain the absolute value of saturation activity D_∞ and the value of ε when measuring the relative spatial distribution of neutron flux or the entire activation reaction rate.

3−2−3 Measurement of Radioactivity Using Gold (Au) Activation Foil

In reactor physics experiments, gold (Au) has been widely utilized as an activation foil for measuring thermal neutrons. Gold in the form of both foil and wire has been utilized in this experiment. For the activation of gold foil, the measurement method of the average counting rate C_{av} is described in this section.

The reasons why gold is widely utilized as the activation foil for measuring thermal neutrons in reactor experiments are:

1) It is well known that Au is 100% composed of ^{197}Au, and the change in energy of the cross-section for the reaction ^{197}Au (n, γ) ^{198}Au by the neutrons approximately conforms to the rule of $1/v$ for thermal area. (Refer to Fig. 3−4).
2) It is well known that the activation cross-section σ_{act} (v_0) of ^{197}Au is 98.5 $\pm$ 0.4 barn for the neutrons with $v_0 = 2{,}200$ m/s.
3) The decay pattern of an induced nuclide ^{198}Au generated by the activation of ^{197}Au is simple, as shown in Fig. 3−1, and the disintegration rate of ^{198}Au can be easily determined.
4) The half-life of ^{198}Au is 2.698 days, which is suitable for measuring radioactivity.

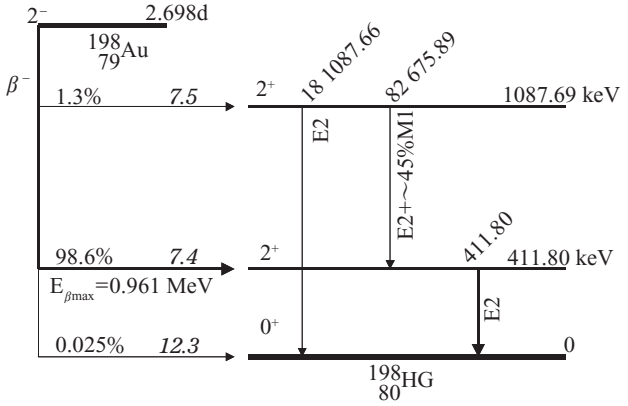

Fig. 3−1 Disintegration of ^{198}Au

The induced nuclide ^{198}Au generated by the activation of ^{197}Au transforms into ^{198}Hg by β-decay, as shown in Fig. 3−1. In this decay pattern, ^{198}Au is decayed under β-ray having a maximum energy of $E_{\beta max} = 0.961$ MeV and is transmitted to the ground state through the 1st excited state of ^{198}Hg after

γ-ray exposure at 411.8 keV. Since the half-life in the 1st excited state is as short as 22 ps, β- and γ-ray can be considered to be coincidently emitted with the transformation of ^{198}Au to ^{198}Hg. The $4\pi\beta-\gamma$ coincidence method is generally used for the absolute measurement of the activation quantity of gold foil in the case of coincident emission of β- and γ-ray. This method is based on determining the disintegration rate of the source, when β-decay occurs and the γ-ray is emitted in the objects of measurement, even if both β- and γ-ray detector efficiencies are unknown. ($4\pi\beta-\gamma$ coincidence method: Refer to Sec. 3A of Appendix 3)

The most accurate method that can be considered to be the absolute value of the activation quantity is widely utilized by a HyperPure Germanium semi-conductor detector (HPGe detector) of which detector efficiency is calibrated beforehand. The main features of the HPGe detector are that it can accurately display energy with a high degree of resolution and obtain the disintegration rate of γ-ray emitted nuclides or the emittance rate of γ-ray photons. Although this method is not considered to be a method for "absolute measurement," as compared with the $4\pi\beta-\gamma$ coincidence method, it is utilized in this experiment for the absolute measurement of the activation quantity of gold foil.

In this experiment, a NaI (Tl) scintillation detector is mainly utilized for the relative measurement of the entire activation reaction rate of the gold wire. Note that the basic measurement principle of the NaI scintillation detector is the same as that of the HPGe detector, although the composition and controls of the measurement system are different.

By using a multi-channel analyzer (MCA), the pulse-height distribution can be measured, the count at peak absorption at the maximum γ-ray energy of 411.8 keV can be obtained, and finally, the activity can be quantitatively determined. (Refer to Sec. 3−4 for details.)

The relationship between C_p and D can be expressed as follows:

$$C_p = \frac{\varepsilon D}{1+\alpha}, \tag{3−17}$$

where C_p indicates the measured counting rate of the absorption peak at full energy level, D is the radioactivity (disintegration rate) of the irradiated gold foil (gold wire), α (0.041) is the internal conversion coefficient, and ε is the detection efficiency for the absorption peak with all the energy. Therefore, it is necessary to know the detection efficiency ε for the absorption peaks corresponding to γ-ray of maximum energy, in order to obtain the absolute value of radioactivity D.

3−2−4 Detection Efficiency

It is necessary to obtain the detection efficiency ε by using a standard source in which the activity of the source is rooted. In case the number of γ-photon or the disintegration rate is rooted in the standard source, the detection efficiency ε in each case can be obtained as follows:

$$\varepsilon_{pi} = \frac{C_{pi}}{Q_i}, \tag{3−18}$$

$$\varepsilon_{pi} = \frac{C_{pi}}{F_i D_i}, \tag{3−19}$$

where C_{pi} indicates the counting rate at the absorption peak corresponding to the γ-ray energy E_i, Q_i is the γ-ray emittance rate [photons/s/4π] in the measurement position of the standard source, D_i is the disintegration rate [Bq] in this position, F_i is the ratio of γ-ray emitted with E_i, and i indicates the type of γ-ray at the measurement position.

The detection efficiency depends on the γ-ray energy for the objects of measurement. When the detection efficiency for the γ-ray of energy 411.8 keV cannot be directly obtained, it is necessary to determine the detection efficiency ε_{pi} by considering the γ-ray emitted from the standard source with energy greater and smaller than 411.8 keV. ε for the γ-ray of energy 411.8 keV can be obtained by considering ε_{pi} as the function of E_i and using the least-squares method or interpolation.

The type of standard source can be determined as follows:

(1) Mixed-Nuclide Standard Source

The mixed-nuclide standard source is a source that comprises a combination of approximately ten types of nuclides whose energy levels range from 60 keV to 1.8 MeV. It is convenient to calibrate the energy of all the ranges and detection efficiencies at one time of measurement. However, since the half-life of some nuclides differ from each other, it is necessary to consider the complicated procedures for correction of attenuation.

(2) Single-Nuclide Standard Source

The single-nuclide standard source is most widely used in the correction of the energy range, which is required when certain nuclides are used. It is necessary to ensure that the position of every nuclide is reproducible.

Subsequently, the detection efficiency depends on the geometric conditions of both detectors and the standard source as well as on the γ-ray

energy. It is also desirable to identify the geometric conditions with the time determined by the detection efficiency when using the standard source, and also with the time measured by the irradiated materials. Note: in order to obtain the spatial distribution of radioactivity, it is very important to ensure that while measuring the radioactivity of a sample, the detection efficiencies of other samples do not change.

3−3 Activation Reaction Rate Contributed by Thermal Neutron Flux

The entire activation reaction rate can be defined as the reaction rate of neutrons having all the energy in the neutron field. Thermal neutron flux is buried in the entire activation reaction rate. In this section, a method for extracting the thermal neutron flux is presented. Attention should be paid to discussions on theoretical as well as experimental reactor physics.

At first, the neutron spectrum in the thermal reactor is described and concepts of thermal and epi-thermal neutrons and neutron spectrum are presented. Secondly, the determination of activation reaction rate contributed by thermal neutron flux is described. Finally, experimental techniques for obtaining thermal neutrons and some corrections based on reactor physics theory are described.

3−3−1 Neutron Spectrum in Reactor Core

In the thermal reactor, the neutron spectrum can be divided into three regions according to neutron energy as follows:

- Nuclear fission energy region.
- Slowing-down energy region.
- Thermal energy region.

Nuclear fission neutrons that are generated in the nuclear fuel have their own kinetic energy with an energy ranging from approximately 75 keV to 17 MeV, regardless of the presence of prompt or delayed neutrons.

As shown in Fig. 3−2, region (i) is formed when the neutrons have been moderated by light nuclides in the media of a reactor core, especially in the moderators. The energy range is 1 eV < E < 100 keV, and the change in neutron energy is proportional to $1/E$, according to the slowing-down theory.

In the final process of slowing-down, the neutrons reach a heat balance with media atoms. In this condition, region (ii) is formed, and the energy

range is $E < 1$ eV.

Regions (i) and (ii) are especially important in the thermal reactor. The media atoms in these states are assumed to be in an infinite system and have a uniform distribution of a fast neutron source. In region (ii), the energy distribution (thermal neutron spectrum) of the thermal neutron flux is fixed to the Maxwell-type distribution with a physical temperature of T_m [K] in the media. When the scattering cross-section is very large and the absorption cross-section is zero, the thermal neutron $\phi_M(E)$ [1/cm^2/s/MeV] with energy E per unit energy width can be approximately expressed as follows:

$$\phi_M(E) \propto E(kT_m)^{-2} e^{-\frac{E}{kT_m}} . \tag{3-20}$$

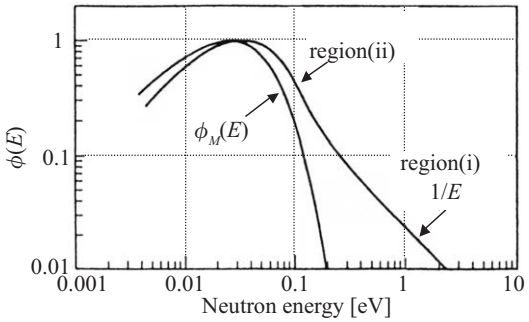

Fig. 3−2 Outline of neutron spectrum in thermal reactor

The energy distribution of the thermal neutron flux is shown in Fig. 3−2. The energy E_p [eV] at which $\phi_M(E)$ is maximized is expressed as follows:

$$E_p = kT_m , \tag{3-21}$$

for instance, when $T_m = 20.4$ ℃ (293.6 K) and the Boltzmann constant $k = 8.6167 \times 10^{-5}$ eV/K, E value can be obtained to be 0.0253 eV by using the above equation. Note that v_p (2,200 m/s) corresponds to the most desirable velocity with energy E_p. However, it is impossible to consider thermal reactors as pure moderators since the actual thermal reactors comprise highly absorptive materials such as the nuclear fuel.

As shown in Fig. 3−2, the neutron spectrum is distributed in three regions as follows:

1) Thermal energy region ($E \leq 0.1$ eV) approximated by the Maxwell distribution corresponding to a neutron temperature T_n that is higher than T_m due to the absorption effect.
2) Region (ii) fixed to the rule of $1/E$ in $E > 1$ eV.
3) Transient region (0.1 eV $< E <$ 1 eV) between epi-thermal energy and region (ii).

The combination of region (i) with the transient region can be called the epi-thermal region, which is distinct from region (ii) of the thermal region.

From the above description, the neutron spectrum in a thermal reactor can be expressed by considering $\phi(E)$ as the neutron flux with energy dependence per unit energy width as follows (Ref. 1):

$$\phi(E) = \phi_{th} \frac{E}{(kT_n)^2} e^{-\frac{E}{kT_n}} + \phi_{epi} \frac{\Delta\left(\frac{E}{kT_n}\right)}{E}, \tag{3−22}$$

where ϕ_{th} indicates the thermal neutron flux, ϕ_{epi} is the neutron flux in the epi-thermal region, and $\Delta(E/kT_n)$ is the joining function for the neutron spectrum in the transient region.

The neutron temperature T_n is given as follows, according to Ref. 2:

$$T_n = \frac{T_m}{1 - \frac{\Sigma_a(T_n)}{\xi\Sigma_s}}, \tag{3−23}$$

where $\xi\Sigma_s$ indicates the average slowing-down power for the epi-thermal neutron in the media of the reactor core.

As shown in Fig. 3−3, the joining function $\Delta(E/kT_n)$ shows different values depending on the value of $\xi\Sigma_s/\Sigma_a(T_n)$. Namely, $\xi\Sigma_s/\Sigma_a(T_n)$ is zero in less than approximately $4kT_n$, maximum at approximately $8kT_n$, and 1 at more than $15kT_n$. (Ref. 2)

3−3−2 Activation Reaction Rate Contributed by Thermal Neutrons

The measurement of activation reaction rate R_{th} [1/s] by thermal neutrons can be expressed as follows:

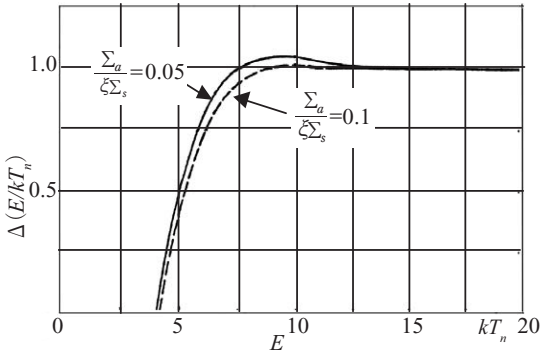

Fig. 3−3 Energy dependence of the joining function $\Delta(E/kT_n)$ for energy E

$$R_{th} = \int_0^{E_{th}} N\sigma(E)\phi(E)\,dE = N\sigma_{act}\phi_{th}, \tag{3−24}$$

where E_{th} indicates the maximum energy of the thermal neutron, N is the number of atoms of the activation foil, $\sigma(E)$ [cm^2] is the activation cross-section, $\phi(E)\,dE$ [1/cm^2/s] is the neutron flux with energy dependence.

The total thermal neutron flux ϕ_{th} and the average activation cross-section σ_{act} for the thermal neutrons in the activation foil can be expressed as follows:

$$\phi_{th} = \int_0^{E_{th}} \phi(E)\,dE, \tag{3−25}$$

$$\sigma_{act} = \int_0^{E_{th}} \frac{\sigma(E)\phi(E)\,dE}{\phi_{th}}. \tag{3−26}$$

(1) Average Activation Cross-Section for Thermal Neutrons

It is necessary to know the value of σ_{act} in order to obtain the total neutron flux ϕ_{th} from the activation reaction rate R_{th} for the thermal neutrons. The activation cross-section $\sigma(v_p)$ for $v_p = 2{,}200$ m/s can be obtained by introducing the Maxwell distribution correction of the neutron temperature T_n if the activation cross sections of the materials are fixed to the rule of $1/v$. However, in case the activation cross sections of some materials are not fixed to the rule of $1/v$, it is necessary to introduce the following correction by using the non−$1/v$ correction factor $g(T_n)$:

$$\sigma_{act} = g(T_n)\left(\frac{293.6\pi}{T_n}\right)^{\frac{1}{2}}\frac{\sigma(v_p)}{2}. \qquad (3\text{−}27)$$

For ^{197}Au, the non−1/v correction factor g (T_n) is presented as a function of T_n, as shown in Table 3−2 (Ref. 3).

Table 3−2 The value of non−1/v correction factor $g(T_n)$ by neutron temperature T_n for ^{198}Au

T_n [℃]	g (T_n)
20	1.0053
40	1.0064
60	1.0075
80	1.0086
100	1.0097

(2) Principle of Cadmium (Cd) Difference Method

The neutron spectrum is fixed in both the thermal region of the Maxwell distribution and the epi-thermal region of 1/E distribution, including the transient region. The boundary energy between the thermal and epi-thermal regions is known as the cut-off energy E_{et} of thermal energy, and it has a value of approximately 0.1 eV.

It is necessary to exclude the effect of epi-thermal neutrons to obtain only information about the thermal neutrons, since the activation reaction rate is inevitably affected not only by the thermal neutrons but also by epi-thermal neutrons when the activation foils are irradiated in the thermal reactor core. For this purpose, it is convenient to use the cadmium (Cd) difference method. The main feature of this method is to utilize the dependence on a specific energy of the absorption cross-section of Cd. It has been widely used in thermal reactor cores, and it is very convenient for this experiment.

The Cd has considerable absorption cross-section for low-energy neutrons with considerable resonance absorption around the energy of 0.18 eV, as shown in Fig. 3−4. Namely, it is necessary to pay attention to the fact that the peak value of the absorption cross-section corresponds to the cut-off energy $E_{et} \fallingdotseq 0.1$ eV of the thermal spectrum and that the absorption cross-section is very high in the energy region corresponding to the Maxwell distribution.

By using the above characteristics of Cd, the activation foil covered with the Cd covers can absorb all the neutrons with energy less than E_{Cd} (E_{Cd}:

effective Cd cut-off energy) and can avoid activation by neutrons with energy less than E_{Cd}. Namely, it is observed that such a foil between the Cd covers can only transmit the neutrons with energy greater than E_{Cd}; further, these neutrons can activate this foil.

The activation contributed by the neutrons with energies over the entire range occurs in the activation foil that is not covered with the Cd covers (bare foil); hence, the activation reaction rate contributed by the neutrons with energy greater than E_{Cd} can be obtained from the difference between the activation reaction rates obtained when using a bare foil and a foil sandwiched with the Cd covers. Moreover, the activation reaction rate contributed only by the thermal neutrons can be obtained by introducing the correction induced by the difference between E_{Cd} and E_{et} and the correction contributed by the thermal neutrons transmitted through the Cd covers.

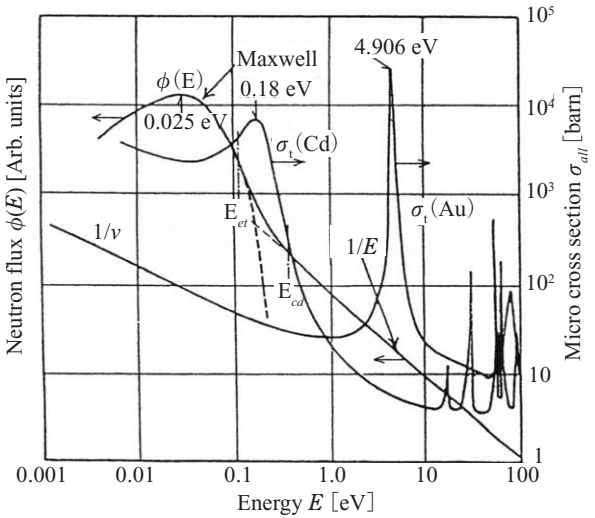

Fig. 3−4 Neutron spectrum in the thermal reactor and energy dependence of all the cross sections of Cd and Au

(3) Effective Cd Cut-off Energy

As mentioned in the previous section, the activation reaction rate of the thermal neutron flux can be obtained on the basis of the difference of the activation reaction rate of the boundary with the effective Cd cut-off energy E_{Cd}. This effective Cd cut-off energy E_{Cd} can be defined as follows:

For energy E, the absorption cross-section σ_a (E) of Cd is assumed to be

∞ when $E \leq E_{Cd}$, 0 when $E > E_{Cd}$, and step approximated when $E = E_{Cd}$. E_{Cd} is defined on the basis of the assumption that the activation reaction rate contributed by the neutron spectrum fixed to $1/E$-type distribution in $E_{Cd} < E < \infty$ is equal to that contributed by the neutron spectrum fixed to $1/E$-type distribution with the joining function, as shown in Eq. (3−22).

(4) Introduction of Cd Ratio

It can be considered that the activation reaction will occur mostly by the epi-thermal neutrons with energy $E > E_{Cd}$ when the activation foil sandwiched with the Cd covers is irradiated. The Cd ratio $(RR)_{Cd}$ of the reaction rate per unit mass is defined as follows:

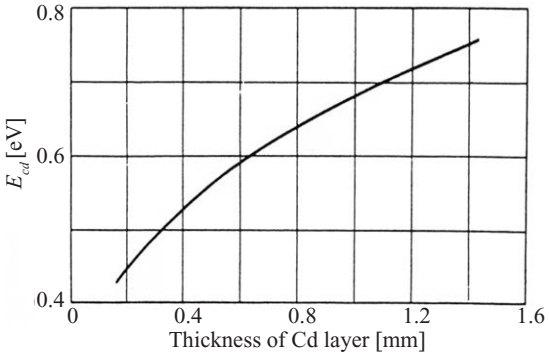

Fig. 3−5 Change in effective Cd cutoff energy E_{Cd} by change in thickness of Cd layer for $1/v$ absorption

$$Cd\ ratio = (RR)_{cd} = \frac{R_{bare} / M_{bare}}{R_{Cd} / M_{Cd}}, \tag{3−28}$$

where M_{bare} and M_{Cd} indicate the masses of the bare gold foil and the foil sandwiched with the Cd covers, respectively; and R_{bare} and R_{Cd} are the activation reaction rates with bare gold foil and the foil sandwiched with the Cd covers, respectively.

By using this Cd ratio $(RR)_{Cd}$, the activation reaction rate contributed by the epi-thermal neutrons in $E > E_{Cd}$ can be expressed as $R_{bare}/(RR)_{Cd}$. Further, R'_{th} by the neutrons in $E < E_{Cd}$ can be obtained by deducting $R_{bare}/(RR)_{Cd}$ from R_{bare} as follows:

$$R'_{th} = R_{bare}\left(1 - \frac{1}{(RR)_{Cd}}\right). \tag{3-29}$$

(5) Correction Factor F_{Cd} for Contribution of Thermal Neutrons

The R'_{th} shown in Eq. (3−29) indicates the activation reaction rate contributed by thermal neutrons with energy less than E_{cd}. Since $E_{Cd} > E_{et}$, it is necessary to correct R'_{th} for the contribution by the neutrons with energy $E_{et} < E < E_{Cd}$ in order to obtain the contribution by the neutrons with energy less than E_{et}.

For this purpose, it is desirable to introduce the correction factor F_{Cd}. In the foils, F_{Cd} is defined as the ratio of the activation reaction rate R_{epi} contributed by the epi-thermal neutrons ($E \geq E_{et}$) and $R_{Cd,epi}$ contributed by the neutrons with energy greater than the effective Cd cut-off energy E_{Cd}. The formula for F_{Cd} is given as follows:

$$F_{Cd} = \frac{R_{epi}}{R_{Cd,epi}} = \frac{\int_{E_{et}}^{\infty} \sigma_{act}(E)\,dE/E}{\int_{E_{Cd}}^{\infty} \sigma_{act}(E)\,dE/E} = 1 + \frac{\int_{E_{et}}^{E_{Cd}} \sigma_{act}(E)\,dE/E}{\int_{E_{Cd}}^{\infty} \sigma_{act}(E)\,dE/E}. \tag{3-30}$$

For the 1/v-type activation of a very thin foil, F_{cd} is expressed as follows:

$$F_{Cd} = \left(\frac{E_{Cd}}{E_{epi}}\right)^{\frac{1}{2}}. \tag{3-31}$$

For instance, a Cd cover of thickness 1 mm for $T_n = 293.6$ K has the value of $F_{Cd} \approx 2.75$. However, F_{Cd} has a low value depending on the thickness of both the bare gold foil and the foil covered with the Cd covers, as shown in Fig. 3−6, since the activation cross-section of Au has a large resonance peak at 4.906 eV, which is greater than E_{Cd}, as shown in Fig. 3−4.

(6) Correction Factor $(TR)_{Cd}$ for Thermal Neutron Permeation through the Cd layer

The Cd covers are utilized for avoiding the absorption of thermal neutrons by the gold foil. As shown in Fig. 3−7, the thickness of the Cd cover should be considered, since the thermal neutrons permeate through the Cd covers. For R_{bare} of the bare gold foil, the activation reaction rate R'''_{th} contributed by the thermal neutrons is given by using the permeation ratio $(TR)_{Cd}$ as follows:

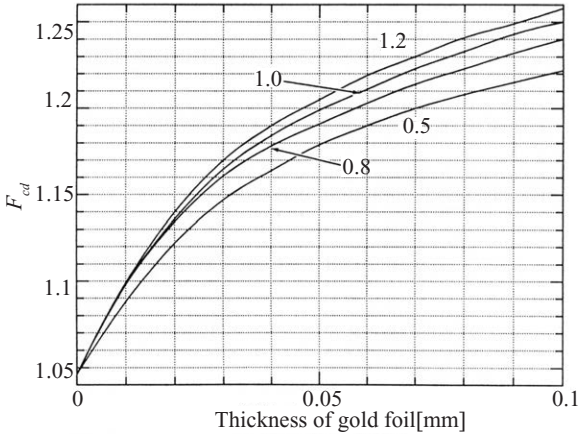

Fig. 3−6 Dependence of thickness of gold foil on F_{Cd} (numbers on the curves indicate thickness [mm] of Cd cover)

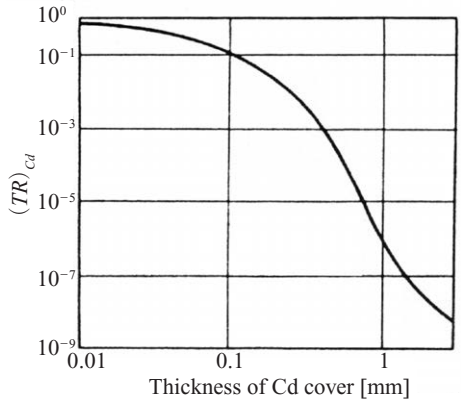

Fig. 3−7 Dependence of thickness of the Cd cover on the permeation ratio $(TR)_{Cd}$

$$R'''_{th} = \frac{R_{bare}\left(1 - \dfrac{F_{Cd}}{(RR)_{Cd}}\right)}{1 - F_{Cd}(TR)_{Cd}} . \tag{3−32}$$

(7) Perturbation by Thermal Neutrons

For determining the activation reaction rate R_{bare} of the bare gold foil, the activation reaction rate contributed by the thermal neutrons in the gold foil can be obtained by combining the Cd ratio $(RR)_{Cd}$, correction factor F_{Cd}, and

permeation rate $(TR)_{Cd}$. Thus, a relationship can be established between the activation reaction rate by the thermal neutrons and the thermal neutrons in the reactor core.

In general, the thermal neutron flux distribution is disturbed and is reduced inside and immediately around the foil, as shown in Fig. 3−8, when the activation foil is placed in the position of thermal neutron flux ϕ_{th}. This phenomenon is known as perturbation. This is due to a reduction in the thermal neutrons around the foil (depression) and also due to a reduction in the neutron flux on the surface of the foil (self-shielding).

The effect of perturbation can be expressed on the basis of the ratio of average thermal neutron flux $\overline{\phi_{th}}$ in the activation foil and thermal neutron flux ϕ_{th} before the reduction. This ratio is known as the perturbation factor f, and it can be expressed as follows:

$$f = \frac{\overline{\phi_{th}}}{\phi_{th}}. \tag{3−33}$$

The depression factor f_1 can be expressed as follows:

$$f_1 = \frac{\phi_s}{\phi_{th}}, \tag{3−34}$$

where ϕ_s indicates the thermal neutron flux in the surface of the foil.

The self-shielding factor f_2 can be expressed as follows:

$$f_2 = \frac{\overline{\phi_{th}}}{\phi_s}. \tag{3−35}$$

By using Eqs. (3−34) and (3−35), the perturbation factor f in Eq. (3−33) can be expressed as follows:

$$f = f_1 \cdot f_2. \tag{3−36}$$

The R'''_{th} in Eq. (3−32) is caused by the average thermal neutron flux $\overline{\phi_{th}}$ in the activation foil, and R_{th} in Eq. (3−24) is caused by the thermal neutron flux ϕ_{th} without the reduction. The relationship between R'''_{th} and R_{th} is expressed as follows:

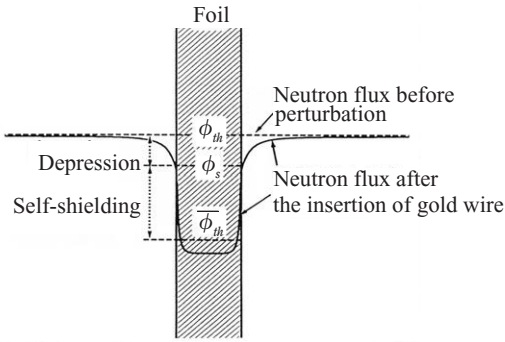

Fig. 3−8 Effect of perturbation in thermal neutron flux

$$R_{th} = R_{th}''' \left(\frac{\phi_{th}}{\overline{\phi}_{th}} \right) = \frac{Q_{th}'''}{f}. \tag{3−37}$$

From Eq. (3−37), the objective value of R_{th} can be obtained by the correction of measured R_{th}''' for the perturbation factor f.

Generally, the depression factor f_1 in the water-moderated and -reflected core (C-core) of KUCA can be considered as $f_1 \approx 1$ when the measurement of neutron flux distribution is conducted by using the gold activation method; otherwise, it can be considered to be $f \approx f_2$.

The self-shielding factor f_2 can be expressed as follows:

$$f \approx f_2 = \frac{1 - 2E_3(\Sigma_a t)}{2\Sigma_a t}, \tag{3−38}$$

where Σ_a [1/cm] indicates the macroscopic absorption cross-section of thermal neutrons in the activation foil, λ_a [cm] is the absorption average mean free path, and $\Sigma_a t$ ($= t/\lambda_a$) is the thickness. Moreover, E_3 indicates the third exponential function (Ref. 3). The results of f_2 are shown in Fig. 3−9. (Refer to Ref. 4 for detailed information regarding f_1 and f_2)

Substituting Eqs. (3−32) and (3−37) in Eq. (3−24), the thermal neutron flux can be obtained as follows:

$$\phi_{th} = \frac{R_{th}}{N\sigma_{act}} = \frac{R_{bare}\left(1 - \dfrac{F_{Cd}}{(RR)_{Cd}}\right)}{N\sigma_{act} f (1 - F_{Cd}(TR)_{Cd})}. \tag{3−39}$$

It is necessary to obtain the absolute value of R_{bare} for the thermal

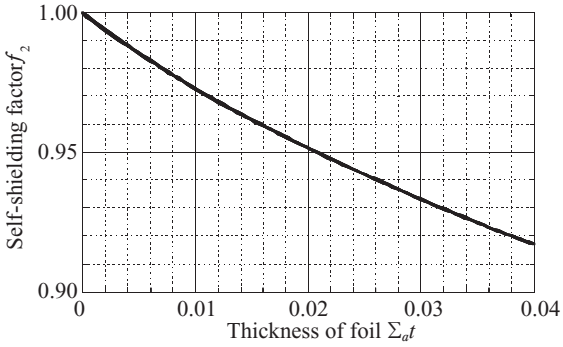

Fig. 3−9 Self-shielding factor f_2 for isotropic injection of thermal neutrons in an infinite plate foil

neutron flux by using Eq. (3−39). The absolute value of the disintegration rate of the activation foil should also be measured. In this experiment, the measurement is conducted by using the HPGe detector. Refer to Sec. 3−4 for detailed explanation of the measurement method.

3−4 Experiments

In this experiment, the bare and Cd-covered gold wires are irradiated to measure the relative spatial distribution of the activation reaction rate, and the foils installed at the core are irradiated to measure the absolute value of thermal neutron flux in the usual core location.

3−4−1 Core Configuration

The irradiated positions of gold wires and foils are described in the document entitled "Order of Core Configurations Change Program," and careful attention should be paid to the core configurations (flux and control rods) and the irradiated positions of gold wires and foils before conducting the experiments.

3−4−2 Equipment and Irradiation of Gold Wires and Foils

(1) Preparation of Gold Wires and Foils

Gold wires

Both the bare and Cd-covered gold wires are irradiated in the core for measuring the relative spatial distribution of the activation reaction rate. Before irradiation, the bare gold wire of diameter 0.5 mm and the gold wire inserted in the Cd tube (inner thickness: 0.05″ and outer thickness: 0.09″) of thickness 0.5 mm are equipped with aluminum (Al) plates. It is imperative

to ensure that water does not seep into the Cd tube during irradiation and that both ends of the Cd tube are sealed with a clamp.

Gold foils

Both the bare and Cd-covered gold foils are irradiated at the typical position of the core for measuring the absolute value of thermal neutrons. Before irradiation, a bare foil of diameter 10 mm and thickness 0.05 mm covered with Al foil and the gold foil sandwiched between the Cd covers of diameter 1.4 mm and thickness 0.8 mm are installed with the fuel. The Cd covers are composed of a cover and a plate. It is imperative to ensure that water does not seep into the Cd tube during irradiation and that the gap between the cover and plate is completely sealed with duct tape.

(2) Installation of Gold Wires and Foils with the Core

For measuring the spatial distribution of neutron flux in the axial direction of the core, the aluminum plates with the bare and Cd-covered gold wires are fixed by inserting them in the fuel frame from the upper core or in the gap between the fuel frames. For measuring the spatial distribution of neutron flux in the horizontal direction of the core, they are also inserted into the gap between the fuel frames.

The fuel plates with the bare and Cd-covered foils are installed in the usual core location.

(3) Neutron Irradiation of Gold Wires and Foils

Neutron irradiation is carried out for approximately 30 min while maintaining the indicator value of the linear power meter Lin-N (UIC#5) constant so that the dose rate of the γ-ray area monitor (γ AREA-C) is approximately 250 μSv/h. It is then necessary to record the start time of irradiation, end time of irradiation, indicator value of the linear power meter, dose rate of the γ-ray area monitor, positioning of the rods, core water level, and core temperature. It is better to confirm the positions of the detectors of the linear power meter and that of the γ-ray area monitor beforehand. The power of the C-core is set to the maximum value throughout these experiments.

In KUCA, the positions of detectors may be frequently changed according to the contents of the experiments; hence, the indicator value of the linear power meter does not always correspond to the absolute value of the reactor power. Therefore, the γ-ray area monitor that is fixed on a wall surface of the core is utilized for attaining the approximate value of the reactor power.

(4) Extraction of the Gold Wires and Foils

The bare and Cd-covered gold wires and foils irradiated in the core are pulled out when the radiation dose is decreased in the C-core. Subsequently, it is possible to enter the core (generally, the day after irradiation). Since the radiation dose rate is high at the upper region of the core, it is necessary to conduct this procedure quickly and to carefully monitor the radiation dose in collaboration with professors. The exposure dose should be carefully monitored while moving the wires and foils to the radiation measurement room.

3−4−3 Measurement of Radiation of Gold Wires and Foils

(1) Measurement of Radiation of Gold Wires

(1−1) Cutting the Gold Wires

The irradiated bare and Cd-covered gold wires should be cut into pins of length 10 mm. Each pin is inserted into a capsule and numbered according to its position along the wire in order to eliminate any error in the number of capsules and positions. The bare and Cd-covered wires should be carefully distinguished. Further, the wires and capsules should be handled with care so that the wires adhere to the bottom of the capsule and not become a mass of gold wire when the gold wire is inserted into the capsule.

(1−2) Measurement of Radiation

The γ-ray (411.8 keV) count can be measured using a γ-ray detection system based on the ^{198}Au in the capsule when the capsules are inserted into a polyethylene capsule, which is then inserted into a well-type NaI (Tl) scintillation counter, as shown in Fig. 3−10.

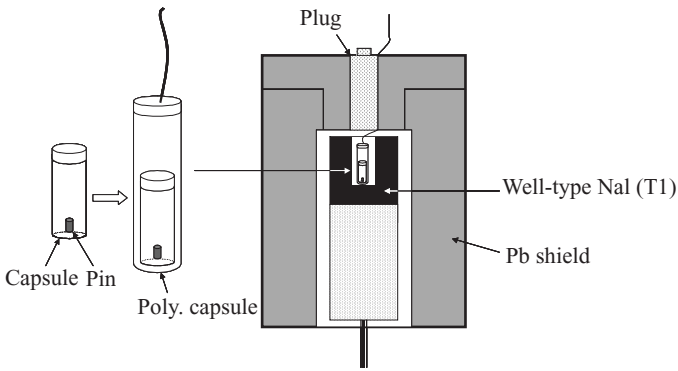

Fig. 3−10 Measurement of activation of sample by a well-type NaI (Tl) scintillation counter

The γ-ray spectrum can be analyzed with a multi-channel analyzer (MCA). The γ-ray peak area value can be obtained by setting the count of the γ-ray peak area corresponding to 411.8 keV as the "ROI" (region of interest) of MCA. The setting of ROI is shown in Fig. 3−11.

The measurement start time, measurement duration, and counting rate of each material in the capsule should be recorded. Further, the counting rate C_{BG} of the background should be also recorded after the measurement.

From these values, the average counting rate $C'_{av,j}$ and the net counting rate $C_{av,j}$ ($= C'_{av,j} - C_{BG}$) of each material j of gold wires can be obtained.

(1−3) Measurement of Mass

The mass M_j of each material should be measured by using a balance.

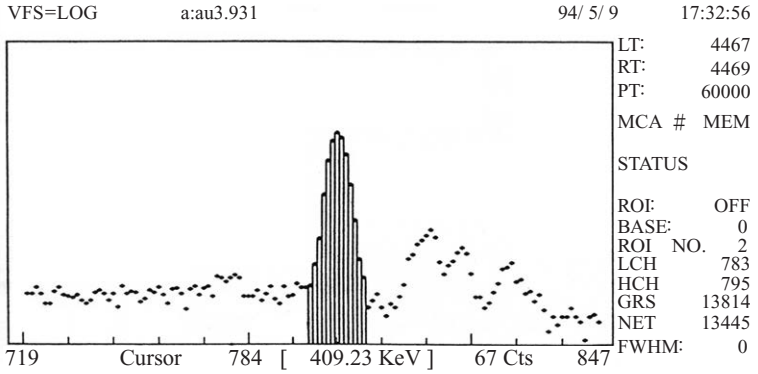

Fig. 3−11 Setting of "ROI" (region of interest) and counting the peak of γ-ray by using the multi-channel analyzer

(1−4) Calculation of Relative Saturation Activity

The value of relative saturation activity $\widetilde{D}_{\infty,j}$ can be obtained by substituting the net counting rate $C_{av,j}$ for C_{av} in the right-hand-side term of Eq. (3−15). The irradiation time T_i can be also obtained from the difference between the start time and the end time of irradiation, and $T_{w,j}$ can be obtained from the difference between the end time of irradiation and the start time of measurement. Note that by carrying out this relative measurement, the requirement of determining the detection efficiency ε is eliminated.

(1−5) Relative Spatial Distribution of Neutron Flux

The relative spatial distribution of the activation reaction rate can be obtained on the basis of the total neutron flux and thermal rate from $(\widetilde{D}_{\infty,j} / M_j)_{bare}$ and $(\widetilde{D}_{\infty,j} / M_j)_{Cd}$, which indicate the relative saturation activity per

unit mass for the position of materials with bare and Cd-covered gold wires, respectively. The spatial distribution of the activation reaction rate contributed by the thermal neutron flux can be approximately obtained from $(\widetilde{D}_{\infty j}/M_j)_{bare} - (\widetilde{D}_{\infty j}/M_j)_{Cd}$, which indicates the difference between the saturation activities per unit mass of bare and Cd-covered gold wires, respectively, by considering its correspondence to the irradiation positions of bare and Cd-covered gold wires.

(2) Measurement of Radiation of Gold Foil and Determination of Thermal Neutron Flux

It is necessary to obtain the absolute value of thermal neutron flux for measuring the radiation of the gold foil and determining thermal neutron flux. The procedure of measurement by using the HPGe detector is presented in the following section. The necessity of determining the detection efficiency for the absolute value of radiation should be considered.

(2−1) Determining the Detection Efficiency for γ-ray of Energy 411.8 keV

(i) Familiarize thoroughly with the instructions for setting and operating the measurement system.

(ii) Control the main amplifier gain by using a set-normalized source when confirming the γ-ray spectrum in order to measure the required energy range. It is better to confirm the relationship between the central peak channel and γ-ray energy to decrease the possibility of any mistake in reading the peak value.

(iii) Obtain the count of all the energy absorption peaks (peak area) for all the set γ-ray. Set the "ROI" in the peak area by confirming the γ-ray spectrum of MCA by moving the cursor near an objective peak and expanding the γ-ray spectrum.

(iv) Determine the detection efficiency ε for the γ-ray at 411.8 keV by calculating the detection efficiency ε_i for each energy level, as shown in Eqs. (3−18) and (3−19), plotting the relationship between the energy and the total energy absorption detection efficiency on a logarithmic graph paper, and by fitting the linear function.

(2−2) Measurement of Activation of Gold Foil

The count rate C_p at all the energy absorption peaks can be obtained by measuring the detection efficiency of γ-ray at 411.8 keV at the position of irradiated foil the same as with the standard source, as is the case with the NaI (Tl) scintillator. Subsequently, the start time and the net time of

measurement should be recorded. Finally, the disintegration rate D can be obtained by using Eq. (3−17) for the counting rate C_p of all the energy absorption peaks.

(2−3) Measuring the Mass of Gold Foil

The mass M of the gold foil should be measured by using a balance and the number N of atoms of Au in the gold foil should be determined.

(2−4) Determination of Thermal Neutron Flux

The absolute value of the activation reaction rate (saturation activity) can be obtained by substituting $C_{av}(C_{av} = D \cdot \varepsilon)$ in Eq. (3−15) in order to correct the time delay for the disintegration rate D. Further, the measurement position of the thermal neutron flux ϕ_{th} can be determined by using Eq. (3−17).

The Cd ratio $(RR)_{Cd}$ shown in Eq. (3−17), correction factor F_{Cd}, permeation ratio $(TR)_{Cd}$, average activation cross-section σ_{act}, and perturbation factor f can be determined as follows:

(a) Cd ratio $(RR)_{Cd}$

The Cd ratio $(RR)_{Cd}$, which can be obtained from Eq. (3−28), can be also determined as the ratio of saturation activity per unit mass as follows:

$$(RR)_{Cd} = \frac{C_{av,bare} / M_{bare}}{C_{av,Cd} / M_{Cd}} . \tag{3−40}$$

(b) Correction factor F_{Cd}

The correction factor F_{Cd} can be determined from the thickness of the gold foil and that of the Cd covers by referring to Fig. 3−6.

(c) Permeation ratio $(TR)_{Cd}$

The permeation ratio $(TR)_{Cd}$ can be determined from the thickness of the Cd cover by referring to Fig. 3−7.

(d) Average activation cross-section σ_{act}

Since σ_{act} is considered to be a function of T_n, as shown in Eq. (3−27), the neutron temperature T_n can be obtained by using Eq. (3−23). Subsequently, the media temperature T_m, absorption cross-section $\Sigma_a(T_n)$, and slowing-down power $\xi\Sigma_s$ can be obtained as follows:

・Media temperature T_m

The media temperature T_m is equal to the temperature of the reactor core.

・Absorption cross-section $\Sigma_a(T_n)$

The absorption cross-section $\Sigma_a(T_n)$ is approximately equal to the Σ_a utilized in the two-energy-group diffusion calculation in Chapter 1 (Approach to Criticality); that is, $\Sigma_a(T_n) \simeq \Sigma_{2a}$, which is shown in Table 1−3 in Chapter 1. It should be carefully noted that the value of Σ_{2a} is different for each fuel composition.

・Average slowing-down power $\xi\Sigma_s$

The slowing-down power $\xi\Sigma_s$ is considered to be homogenous in the core cell and as the average slowing-down power in the whole core. It can be also obtained from both the volume ratio and slowing-down power of certain composition materials (U, H_2O, and Al). Their volume ratios are shown in Figs. 4 and 5 of the "General Description of the KUCA Facility" in this textbook, and the slowing-down power is shown in Table 3−3.

For determining the volume ratio, the horizontal section of the fuel unit cell of length 142 mm and width 71 mm is assumed in the fuel frame containing the fuel meat region. The volume ratio of this section is approximately equal to the area ratio of certain materials.

For determining the volume ratio of U and Al in the fuel meat, the volume of U, which is composed of U-Al metal, can be obtained by using the values of 9.55 g and 18.7 g/cm^3 as the mass and density of U in the fuel plate, respectively, and assuming a value for the volume of Al.

The size of the fuel assembly and the number of fuel plates loaded in the unit fuel assembly (maximum number of fuel plates) should be considered in detail.

Table 3−3 Slowing-down power $\xi\Sigma s$ of certain composition materials (U, H_2O, and Al)

Material	Slowing-down power $\xi\Sigma_s$
U	0.003
H_2O	1.35
Al	0.0061

The average activation cross-section σ_{act} for thermal neutrons in the gold foil can be obtained on the basis of the neutron temperature T_n using Eq. (3−27). The non−1/v correction factor g (T_n) can be obtained by interpolation, and the activation cross-section σ (v_p) of the gold foil for v_p = 2,200 m/s can be obtained by using the value shown in Table 3−1.

(e) Perturbation factor f

The perturbation factor f can be obtained by using the macroscopic cross-section Σ_a through the average activation cross-section σ_{act} for thermal neutrons in the gold foil of thickness t, as shown in Fig. 3−9 or Eq. (3−38), when f is assumed to be equal to f_2.

3−5 Discussion

As a general rule, the experimental report of each member should be prepared as mentioned herein. However, the method, results of the experiments, and the common terms in each group can be shared and copied (terms (1) through (4) as follows):

(1) Purpose

(2) Experimental conditions

1) Core name, core configuration, irradiation positions of the gold foils (this can be substituted for the documents on "order" and distribution).
2) "Run No." of irradiation, positions of control and safety rods, water level, core temperature, indicator value of linear power and γ-ray area monitor, start and end times of irradiation of the gold foils.
3) Type of γ-ray detectors utilized for measuring activation and block diagram of the measurement circuit.

(3) Measurement data from the activation in the gold wire

The results of the measurements of the activation in the bare and Cd-covered gold wires should be arranged by creating a table comprising the following criteria:

- Material number of gold wires
- Positions of gold wires in the core
- Start time of the irradiation
- Irradiation time
- Waiting time
- Measuring time
- Count and counting rate of γ-ray at 411.8 keV
- Count and counting rate of the background
- Net count rate of γ-ray at 411.8 keV
  (the difference in the counting rates between the γ-ray and background)
- Relative saturation activity

- Mass of the gold wires
- Relative saturation activity per unit mass (specific saturation activity)

(4) Measurement data of the activation in the gold foils

The results of the measurements of the activation in the bare and Cd-covered gold foils should be arranged by making a table with the following criteria. It is also better to arrange the results of the measurement of activation in the standard source for the determination of detection efficiency of γ-ray at 411.8 keV:

- Positions of gold foils in the core
- Start time of the irradiation
- Irradiation time
- Waiting time
- Measuring time
- Count and counting rate of γ-ray at 411.8 keV
- Count and counting rate of background
- Net counting rate of γ-ray at 411.8 keV (the difference in the counting rates between γ-ray and the background)
- Relative saturation activity
- Mass of the gold foils
- Relative saturation activity per unit mass (specific saturation activity)

(5) Relative spatial distribution of the activation reaction rate obtained by the gold wires

The relative spatial distribution of the activation reaction rate contributed by the entire neuron flux as well as the epi-thermal neutron flux should be obtained by plotting the position in the core of the bare and Cd-covered gold wire sample j on the horizontal axis and the relative value of saturation activity (specific saturation activity) on the vertical axis. The relative spatial distribution should also be obtained by using the approximate value of the activation reaction rate contributed by the thermal neutron flux on the basis of the difference in the activation reaction rates between the entire neutron flux and the thermal neutron flux.

Subsequently, the spatial distribution should be obtained by calculating the ratio of specific saturation activity shown in Eq. (3−40) as the Cd ratio of the gold wires.

(6) Absolute value of the thermal neutron flux obtained by the gold foil and reactor power

The absolute value of the thermal neutron flux in the irradiation position of gold foil and the reactor power according to the procedures of Question [b] of "Sec. 3−6" should be obtained on the basis of the results of the activation measurement. The Cd ratio of gold foils and some correction factors should be arranged.

(7) Comparison with the results of two-energy-group calculations

Three kinds of relative spatial distributions of activation reaction rates obtained by the experiments should be compared. The result of the Cd ratio of the gold foil should also be examined as follows:

1) Examine which group is closest to the neutron flux distribution in the fast or thermal group, by comparing with three kinds of relative spatial distributions of activation reaction rates obtained by the experiments, respectively, and that of the Cd ratio of gold wires. Theoretically explain the above examination and be careful of the facts such as (Experiment = Reaction rate) and (Calculation = Neutron flux).
2) Explain the physical configuration and spatial distribution of the Cd ratio in the gold wires and their relation with the results of the two-energy-group calculations.
3) Explain the physical configuration and spatial distribution of the Cd ratio in the gold foils and their relation with the results of the two-energy-group calculations.
4) Examine the differences in the configuration of the activation reaction rate of the gold wires by the loading method (x, y, and z axes) of the gold wires and determine what causes the differences and the effects of reactor composition. (Composition of fuel frame, control and safety rods, and so on).
5) Examine the reason underlying the difference between the experimental and calculated results.

3−6 Preparatory Report

Note that in order to prepare this preparatory report, the preparatory report in Chapter 1 should be referred to.

The neutron flux with fast and thermal groups could be expressed in the core and reflector regions as follows:

$$\phi_{1c}(x) = A\cos(\mu x) + C\cosh(\lambda x), \tag{3−41}$$

$$\phi_{2c}(x) = S_1 A\cos(\mu x) + S_2 C\cosh(\lambda x), \tag{3−42}$$

$$\phi_{1r}(x) = Fe^{-\kappa_{1r}|x|}, \tag{3−43}$$

$$\phi_{2r}(x) = S_3 Fe^{-\kappa_{1r}|x|} + Ge^{-\kappa_{2r}|x|}. \tag{3−44}$$

The continuity of neutron flux and neutron current $J = Dd\phi/dx$ at the core-reflector boundary ($x = a$) is utilized as the boundary condition. Substituting the boundary condition in Eqs. (3−41) through (3−44), the following equations can be obtained when the critical x-direction length is set to $2a$:

$$\phi_{1c}(a) = \phi_{1r}(a), \tag{3−45}$$

$$D_{1c}\frac{d}{dx}\phi_{1c}(a) = D_{1r}\frac{d}{dx}\phi_{1r}(a), \tag{3−46}$$

$$\phi_{2c}(a) = \phi_{2r}(a), \tag{3−47}$$

$$D_{2c}\frac{d}{dx}\phi_{2c}(a) = D_{2r}\frac{d}{dx}\phi_{2r}(a). \tag{3−48}$$

The following equations for determining the unknown constants A, C, F, and G can be obtained:

$$A\cos(\mu a) + C\cosh(\lambda a) = Fe^{-\kappa_{1r}a}, \tag{3−49}$$

$$-A D_{1c}\mu\sin(\mu a) + C D_{1c}\lambda\sinh(\lambda a) = -F D_{1r}\kappa_{1r}e^{-\kappa_{1r}a}, \tag{3−50}$$

$$S_1 A\cos(\mu a) + S_2 C\cosh(\lambda a) = S_3 Fe^{-\kappa_{1r}a} + Ge^{-\kappa_{2r}a}, \tag{3−51}$$

$$-S_1 A D_{2c}\mu\sin(\mu a) + S_2 C D_{2c}\lambda\sinh(\lambda a) = -S_3 F D_{2r}\kappa_{1r}e^{-\kappa_{1r}a} - G D_{2r}\kappa_{2r}e^{-\kappa_{2r}a}. \tag{3−52}$$

Note that, among the unknown constants A, C, F, and G, only three constants are independent. Therefore, A is set to one.

[a] For setting A = 1,

(1) Determine the unknown constants C, F, and G by using Eqs. (3−49) through (3−52).
(2) Plot the fast and thermal neutron flux distributions by using Eqs. (3−41)

through (3−44).
(3) Examine the relative neutron flux distributions in the fast and thermal groups.
(4) Observe the large differences between the fast and thermal neutron flux distributions in the reflector region.

[b] Activation reaction rate of gold wire can be obtained by using Eq. (3−3) as follows:

$$R_{act} = \int_0^{E_{\max}} N\sigma_{act,Au}(E)\,\phi(E)\,dE, \tag{3−53}$$

where $\sigma_{act,Au}(E)$ indicates the activation cross-section of Au.

Separate the R_{act} into fast and thermal components as follows:

$$R_{act} = R_1 + R_2, \tag{3−54}$$

and assume the following equations:

$$R_1 = \overline{\sigma}_{act,Au,1}\,\overline{\phi}_1, \tag{3−55}$$

$$R_2 = \overline{\sigma}_{act,Au,2}\,\overline{\phi}_2, \tag{3−56}$$

where $\overline{\sigma}_{act,Au}$ indicates the average activation cross-section of Au and $\overline{\phi}$ is the average neutron flux. For setting $(\overline{\sigma}_{act,Au,2} / \overline{\sigma}_{act,Au,1}) = 7$,

(1) Calculate R_1 and R_2 by using the neutron flux distributions with fast and thermal groups.
(2) Plot $R_{act} = R_1 + R_2$ with x (R_{act} may be normalized to unity at core center).
(3) Observe how the overall configuration of R_{act} looks like.

[c] In the experiment, the Cd covers are utilized for eliminating the activation thermal neutrons. This means that the calculated R_1 corresponds to the Cd-covered gold wire and $R_1 + R_2$ to the bare gold wire.

(1) Explain why the Cd could be utilized for eliminating the thermal neutrons.
(2) Calculate the Cd ratio $(R_1 + R_2)/R_1$ and plot it with x.
(3) Examine why it shows very small variation within the core on the basis of the overall configuration of Cd ratio.

[d] Relationship between thermal neutron flux and reactor power

A critical assembly comprises a rectangular parallelepiped core with three sides equal to a, b, and c [cm] in x, y, and z directions, respectively. It can be expressed as the extrapolation lengths $a^* = a + 2\delta_x$, $b^* = b + 2\delta_y$, and $c^* = c + 2\delta_z$ on the basis of the assumption that the reflector savings δ_x, δ_y, and δ_z [cm] become in x, y, and z directions, respectively.

(1) Derive the following equation, on the basis of the assumption that the thermal neutron flux distribution can be expressed as cosine functions in x, y, and z directions, and that an average thermal neutron flux ϕ_{av} [1/cm^2/s] can be regarded as the thermal neutron flux ϕ_0 [1/cm^2/s] at the center of the core:

$$\phi_{av} = \phi_0 \frac{8a^*b^*c^*}{\pi^3 abc} \sin\left(\frac{\pi a}{2a^*}\right) \sin\left(\frac{\pi b}{2b^*}\right) \sin\left(\frac{\pi c}{2c^*}\right). \tag{3−57}$$

(2) Derive the following equation, namely reactor power P [W], on the basis of the assumption that a single fission reaction would occur in unit time, for macro fission cross-section Σ_f and emission energy γ:

$$P = \gamma \Sigma_f abc \phi_{av}. \tag{3−58}$$

[e] Measurement of thermal neutron flux and determination of reactor power by activation foil method of Au foil

It was assumed that Au wires and foils were irradiated in the center of KUCA C-core (C45G0(5) core) and the γ-ray of energy 411.8 keV emitted from ^{198}Au was measured by the HPGe detector after the radiation dose was fully decreased. The Au foil is of diameter 9.5 mm and thickness 0.05 mm, the Cd cover is of thickness 0.8 mm, and the detection efficiency of the HPGe detector is 28.9% for γ-ray of 411.8 keV.

The experimental data are as follows;

- Data of Au foil irradiation
  1) Start time of irradiation: 16:30
  2) Stop time of irradiation: 17:00
  3) Temperature of the core: 23.5 ℃
  4) Indicator value of the linear power meter: 50 W
- Measurement results of irradiated Au foil

Table 3−4 Measurement results of irradiated Au foil

Sample No.	Start time of Measurement	Measurement time [s]	Count
BG (Background)		300	316
1 (Bare)	11:30	60	31521
2 (Cd cover)	11:40	180	28846
1 (Bare)	13:30	60	30909
2 (Cd cover)	13:40	180	28215
BG (Background)		300	321

(1) Obtain the absolute value of saturation activity of both bare Au foil and Cd-covered Au foil.
(2) Obtain the value of Cd ratio $(RR)_{Cd}$
(3) Obtain the value of F_{Cd}
(4) Obtain the value of $(TR)_{Cd}$
(5) Obtain the value of T_n
(6) Obtain the absolute value of average activation cross-section σ_{act}
(7) Obtain the value of perturbation factor f
(8) Obtain the absolute value of thermal neutron flux ϕ_{th} in the center of the core
(9) Obtain the value of reactor power P [W] by using Question [d]

In this case, three sides equal to a, b, and c [cm] in x, y, and z directions are 28.5, 35.5, and 57.0 cm, respectively. Any of the reflector savings δ_x, δ_y, and δ_z [cm] in x, y and z directions, respectively, corresponds to δ of C45 core shown in Table 1−2. The macro fission cross-section Σ_f corresponds to the value obtained by dividing $\nu\Sigma_{2f}$ of C45 core with $\nu = 2.44$ shown in Table 3−1. The emission energy is 3.2×10^{-11} J/fission/s.

References

1. K. H. Beckurts and K. Wirtz, *Neutron Physics*, Springer-Verlag, (1964).
2. D. Jakeman, *Physics of Nuclear Reactor*, Charles E. Tuttle Co., Inc., (1966).
3. J. R. Lamarsh, *Introduction to Nuclear Reactor Theory*, Addison-Wesley Pub. Co., (1966).
4. F. H. Helm, *Nucl. Sci. Eng.*, **16**, 235 (1963).

Appendix 3

3A. Activation Reaction Rate by 4$\pi\beta$–γ Coincidence Method

3A−1 Principle of 4$\pi\beta$–γ Coincidence Method

The absolute value of D_∞ can be obtained by determining the absolute value of the disintegration rate D of ^{198}Au generated in gold foil by observing the coincidence phenomena of the emittance of β- and γ-ray and by measuring the reaction rates C_β, C_γ, and $C_{\beta,\gamma}$ of β-ray, γ-ray, and their coincidence, respectively. In the 4$\pi\beta$–γ coincidence method, the 4π gas flow counter is often utilized as the detector of β-ray and the NaI (Tl) scintillation counter is utilized for detecting γ-ray.

The reaction rates C_β, C_γ, and $C_{\beta,\gamma}$ can be expressed by using the detection efficiencies ε_β and ε_γ for gold foil sources of these detectors as follows:

$$C_\beta = D\varepsilon_\beta\left\{1+\frac{(1-\varepsilon_\beta)\,\alpha\varepsilon_c}{\varepsilon_\beta(1+\alpha)}\right\}, \tag{3A−1}$$

$$C_\gamma = \frac{D\varepsilon_\gamma}{1+\alpha}, \tag{3A−2}$$

$$C_{\beta,\gamma} = \frac{D\varepsilon_\beta\varepsilon_\gamma}{1+\alpha}. \tag{3A−3}$$

From these equations, the disintegration rate D can be expressed as follows:

$$D = \frac{C_\beta\, C_\gamma}{C_{\beta,\gamma}\left\{1+\dfrac{(1-\varepsilon_\beta)\,\alpha\varepsilon_c}{\varepsilon_\beta(1+\alpha)}\right\}}, \tag{3A−4}$$

where the internal conversion coefficient α is 0.041 for γ-ray of energy 411.8 keV.

ε_β is given by the measurement values of C_γ and $C_{\beta,\gamma}$ as follows:

$$\varepsilon_\beta = \frac{C_\gamma}{C_{\beta,\gamma}}, \tag{3A−5}$$

and ε_c indicates the detection efficiency of the 4π counter for inversion electrons obtained by the γ-ray emittance of 411.8 keV. It is determined mainly on the basis of the thickness of gold foil, as shown in Table 3A−1.

Table 3A−1 Detection efficiency of 4π counter for inversion electrons obtained by γ-ray emittance at 411.8 keV

Thickness of gold foil [mg/cm^2]	ε_c
6	0.975
31	0.880
49	0.820
110	0.610

Eq. (3A−4) is simplified by the disintegration system of ^{198}Au, as shown in Fig. 3−1, and the specific activation is assumed to be a constant; ε_β and ε_γ are also assumed to be constant regardless of the position of the gold foil. For the latter condition, the gold foil is preferable, since a thick gold foil reduces the activation. However, a statistically high degree of precision can be maintained by using the 4π counter with maximum geometric efficiency for the β-ray detector and a large size NaI (Tl) scintillator for the γ-ray detector by keeping a check on the value of neutron flux density and the mass of the gold foil.

The following corrections for C_β, C_γ, and $C_{\beta,\gamma}$ should be introduced in order to obtain the absolute value of the disintegration rate, as shown in Eq. (3A−4):

a) Correction of the background for C_β, C_γ, and $C_{\beta,\gamma}$
b) Correction for resolving time, especially for C_β
c) Correction of the random coincidence for $C_{\beta,\gamma}$

When the resolution time of coincidence circuit is 2τ, the random coincidence C_{ch} can be expressed as follows:

$$C_{ch} = 2\tau C_\beta C_\gamma, \tag{3A−6}$$

where it is desirable for C_{ch} to be less than 10% of $C_{\beta,\gamma}$. Therefore, the following equations are preferable:

$$2\tau\varepsilon_\beta\,\varepsilon_\gamma\,D^2 \le 0.1\varepsilon_\beta\,\varepsilon_\gamma\,D, \tag{3A−7}$$

$$D < 0.1 \times \left(\frac{1}{2\tau}\right). \tag{3A−8}$$

For example, it is preferable for the value of D to be less than $0.1 \times \{1/(2$

$\times 10^{-6})\} = 5 \times 10^4$ Bq (= 1.35 μCi).

3A−2 Absolute Measurement by 4$\pi\beta$−γ Coincidence Method

The absolute value of the activation of ^{198}Au in the irradiated bare and Cd-covered gold foil can be obtained by the 4$\pi\beta$−γ coincidence method. The counting rates of the β, γ, and $\beta\gamma$ coincidences can be obtained in the respective gold foils. The equipment for the 4$\pi\beta$−γ coincidence detector is shown in Fig. 3A−1.

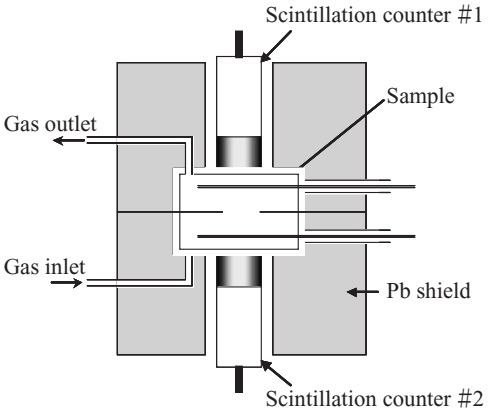

Fig. 3A−1 4$\pi\beta$−γ coincidence detector

The β-ray detector is a horn 4π counter and comprises a source support membrane in the central position holding conductivity with deposition. It also includes gas-flow-type proportional counters at the top and bottom and a counter gas (PR gas) flows through the counter.

The γ-ray detector is arranged by placing the β-ray detector between the two NaI (Tl) scintillation counters that are located at the top and bottom of the detector. The outputs of the β- and γ-ray detectors are directed to the coincidence circuit through a pre-amplifier, main-amplifier, and a single-channel wave-height analyzer. C_β, C_γ, and $C_{\beta,\gamma}$ can then be obtained.

The resolution time τ of the β-ray detector is less than 5 μs and that of the γ-ray is less than 0.5 μs.

Careful attention should be paid when handling the β-ray detector:

a) Be careful while inserting and retracting the sample, and while handling the source support membrane
b) Confirm the impressed voltage of zero of the detector in case of a sample change

c) Be careful while handling the platinum electrode below the source support membrane

The counting rates of the background $(C_\beta)_{BG}$, $(C_\gamma)_{BG}$, and $(C_{\beta,\gamma})_{BG}$ in C_β, C_γ, and $C_{\beta,\gamma}$, respectively, should be obtained before and after the start of measurements. Successively measure the number of bare and Cd-covered gold foils. When the total counting rates $C_{\beta total}$, $C_{\gamma total}$, and $C_{\beta,\gamma total}$ are within time T_c after the waiting time T_w, the average counting rates $C_{av\beta}$, $C_{av\gamma}$, and $C_{av\beta,\gamma}$ are given as follows:

$$C_{av\beta} = \frac{\left(\frac{C_{\beta total}}{T_c}\right)}{1 - \left(\frac{C_{\beta total}\,\tau_\beta}{T_c}\right)} - (C_\beta)_{BG}, \tag{3A−9}$$

$$C_{av\gamma} = \left(\frac{C_{\gamma total}}{T_c}\right) - (C_\gamma)_{BG}, \tag{3A−10}$$

$$C_{av\beta,\gamma} = \left(\frac{C_{\beta,\gamma total}}{T_c}\right) - 2\tau\left(\frac{C_{\beta total}}{T_c}\right)\left(\frac{C_{\gamma total}}{T_c}\right), \tag{3A−11}$$

where the counting loss in the measurement systems of β and $\beta\gamma$ may be ignored. Further, 2τ indicates the resolution time of the coincidence circuit.

The average disintegration rate D can be obtained by substituting Eqs. (3A−9) through (3A−11) in Eq. (3A−4) and considering C_{av} as $D = C_{av}/\varepsilon$. Moreover, the saturation activity D_∞ can be obtained by substituting C_{av} in Eq. (3−15); finally, the saturation activities $(D_\infty)_{bare}$ and $(D_\infty)_{Cd}$ of the bare and Cd-covered gold foils, respectively, can be obtained.

3B. Outline of the HPGe Detector

The HPGe detector comprises a single crystal germanium (Ge) of high purity, gold finger, clinostat, pre-amplifier, and a dewar of liquid nitrogen, as shown in Fig. 3B−1.

(1) Coolant of detector

The detecting element of the HPGe detector should be completely cool when in use, although this detector can be stored at ambient temperature. This is because the Ge crystal and the FET of the pre-amplifier can break easily when the bias voltage is applied to the detector without sufficient coolant or at ambient temperature. The coolant time of an I-type (inverse L-type) detector is approximately 6 to 8 h. It is preferable to cool within 12

h for carrying out a stable measurement.

(2) Supplement of liquid nitrogen

Liquid nitrogen should be carefully handled so that the temperature of the crystal does not inadvertently rise when the amount of liquid nitrogen is decreased during the measurement. Especially, it is important to supply the liquid nitrogen in a small dewar during the measurement. It is then necessary to decrease the bias voltage once and continue to supply it again in order to avoid a short circuit due to condensation. After the supplement, it is important to apply the bias voltage to the detector after a delay of approximately 30 min to 1 h.

(3) Re-cooling the detector

When the amount of liquid nitrogen decreases and the temperature of the

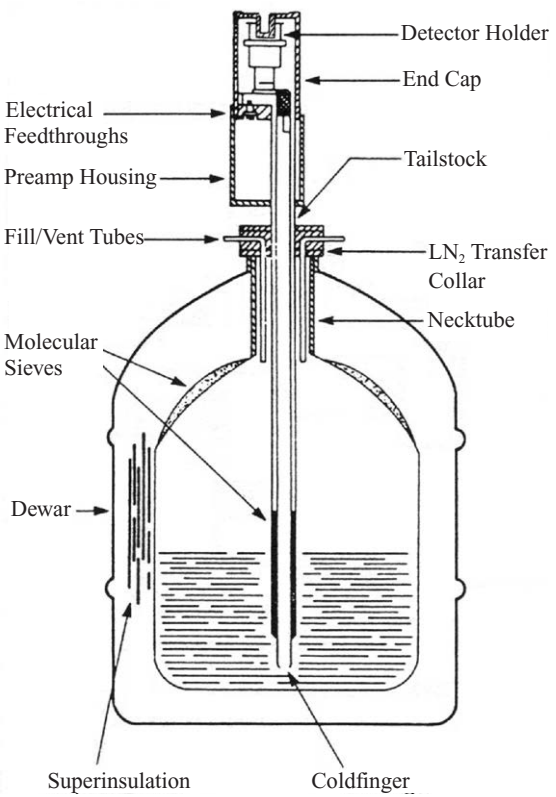

Fig. 3B−1 HPGe detector

clinostat is higher than that of liquid nitrogen, it is necessary to re-cool the detector by completely removing the liquid nitrogen in the dewar, warming the clinostat to ambient temperature, and letting them sit for a few hours.

(4) Application of detector bias voltage

The bias voltage to the HPGe detector should be supplied gradually by applying a voltage less than the booster rate of 100 V/s. A rapid change in the bias voltage of the HPGe detector can cause the Ge crystal and the pre-amplifier to break, regardless of the change in the booster. This slow booster is common to the pre-amplifier.

Chapter 4 Feynman-α Method

4−1 Purpose

The purpose of the reactor (zero power reactor) noise experiment is to measure the fluctuation in the average value of neutron density and to determine certain parameters of the reactor. The reactor noise can be analyzed either in the time region or in the frequency region. For discussion in the context of the time region, the Feynman-α experiment is to be conducted for estimating the variance-to-mean ratio of the counting rate by using a neutron detector. The reactor noise experiment for the time region is known as the neutron correlation experiment.

The fluctuation of the counting rate can be determined by measuring the neutron flux for the time when the automatic control system on the reactor core is either in the critical state or the subcritical state. The index of this fluctuation is the variance. When the neutrons are generated randomly and uniformly in the neutron source, such as an Am-Be neutron source or cosmic rays, it is well known that the count of neutrons per unit time obeys the Poisson distribution law. The mean of a Poisson distribution is equal to its variance, and hence, the ratio of the variance to mean is one.

Some of the neutrons generated in the neutron source die, and the others are born by the fission reactions. These progeny neutrons are generated by a long chain reaction, considering the presence of a chain reaction reactor between this uniform and random neutron source and the neutron counter. This chain reaction family increases the variation of the counting rate to a value higher than that of the abovementioned Poisson distribution. Moreover, the neutrons per unit of fission reaction are statistical, and hence, would affect the variation of variance of the counting rates.

In this experiment, this variance is measured as the ratio of variance to the mean, and this variance is compared with the theoretically obtained values. It is also possible to determine what parameters of the reactor core can be determined by using this methodology.

4−2 Variance-to-Mean Ratio in Multiplication System

M refers to the count per measurement time t (gate width), and the "variance-to-mean" of M can be expressed as follows:

$$\frac{\sigma_M^2}{\overline{M}} = \frac{\overline{M^2} - (\overline{M})^2}{\overline{M}} \equiv 1 + Y, \tag{4−1}$$

where $\overline{M}$ indicates the average of the measurements, $\overline{M^2}$ is the square of the average, and σ_M^2 is the square of standard deviation. Further, Y is zero in the Poisson distribution and indicates excess variation in the multiplication system.

The average of $\overline{M}$ and square of the average $\overline{M^2}$ can be expressed as follows:

$$\overline{M} = \sum_{n=0}^{\infty} nP(n), \tag{4−2}$$

$$\overline{M^2} = \sum_{n=0}^{\infty} n^2 P(n), \tag{4−3}$$

where $P(n)$ indicates the probability of precisely counting the value of n per unit time t and would be expressed as $P(n; t)$.

Y is given in the one-point reactor approximation as follows:

$$Y(t) = \frac{\varepsilon \overline{\nu(\nu-1)}}{\alpha^2 \tau_f^2} \left(1 - \frac{1 - e^{-\alpha t}}{\alpha t}\right), \tag{4−4}$$

ε: counting efficiency per unit of all fission reactions,
$\tau_f = (\nu\Sigma_f)^{-1}$: average lifetime of neutrons up to the fission reaction,
t: time duration of the count,
ν: the number of prompt neutrons per fission reaction unit.

ν has a $p(\nu)$ distribution and the average of $\overline{\nu}$ is 2.42 for ^{235}U; $\overline{\nu(\nu-1)}$ in Eq. (4−4) is given as follows:

$$\overline{\nu(\nu-1)} = \sum_{n=0}^{\infty} \nu(\nu-1)p(\nu), \tag{4−5}$$

where the ratio of Eq. (4−5) to $\overline{(\nu)^2}$ is called the Diven factor D; for ^{235}U, it is determined to be as follows:

$$D = \frac{\overline{\nu(\nu-1)}}{\overline{(\nu)^2}} = 0.795. \tag{4-6}$$

4-2-1 Decay Constant α

In the subcritical system, the fission neutrons (2nd neutrons) generated by neutrons (1st neutrons) in the source decrease gradually. This decrease can be expressed on the basis of neutron production and loss as follows:

$$\frac{d\overline{N}}{dt} = \frac{\overline{\nu N}}{\tau_f} - \frac{\overline{N}}{\ell} = \frac{k_p - 1}{\ell}\overline{N}. \tag{4-7}$$

Careful attention should be paid to the prompt neutrons. ℓ, which indicates the neutron lifetime and the multiplication rate k_p of prompt neutrons, is expressed as follows:

$$k_p \equiv \frac{\bar{\nu}\ell}{\tau_f}. \tag{4-8}$$

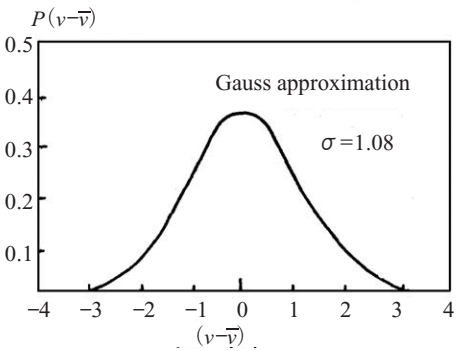

Fig. 4-1 Configuration of $p(\nu-\bar{\nu})$

By integrating Eq. (4-8):

$$\overline{N} = \overline{N_0} e^{\frac{k_p - 1}{\ell}\ell} \equiv \overline{N_0} e^{-\alpha t}, \tag{4-9}$$

and the decay constant α can be expressed as follows:

$$\alpha \equiv \frac{1 - k_p}{\ell}. \tag{4-10}$$

As shown in Appendix 4, the decay constant α can be expressed by considering the counting loss as follows:

$$\alpha = v[\{\Sigma_c + (1+\varepsilon)\Sigma_f\} - \bar{v}\,\Sigma_f]. \tag{4−11}$$

The neutron lifetime ℓ can be expressed as follows:

$$\ell = \frac{1}{v\{\Sigma_c + (1+\varepsilon)\Sigma_f\}} = \frac{\tau_f \tau_c}{\tau_f + (1+\varepsilon)\tau_c}, \tag{4−12}$$

where $\tau_c (= (v\Sigma_c)^{-1})$ indicates the average lifetime up to neutron capture.

4−2−2 *Y* Value Expressed by Reactivity

In the reactor core, the *Y* value is given as follows:

$$Y(t) = \varepsilon \left\{ \frac{\overline{v(v-1)}}{(\bar{v})^2} \right\} \left\{ \frac{(1-\beta)^2}{(\beta-\rho)^2} \right\} \left(1 - \frac{1 - e^{-\frac{\beta-\rho}{\ell}t}}{\frac{\beta-\rho}{\ell}t} \right), \tag{4−13}$$

where β indicates the delayed neutron fractions among all the fission neutrons and ρ is the reactivity. The multiplication rate k_p and the decay constant α can be expressed by using the multiplication factor k and reactivity ρ ($= (k-1)/k$), respectively, as follows:

$$k_p = k(1-\beta) = \frac{\bar{v}\ell}{\tau_f}, \tag{4−14}$$

$$\alpha = \frac{\beta-\rho}{\ell(1-\rho)} \simeq \frac{\beta-\rho}{\ell}. \tag{4−15}$$

4−2−3 *Y* Value

When $\rho = 0$, $\beta = 0.0064$, $\overline{v(v-1)}/(\bar{v})^2 = 0.795$, and the gate width t is considered to be $\ell/(\beta-\rho)$, the *Y* value is $0.7 \times 10^4 \varepsilon$. On the basis of this value, the counting efficiency should be more than 10^{-4} (Count/Fission).

4−2−4 Asymptotic Behavior of *Y* Value

For the measurement of *Y*, it is necessary to have the measurement value fit Eq. (4−4) or (4−13) on the basis of the least squares method in order to determine the decay constant α and the reactivity ρ. However, α can be approximately inferred by increasing t or the asymptotic behavior for $t = 0$

as follows:

$$\left(1-\frac{1-e^{-\alpha t}}{\alpha t}\right)\rightarrow 1, \quad for\ t\rightarrow\infty, \tag{4-16}$$

$$\left(1-\frac{1-e^{-\alpha t}}{\alpha t}\right)\rightarrow \frac{1}{2}\alpha t, \quad for\ t\rightarrow 0. \tag{4-17}$$

The Y value is saturated for $t\rightarrow\infty$, and this is defined as Y_{sat}. For $t\rightarrow 0$, the Y value can be brought to be asymptotically close to a certain value by dividing it by t.

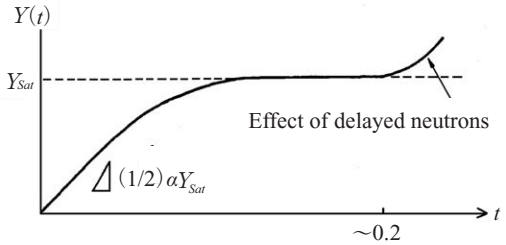

Fig. 4-2 Results of $Y(t)$ for gate time

As shown in Fig. 4-2, $Y(t)$ increases beyond Y_{sat} when the effect of delayed neutrons is considered, while it is asymptotically close to Y_{sat} for $t\rightarrow\infty$ when only the effect of prompt neutrons is considered.

4-2-5 *Y* Value in a Critical System by Delayed Neutrons

The following equation can be obtained in Eq. (4-13) for $\rho = 0$:

$$Y_c(t) = \varepsilon\left\{\frac{\overline{\nu(\nu-1)}}{(\overline{\nu})^2}\right\}\left(\frac{1-\beta}{\beta}\right)^2\left(1-\frac{1-e^{-\frac{\beta}{\ell}t}}{\frac{\beta}{\ell}t}\right). \tag{4-18}$$

By dividing the saturated value $Y_{c,\,sat}$ by Y_{sat} in a subcritical system, the following equation can be obtained:

$$\frac{Y_{c,sat}}{Y_{sat}} = \frac{(\beta-\rho)^2}{\beta^2} = \left(1-\frac{\rho}{\beta}\right)^2. \tag{4-19}$$

From this equation, either β or ρ can be obtained or the reactivity can be expressed by a dollar unit.

4−2−6 Relationship between Power and *Y* Value

The fission reaction rate and final reactor power can be obtained by considering the following detection efficiency ε obtained from the measured values of both β/ℓ and ρ/β and D and β:

$$\varepsilon = \frac{(Average\ count\ rate)}{(All\ fission\ reaction\ rate)}. \tag{4−20}$$

4−3 Experiments

4−3−1 Experimental Equipment

The 1st neutron source is Am-Be (2 Ci). (5×10^6 *n*/*s*)

Either a ^{3}He- or BF_3-proportional counter is utilized as the neutron detector. The detectors are utilized in combination with a pulsed count-rate analyzer (PRA) and a multi-channel analyzer (MCA), as shown in Figs. 4−3 and 4−4.

The histogram $F(n; t)$ of the value of n for the gate width t [s] can be obtained by using the abovementioned experimental equipment. The $Y(t)$ can be easily obtained by using the following equations:

- Total number of gates:

$$n_T = \sum_{n=0}^{\infty} F(n; t), \tag{4−21}$$

- Probability density function:

$$P(n; t) = \frac{F(n; t)}{n_T}, \tag{4−22}$$

- Average count:

$$\overline{M} = \frac{1}{n_T} \sum_{n=0}^{\infty} nF(n; t), \tag{4−23}$$

- Square average of the count:

$$\overline{M^2} = \frac{1}{n_T} \sum_{n=0}^{\infty} n^2 F(n; t). \tag{4−24}$$

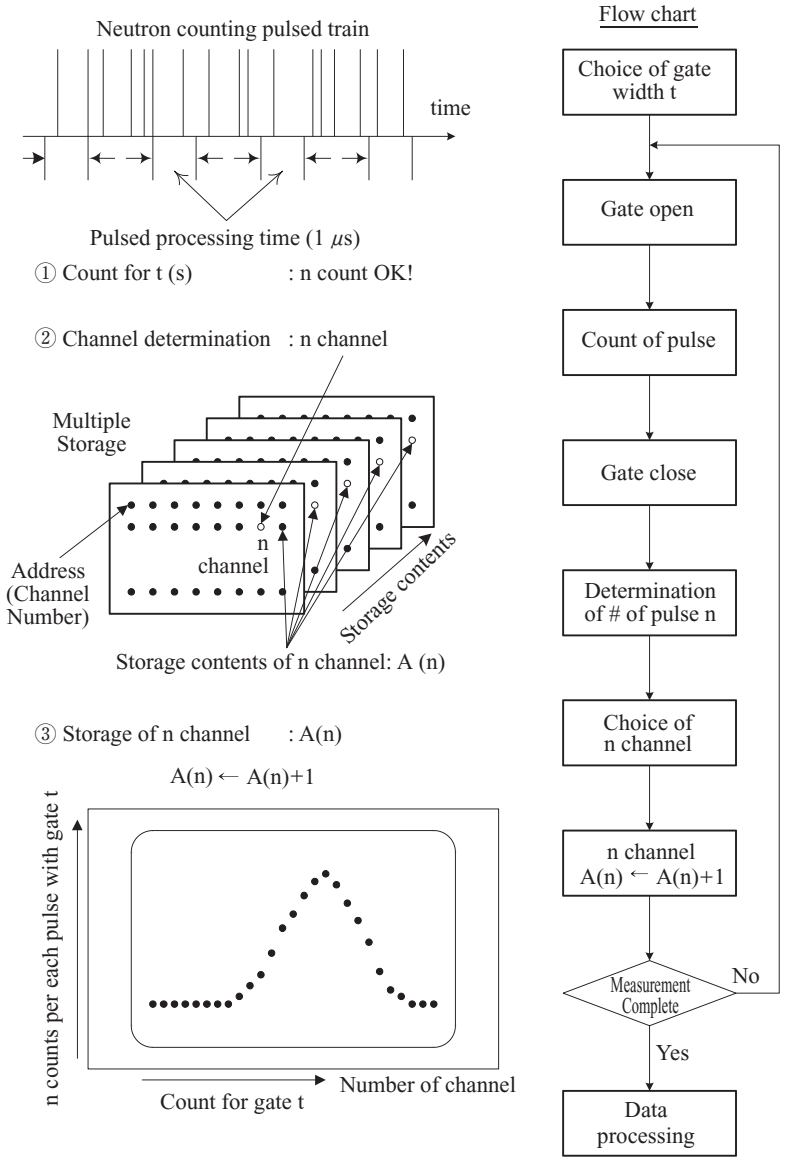

Fig. 4−3 Flow chart of the pulsed count-rate analyzer (PRA)

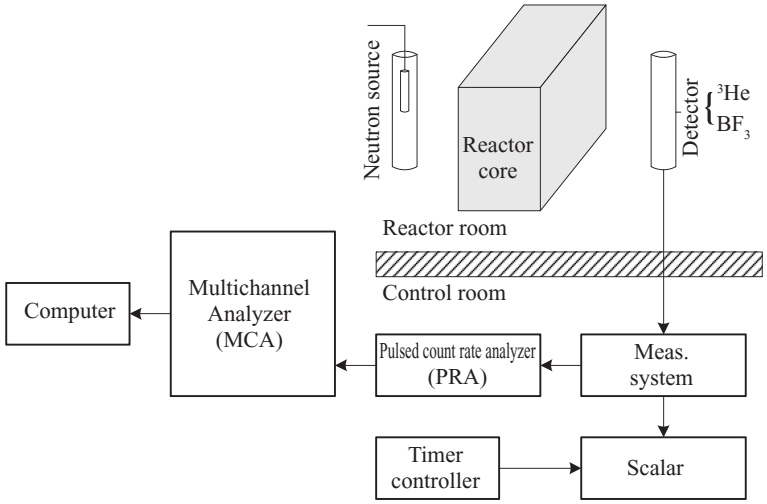

Fig. 4−4 Measurement system

4−3−2 Experimental Methods

(1) Measurement of the counting histogram distribution of a Poisson distribution

The distribution of the neutron count per gate unit in a gate width of 10 ms should be measured by inputting the signal from the ^{3}He-proportional counter that is set near the Am-Be neutron source storage of the pulsed count-rate analyzer (PRA). (Measurement time: 100 s.)

(2) Measurement of the histogram distribution count and $Y(t)$ in the core

First, the criticality point of the core should be confirmed. Choose the four points (Subcriticality I, II, III, and IV) of the subcritical control rod positions in the experiments and infer the reactivity from the control rod calibration curve. The following procedures 1) through 8) should be conducted by the operators:

1) The calibrated control rods are inserted in the core up to the subcritical state. The distance between the outer neutron source and the core should be controlled to the same power level in Subcriticality I, II, III, and IV.
2) Set the gate width t of a fixed time width, as shown in Table 4−1.
3) Set the operation time (measurement time) of the multi-channel analyzer (MCA) according to the gate width, as shown in Table 4−2.

4) Prepare the scalar for monitoring the entire operation of neutron counting N of the detector. Set the measurement time by the scalar shown in Table 4−2 after "resetting" both the scalar and MCA, and start them simultaneously.
5) Record the number of data, detector number, core system, the value of t, and so on.
6) After counting, reserve the data by MCA and record the entire neutron count (N).
7) Repeat procedures 2) through 6) for each gate width shown in Table 4−2.
8) Repeat procedures 1) through 7) for each subcritical state of the core.

Table 4−1 Setting of time width

Subcriticality	Gate Width (Time Width) t (s)	Group
I	1, 2, 3, 5, 7, 10, 20, 30, 50, 70, 100, 150	
II	1, 2, 3, 5, 7, 10, 20, 30, 50, 70, 100	
III	1, 2, 3, 5, 7, 10, 20, 30, 50, 70, 100	
IV	1, 2, 3, 5, 7, 10, 20, 30, 50	

Table 4−2 Setting of measurement time by multi-channel analyzer (MCA)

Gate width (ms)	1	2	3	5	7	10	20	30	50	70	100	150
Frequency (Hz)	1000	500	333	200	143	100	50	33	20	14	10	6.7
Time (s)	10	20	30	50	70	100	200	300	500	700	900	1000

(3) Measurement of $Y(t)$ in the delayed subcriticality of the core

The $Y(t)$ of the self-stable state, excluding the neutron source, can be measured even in the delayed subcriticality state. Subsequently, the delayed neutron precursor can be considered as the neutron source. In fact, since it is difficult to determine the criticality state at a low level, α and $Y(t)$ can be determined by extrapolation.

4−3−3 Data Processing

Electronic calculators and computers should be used to process data. Obtain the variance, mean, and Y (10 ms) by using the electronic calculators and printing the data (Subcriticality I, II, III, and IV) for the time width of 10 ms.

The data processing for periods other than 10 ms in each group should be conducted by using computers.

1) Select the Poisson distribution shown in (1) of Sec. 4−3−2 and the counting histogram distribution on certain gate widths, as shown in (2) of Sec. 4−3−2. Further, plot the same average Poisson distribution by using the above distributions. Note that the Poisson distribution can be obtained mathematically.
2) Plot $Y(t)$ obtained by (2) of Sec. 4−3−2 on the vertical axis and the gate width on the horizontal axis.
3) Obtain the Y_{sat} and α of each subcriticality state. α can be obtained by using the gradient $1/2\alpha\ Y_{sat}$, which approaches zero at $Y(t)$, or by using Z_0 obtained from Eq. (4−26).
4) Obtain the $Y_{c,sat}$ in the critical state by extrapolating Y_{sat} in the four subcriticality states. In this case, it is convenient to use $\{(1-\rho)/\beta\}^2$ obtained by the control rod calibration curve on the vertical axis and Y_{sat}^{-1} on the horizontal one. Compare it with the result of (3) of Sec. 4−3−2.
5) Compare the control rod calibration curve with the reactivity ρ/β in the four subcriticality states.
6) Plot $(\beta-\rho)/\beta$ (both obtained in the above five steps) and the control rod calibration curve on the vertical axis and $\alpha=(\beta-\rho)/\ell$ on the horizontal axis. $\alpha_c=\beta/\ell$ can be obtained from this procedure. Determine the neutron lifetime ℓ by using β (effective value) by referring to Table 2−6.
7) Obtain the power in each subcritical state. It is desirable to compare it with the results of the activation detection method in Chapter 3 and the method of calibration of the power output meter.

4−4 Discussion

From the results of this experiment, several reactor parameters from the variance-to-mean value can be obtained. The reports and discussions are presented in the following sections.

1. Reports

(1) Present the measurement condition and results obtained from (1) through (7) in Sec. 4−3−3.
(2) It is preferable to use not only the value of Y but also that of Z for data processing by the Feynman-α method. Z can be obtained as follows:

$$Z\equiv\frac{\overline{M^2}-(\overline{M})^2-\overline{M}}{(\overline{M})^2}\quad\text{or}\quad Z\equiv\frac{Y}{\overline{M}},\tag{4−25}$$

where $\overline{M}$ is equal to εFt. F indicates the average fission reaction rate and εF is the counting rate per minute. Z obtained from the data should be compared with that obtained from the Y plot. It is very interesting to observe the result Z_0 for $t \rightarrow 0$ as follows:

$$Z_0 = \frac{\overline{\nu(\nu-1)}}{2\alpha^2 \tau_f F} = \frac{\overline{\nu(\nu-1)}}{2\alpha^2 (\bar{\nu})^2 \ell^2 F} = \frac{1}{2} \alpha \frac{Y_{sat}}{\varepsilon F}. \qquad (4\text{−}26)$$

From Eq. (4−26), it can be observed that Z_0 is a specific value for the core by disregarding the counting efficiency and adding the fission reaction rate F, compared with Y_{sat}.

α should be obtained by using Eq. (4−26) and the data of (2), as obtained in Sec. 4−3−3.

(3) List the reactor constants obtained from the Feynman-α experiment. It is desirable to clearly understand which of the experiments can be carried out to obtain the experimental results.

[Example] Factors affecting the counting procedure:
(1) Dispersion of counting rate
(2) Degree of criticality in the system
(3) Efficiency of detectors
(4) Dependence on the removal rate of neutrons in the system

Experimental results
(1) Y_{sat}
(2) Gradient for $t \rightarrow 0$
(3) Counting rate

2. Discussion

(1) It has been shown that the variance in the critical state has a divergence. However, the Feynman-α experiment can be also carried out in the delayed subcritical state, and the reason underlying this should be theoretically explained; for instance, the feasibility of carrying out the Feynman-α experiment, when the gate width is more than 10 ms, should be explained.

(2) Any differences in the results obtained by using the least squares method of fitting the Y curve for gate width t in the Feynman-α experiment should be noted.

(3) The equations in the Feynman-α method should be derived by considering the delayed neutrons shown in Appendix 4, and it is noted that the solution of kinetic-inverse equations is required.

References

1. M. Otsuka, *Nuclear Reactor Theory*, Kyoritu Shuppan (1972). (in Japanese)
2. A. Furuhashi and T. Iijima, *J. Nucl. Sci. Technol.*, **16**, 117 (1974).
3. K. Saito, *JAERI 1187* (1970).
4. M. M. R. Williams, *Random Processes in Nuclear Reactors*, Pergamon Press, (1974).
5. R. E. Uhrig, *Random Noise Techniques in Nuclear Reactor Systems*, Ronald Press, (1970).
6. J. A. Thie, *Reactor Noise*, Rowman and Littlefield, (1963).
7. E. D. Courant and P. R. Wallace, *Phys. Rev.*, **72**, 1038 (1947).
8. F. de Hofmann, *The Science and Engineering of Nuclear Power*, (1948).
9. R. P. Feynman, F. de Hofmann, and R. Serber, *J. Nucl. Energy*, **3**, 64 (1956).
10. R. W. Albrecht, *Nucl. Sci. Eng.*, **14**, 153 (1962).
11. Y. Gotoh, *J. Nucl. Sci. Technol.*, **1**, 11 (1964).
12. E. F. Bennett, *Nucl. Sci. Eng.*, **8**, 53 (1960).
13. A. Furuhashi and S. Izumi, *J. Nucl. Sci. Technol.*, **4**, 99 (1967).
14. R. W. Albretcht, *IRE. Trans. Nucl. Sci.*, **1**, (1962).
15. S. Okajima, M. Narita, and K. Kobayashi, *Ann. Nucl. Energy*, **14**, 673 (1987).
16. G. R. Keepin, *Physics of Nuclear Kinetics*, Addison Wesley, (1964).

Appendix 4

4A. Derivation of Equations for Feynman-*α* Method

In this section, the derivation of Eq. (4−4) shown in Sec. 4−2 is presented by using several methods such as:

(1) Feynman method (de Hoffmann) [5, 8, 9, 15]
(2) Kolmogorov method (Courant-Wallace [1, 3, 4, 7] and Pal-Bell [2, 3])
(3) Langevin method (Moore-Cohn [1, 3])
(4) Power spectrum

In this section, the Kolmogorov Method is used for the derivation.

The P (N, M; t) is the probability given by counting M in the time distance (0, t) to the counting detectors. The change in the probability P (N, M; Δt) after Δt (s) is expressed as follows:

$$\begin{aligned} P(N, M; t+\Delta t) = & P(N-1, M; t) \times S\Delta t \\ & + P(N+1, M; t) \times (N+1)\nu\Sigma_c\Delta t \\ & + \sum_{n=0}^{\infty} P(N+1-n, M; t) \times p(n) \times (N+1-n)\nu\Sigma_f\Delta t \\ & + P(N+1, M-1; t) \times (N+1)\varepsilon\nu\Sigma_f\Delta t \\ & + P(N, M; t) \times \{1 - S - (\nu\Sigma_f + \nu\Sigma_c + \varepsilon\nu\Sigma_f)N\}\Delta t \\ & + O(\Delta t), \end{aligned} \tag{4A−1}$$

where the phenomena with these above terms in Eq. (4A−1) would occur exclusively, and the two coincident phenomena are assumed to be less than the order of Δt. S indicates the average number of neutron source emitted per unit time and $\nu\Sigma_f \equiv \tau_f^{-1}$, $\nu\Sigma_c \equiv \tau_c^{-1}$, and $\varepsilon\nu\Sigma_f \equiv \varepsilon\tau_f^{-1}$ are the fission rate, absorption rate, and detection rate, respectively.

For $t \to 0$, the differential difference equation to P (⋯, t) is given as follows:

$$\begin{aligned} \frac{dP(N, M; t)}{dt} = & S\{P(N-1, M; t) - P(N, M; t)\} \\ & + \nu\Sigma_c(N+1)P(N+1, M; t) - \nu\{\Sigma_c + (\varepsilon+1)\Sigma_f\}NP(N, M; t) \end{aligned}$$

$$+\varepsilon v\Sigma_f(N+1)P(N+1, M-1; t)+v\Sigma_f\sum_{n=0}^{\infty}p(n)(N+1-n)P(N$$

$$+1-n, M; t). \tag{4A-2}$$

It is convenient to use the following probability generating function $F(x, z)$ so that the low-order moment can be obtained:

$$F(x, z)=\sum_{N=0}^{\infty}\sum_{M=0}^{\infty}x^N z^M P(N, M; t), \tag{4A-3}$$

$$f(x)\equiv\sum_{n=0}^{\infty}x^n p(n). \tag{4A-4}$$

Multiplying Eq. (4A−2) by $x^N z^M$ and summing N and M, the following equation can be obtained:

$$\frac{\partial F}{\partial t}=(x-1)SF+[v\Sigma_c(1-x)+v\Sigma_f\{f(x)-x\}+\varepsilon v\Sigma_f(z-x)]\frac{\partial F}{\partial x}. \tag{4A-5}$$

The probability generating function is presented as follows:

$$F(x, z; t)\big|_{x=z=1}=\sum_{N=0}^{\infty}\sum_{M=0}^{\infty}P(N, M; t)=1, \tag{4A-6}$$

$$\left.\frac{\partial F(x, z; t)}{\partial x}\right|_{x=z=1}=\sum_{N=0}^{\infty}\sum_{M=0}^{\infty}NP(N, M; t)=\overline{N}, \tag{4A-7}$$

$$\left.\frac{\partial F(x, z; t)}{\partial z}\right|_{x=z=1}=\sum_{N=0}^{\infty}\sum_{M=0}^{\infty}NP(N, M; t)=\overline{M}, \tag{4A-8}$$

$$\left.\frac{\partial^2 F(x, z; t)}{\partial x^2}\right|_{x=z=1}=\sum_{N=0}^{\infty}\sum_{M=0}^{\infty}N(N-1)P(N, M; t)=\overline{N^2}-\overline{N}, \tag{4A-9}$$

$$\left.\frac{\partial^2 F(x, z; t)}{\partial x\partial z}\right|_{x=z=1}=\sum_{N=0}^{\infty}\sum_{M=0}^{\infty}NMP(N, M; t)=\overline{NM}, \tag{4A-10}$$

$$\left.\frac{\partial^2 F(x, z; t)}{\partial z^2}\right|_{x=z=1}=\sum_{N=0}^{\infty}\sum_{M=0}^{\infty}M(M-1)P(N, M; t)=\overline{M^2}-\overline{M}. \tag{4A-11}$$

By using the above equations, the 2nd order of moment, modified variance, and co-variance can be obtained as follows:

- Factorial accumulation of neutrons:

$$\mu_{NN} \equiv \overline{N^2} - (\overline{N})^2 - \overline{N} = \sigma_N^2 - \overline{N}, \tag{4A−12}$$

- Factorial accumulation of the counting:

$$\mu_{MM} \equiv \overline{M^2} - (\overline{M})^2 - \overline{M} = \sigma_M^2 - \overline{M}, \tag{4A−13}$$

- Co-variance:

$$\mu_{NM} \equiv \overline{(N-\overline{N})(M-\overline{M})} = \overline{NM} - \overline{M}\,\overline{N}. \tag{4A−14}$$

The average values can be obtained as follows:

- Average number of neutron generation:

$$\overline{\nu} = \frac{\partial f(x)}{\partial x}\bigg|_{x=1} = \sum_{n=0}^{\infty} nP(n), \tag{4A−15}$$

- 1st factorial moment of the average neutron generation rate:

$$\overline{\nu(\nu-1)} = \frac{\partial^2 f(x)}{\partial x^2}\bigg|_{x=1} = \sum_{n=0}^{\infty} n(n-1)P(n). \tag{4A−16}$$

As a result, the following series of equations can be obtained:

$$\frac{d\overline{N}}{dt} = \nu\{(\overline{\nu}-1-\varepsilon)\Sigma_f - \Sigma_c\}\overline{N} + S,$$

or

$$\frac{d\overline{N}}{dt} = \frac{k_\rho - 1}{\ell}\overline{N} + S,$$

$$\frac{d\overline{N}}{dt} = -\alpha\overline{N} + S. \tag{4A−17}$$

The reactor kinetics equation for prompt neutrons can be obtained as follows:

$$k_\rho \equiv \frac{\overline{\nu}\Sigma_f}{\Sigma_c + (1+\varepsilon)\Sigma_f} \equiv k(1-\beta), \tag{4A−18}$$

$$\ell \equiv \frac{1}{v\{\Sigma_c + (1+\varepsilon)\Sigma_f\}}, \tag{4A−19}$$

$$\alpha \equiv -v\{(\bar{\nu} - 1 - \varepsilon)\Sigma_f - \Sigma_c\}. \tag{4A−20}$$

The average counting $\overline{M}$ in gate width t is determined in accordance with the following equation:

$$\frac{d\overline{M}}{dt} = \varepsilon v \Sigma_f \overline{N}. \tag{4A−21}$$

μ_{NN}, μ_{MM}, and μ_{NM} are determined by using the following equations:

$$\frac{d\mu_{NN}}{dt} = 2\mu_{NN} v\{(\bar{\nu} - 1 - \varepsilon)\Sigma_f - \Sigma_c\} + v\Sigma_f \overline{N}\ \overline{\nu(\nu-1)}, \tag{4A−22}$$

$$\frac{d\mu_{MM}}{dt} = 2\varepsilon v \Sigma_f \mu_{NM}, \tag{4A−23}$$

$$\frac{d\mu_{NM}}{dt} = \mu_{NM} v\{(\bar{\nu} - 1 - \varepsilon)\Sigma_f - \Sigma_c\} + \varepsilon v \Sigma_f \mu_{NM}. \tag{4A−24}$$

4A−1 Steady State

Both reactivity and the outer neutron source are held constant, since the Feynman-α experiment is carried out in a steady state of a delayed critical or subcritical system.

The $\overline{N}$ and μ_{NN} in the steady state are obtained by using Eqs. (4A−17) and (4A−22) as follows:

$$\overline{N} = \frac{S\ell}{1 - k_P} = \frac{S}{\alpha}, \tag{4A−25}$$

$$\mu_{NN} = \frac{\overline{\nu(\nu-1)} v \Sigma_f \overline{N}}{2v\{\Sigma_c - \Sigma_f(\bar{\nu} - 1 - \varepsilon)\}} = \frac{\overline{\nu(\nu-1)} v \Sigma_f}{2\alpha} \overline{N}. \tag{4A−26}$$

The objective equation of the Feynman-α method is given as follows:

$$\frac{\overline{M^2} - (\overline{M})^2}{\overline{M}} = 1 + \frac{\mu_{MM}}{\overline{M}} \equiv 1 + Y. \tag{4A−27}$$

Y can be obtained by substituting $\overline{M}$ and μ_{MM} given in Eqs. (4A−21) and (4A−23), respectively, in Eq. (4A−27).

For applying a Laplace transformation to Eqs. (4A−23) and (4A−24), the matrix expression can be obtained by considering the initial value to be zero as follows:

$$\begin{pmatrix} s & -2\varepsilon\nu\Sigma_f \\ 0 & s(s+\alpha) \end{pmatrix} \begin{pmatrix} \tilde{\mu}_{MM}(s) \\ \tilde{\mu}_{NM}(s) \end{pmatrix} = \begin{pmatrix} 0 \\ \varepsilon\nu\Sigma_f \mu_{NM} \end{pmatrix}. \tag{4A−28}$$

By solving Eq. (4A−28), the following equations can be obtained:

$$\tilde{\mu}_{MM}(s) = \frac{2\varepsilon^2(\nu\Sigma_f)^2\mu_{NN}}{\alpha}\left\{\frac{1}{s^2} - \frac{1}{\alpha s} + \frac{1}{\alpha(s+\alpha)}\right\}, \tag{4A−29}$$

$$\tilde{\mu}_{NM}(s) = \frac{\varepsilon\nu\Sigma_f \mu_{NN}}{\alpha}\left\{\frac{1}{s} - \frac{1}{s+\alpha}\right\}. \tag{4A−30}$$

The following equation can be obtained by applying an inverse-Laplace transform to Eq. (4A−29) and substituting μ_{NN}, which is shown in Eq. (4A−26), in Eq. (4A−29):

$$\mu_{MM}(t) = \frac{\overline{N}\varepsilon^2(\nu\Sigma_f)^3\overline{\nu(\nu-1)}}{\alpha^2}\, t\left(1 - \frac{1-e^{-\alpha t}}{\alpha t}\right). \tag{4A−31}$$

By using Eq. (4A−27) and an integration value $\overline{M} = \varepsilon\nu\Sigma_f\overline{N}t$ given by Eq. (4A−21), Eq. (4−4) can be expressed as follows:

$$Y(t) = \frac{\mu_{MM}}{\overline{M}} = \frac{\varepsilon(\nu\Sigma_f)^2\overline{\nu(\nu-1)}}{\alpha^2}\left(1 - \frac{1-e^{-\alpha t}}{\alpha t}\right). \tag{4A−32}$$

4A−2 Consideration of Delayed Neutrons

When the delayed neutrons can be considered for up to the six-energy-group, the following equation can be obtained by using the same methodology as that of the above procedures:

$$\frac{\mu_{MM}}{\overline{M}} = \sum_{i=1}^{7} Y_i\left(1 - \frac{1-e^{-\alpha_i t}}{\alpha_i t}\right). \tag{4A−33}$$

Y_1 is equal to the Y shown in Eq. (4A−32), and the general expression is given as follows:

$$Y_i = 2\varepsilon \frac{\overline{\nu(\nu-1)}}{\alpha_i (\bar{\nu})^2} A_i G(\alpha_i), \tag{4A−34}$$

where α_i indicates the solution $s = -\alpha_i$ of a "within-an-hour" equation and $G(s)$ is a transfer function of the zero power reactor. α_1 is the prompt neutron decay for the gate width t, and it is expressed as follows:

$$\frac{1}{\alpha_1} = t = \frac{1}{\alpha_2}. \tag{4A−35}$$

The above experiment can be possibly carried out by considering only the first term ($i = 1$), shown in Eq. (4A−33), while the experiment cannot be carried out because of a divergence of Y_7 for $\alpha_7 = 0$ in the delayed criticality.

4A−3 Initial Correlation Correction, Spatial Dependence, and Fission Counter

When the neutron density is small and the effect of the neutron source is large, the effect of spatial higher-mode would be strong for the core. However, it is necessary to multiply the spatial correction factor g (1.1−1.3)[2,15] considering the effects of spatial distribution of the neutron source, even when the fundamental-mode neutron flux can be approximately obtained in a low-subcriticality state. This correction is important especially for the measurement of reactor power. However, this correction is too small[3] for using a fission counter, although the correlation by the detection of a second neutron would be added.

Chapter 5 Pulsed Neutron Source Method

5−1 Purpose

The pulsed neutron source method is a technique for measuring the time change in neutron density in a system in which pulsed neutrons are generated by an accelerator and injected into either a moderated or multiplication system. This method is considered as one of the basic measurement techniques for obtaining several integrated reactor physics parameters.

In this experiment, the measurement of negative reactivity is carried out in the multiplication system by using the pulsed neutron method. The purpose of this experiment is to learn the fundamentals and experimental techniques of the pulsed neutron method.

5−2 Principle

In this section, the time change in neutron density in the multiplication system, when the high-energy neutrons are injected into the multiplication system below criticality, is presented quantitatively. Also, physical consideration is presented theoretically for the relationship[1] between the decreased neutron density and the reactivity in the system.

When the high-energy neutrons are injected in the system, all the neutrons are emitted at the time interval (10 μs order) of neutron burst and are diffused throughout the system. For carrying out these procedures, the neutrons are moderated repeatedly through collisions with nuclei. The time in which the high-energy neutrons are moderated to thermal neutrons depends on the energy and slowing-down power of the injected neutrons. Namely, the start-up time depends on the neutron burst width and the average slowing-down time required for moderating the energy of the injected neutrons to that of the thermal neutrons, although the thermal neutron density in the system is considerably large after the neutron burst. Note that this holds for the case in which the neutron moderation time is shorter than the average lifetime of the thermal neutrons to a greater extent.

By following the abovementioned procedure, the thermal neutrons are diffused in the system, and they either get absorbed inside the system or

leak outside. However, in the multiplication system, the neutrons absorbed in nuclear fuel produce some new fast neutrons by fission reactions. Since delayed neutrons are reserved in a corresponding precursor and the decay time ratio is very small in the time region for a measuring object, it is important to consider the prompt neutrons. The prompt neutrons generated by the fission reaction are moderated to the thermal neutrons. They are then absorbed inside or leak outside the system. In this subcritical system, the number of thermal neutrons in the system decreases exponentially, and this decay constant is related to the reactivity in the system.

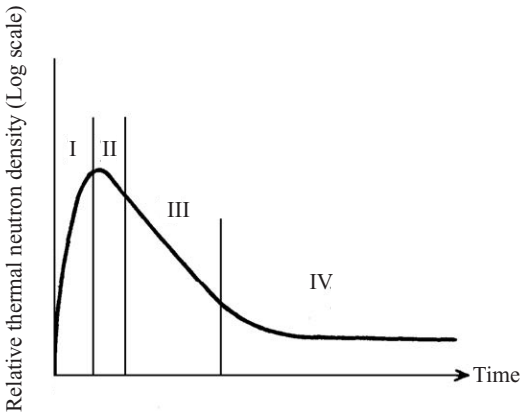

Fig. 5−1 Change in thermal neutron density after injection of pulsed neutrons

As shown in Fig. 5−1, the time change in the thermal neutron density of the system after the injection of high-energy neutrons into the system is presented as follows:

(Region I)

The thermal neutron density increases by moderating the neutron source injected into the thermal neutrons.

(Region II)

The neutron spectrum reaches equilibrium and the spatial distribution in the higher-mode decreases.

(Region III)

The thermal neutron density exponentially decreases in accordance with

the specific decay constant. This decay is caused by the prompt neutrons.

(Region IV)

The thermal neutron density in this region is smaller than that in Region III and decreases gradually. The change in thermal neutron density of Region IV is caused mainly by the delayed neutrons, and this decay depends on the average lifetime (less than 12 s) and amplitude of the reactivity of the system.

The characteristic of Region III is an exponential decrease in the thermal neutron density. Namely, in this region, neutron production is caused only by the prompt neutrons, since the contribution of delayed neutrons is relatively low. The ratio of the contribution is constant, and it can be expressed as follows:

$$k_p = (1-\beta)k, \tag{5−1}$$

where k_p is the prompt neutron multiplication coefficient, k is the multiplication factor including the delayed neutrons, and β is the effective delayed neutron fraction.

The rate of change in the neutrons of the system is given as follows, in accordance with the generation of pulsed neutrons:

$$\frac{\Delta n}{n} = (1-\beta)k - 1. \tag{5−2}$$

By introducing the prompt neutron lifetime ℓ, Eq. (5−2) can be expressed per unit time as follows:

$$\frac{dn/n}{dt} = \frac{(1-\beta)k-1}{\ell}. \tag{5−3}$$

The time change over the number of neutrons can be given as follows:

$$n(t) \simeq n_o \exp\left\{-\frac{1-(1-\beta)k}{\ell}t\right\}. \tag{5−4}$$

Finally, the decay constant α after the injection of pulsed neutrons into the multiplication system can be expressed as follows:

$$\alpha = \frac{1-(1-\beta)k}{\ell} = \frac{\beta}{\ell}k\left(\frac{1-k}{\beta k}+1\right). \tag{5-5}$$

On the other hand, reactivity ρ, negative reactivity \$ (dollar units), and prompt neutron generation time Λ are defined as follows:

$$\rho = \frac{k-1}{k}, \tag{5-6}$$

$$\$ = \frac{\rho}{\beta} = \frac{k-1}{\beta k}, \tag{5-7}$$

$$\Lambda = \frac{\ell}{k}. \tag{5-8}$$

By using Eqs. (5-6) through (5-8), the decay constant α can be expressed as follows:

$$\alpha = \frac{\beta}{\ell}k(1+\$) = \frac{\beta}{\Lambda}(1+\$). \tag{5-9}$$

When the pulsed neutron experiment is carried out in a delayed critical system, the decay constant α_c can be expressed as follows:

$$\alpha_c = \frac{\beta}{\Lambda}. \tag{5-10}$$

α_c can be considered as an index of reactivity measurement in the subcritical system. Namely, since Λ can be considered to be constant for the experiment in the state of $k \fallingdotseq 1$, the reactivity \$ in the dollar units is determined as follows:

$$\$ = \frac{\alpha}{\alpha_c} - 1. \tag{5-11}$$

This is known as the Simmons-King method.[2] (However, α_c is obtained by the extrapolation of the result from the measurement in a subcritical system in which the reactivity is known beforehand, since it is very difficult to measure its value directly).

The decay of the number of neutrons observed practically is the sum

of the region of exponential change and that of the background of delayed neutrons, and is given as follows:

$$n = Ce^{-\alpha t} + B. \tag{5−12}$$

(Note that it is not suitable to set B = const. in case the system is very close to criticality.)

From this discussion, the change in the number of neutrons can be expressed as follows:

$$\frac{dn}{dt} = -\alpha Ce^{-\alpha t} = -\alpha(n - B). \tag{5−13}$$

On the other hand, on the basis of the reactor kinetics equation, the change in the number of neutrons can be expressed as follows:

$$\frac{dn}{dt} = \frac{\rho - \beta}{\ell(1-\rho)} n + \sum_{i=1}^{6} \lambda_i C_i, \tag{5−14}$$

and by using Eq. (5−6), Eq. (5−14) can be expressed as follows:

$$\frac{dn}{dt} = \frac{(1-\beta)k - 1}{\ell} n + \sum_{i=1}^{6} \lambda_i C_i. \tag{5−15}$$

Assuming that the coefficients of the number of neutrons n in both Eqs. (5−13) and (5−15) are equal to each other, the following equation can be obtained:

$$\alpha = \frac{1 - (1-\beta)k}{\ell}. \tag{5−16}$$

It is necessary to introduce some approximations to the neutron transport equation and describe the behavior of neutrons for the injection of pulsed neutrons into the multiplication system in order to completely address this problem.[2, 3] In general, the calculations are conducted with energy groups 1 and 2 of the delayed neutrons and the bare core system. By deriving the neutron diffusion equation using the abovementioned method, the conventional time dependence equation can be obtained for the neutron density.

The spatial higher-mode effect can be observed in the measurement. The

objective reactivity is one for the fundamental-mode, although the higher-mode effect can be expressed by eigenfunctions in a wave equation of the spatial neutron flux distribution. Therefore, when all the higher-mode components are fully attenuated, it is necessary to determine the decay constant by carrying out measurements. This condition can be easily found in the system that is approaching criticality. However, the effect on the decay constant can be observed, since the attenuation of the fundamental-mode component is quickly increased and the split with higher-mode ones is difficult, as the subcriticality in the system deepens. The effect of higher-mode components can be measured experimentally by setting some detectors in several locations throughout the system. Regardless of the energy dependence of the detectors, it is possible to carry out the reactivity measurement.

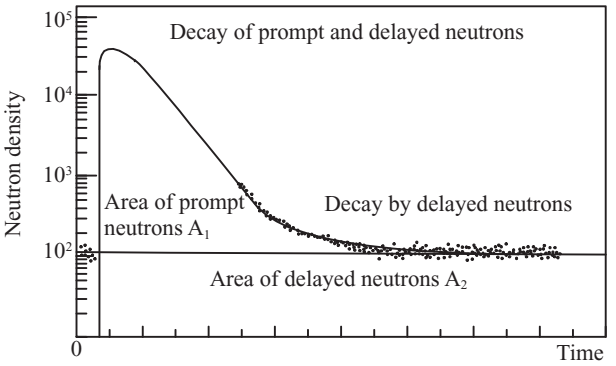

Fig. 5−2 Decay of neutron density

The method of reactivity measurement was proposed by Sjostrand.[4] This method involves the determination of the area ratio of attenuation distribution of the delayed neutrons, as shown in Fig. 5−2. The areas A_1 and A_2 corresponding to the prompt and delayed neutrons, respectively, as shown in Fig. 5−2, are given as follows:

$$A_1 = \frac{S}{1-(1-\beta)k}, \tag{5−17}$$

$$A_1 + A_2 = \frac{S}{1-k}, \tag{5−18}$$

where S indicates the number of injected neutrons.

ρ/β can be obtained from the ratio of A_1 to A_2 by using the following equation:

$$\frac{A_1}{A_2} = \frac{1-k}{\beta k} = -\left(\frac{\rho}{\beta}\right)_{sj}. \tag{5−19}$$

The main feature of this method is that it is independent of an index of reactivity measurement, such as α_c, which is required in the Simmons-King method. The higher-mode components in the system would be affected, since the fundamental-mode is assumed to be dominant in the system.

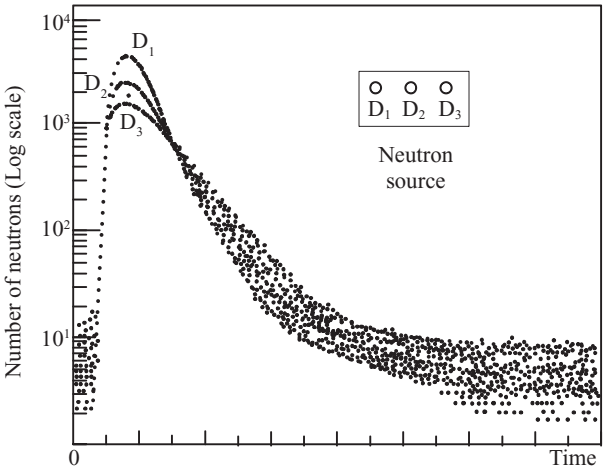

Fig. 5−3 Spatial dependence on decayed neutron density

As shown in Fig. 5−3, it was observed that the configuration at start-up varied according to the positions of both the neutron source and detectors and that the value of A_1 varied according to the configuration of the attenuation curve at start-up.

For decreasing the effect by spatial higher-mode components, the "extrapolation area ratio method" was proposed by Gozani,[5] and the reactivity was expressed as follows:

$$-\left(\frac{\rho}{\beta}\right)_{Go} = e^{\alpha t_w} \frac{\int_{t_w}^{T} X_p(t)\,dt}{\int_0^T X_d(t)\,dt}, \tag{5−20}$$

where $X_p(t)$ indicates the area of the decay curve by prompt neutrons, $X_d(t)$

is the delayed neutron level, T is the pulsed repetition period, and t_w is the waiting time of decreasing higher-mode components.

The Simmons-King method was modified by Garelis and Russell.[6] The spatial dependence of reactivity measurement is found in the core with a reflector, since the above methods are assumed to be in a one-region bare core with one-energy-group even if these analyses would be performed at full attenuation of higher-mode components.[7] Note that the analyses conducted so far are mentioned in Refs. 8 through 11.

5−3 Experimental Equipment

(1) Selected Core
One of the three KUCA cores (A, B, or C) is selected.

(2) Pulsed Neutron Source
The shield tube (Kaman Corp.) is utilized as the pulsed neutron source (PNS) in this experiment. This tube is divided into a console and a neutron generation pipe of diameter approximately 10 cm and length approximately 60 cm. The 14 MeV neutron burst is generated by a D-T reaction with a pulsed width in the range of 2 to 5 μs and a repetition frequency of less than 10 pps. The console is set in the control room (CR) or measurement room and the neutron generation tube is placed in the reflector region. These two pieces of equipment are joined by a strong cable.

(3) Neutron Measurement System
Counting detectors such as the BF_3 proportional and ^3He proportional counters, which are used in the fission chamber (starting system), are utilized in this experiment. The time change over these counts is measured by a multi-channel scalar (MCS), as shown in Fig. 5−4.

5−4 Experimental Methods

Note that the differential reactivity of the control rod is measured beforehand.

(1) Maintain the criticality by using the other control rods, with the control rod whose differential reactivity is known fully withdrawn. Then insert this control rod completely into the core. Wait until the background count is constant and measure the background count.
(2) Start the operation of the PNS after confirming that the measurement

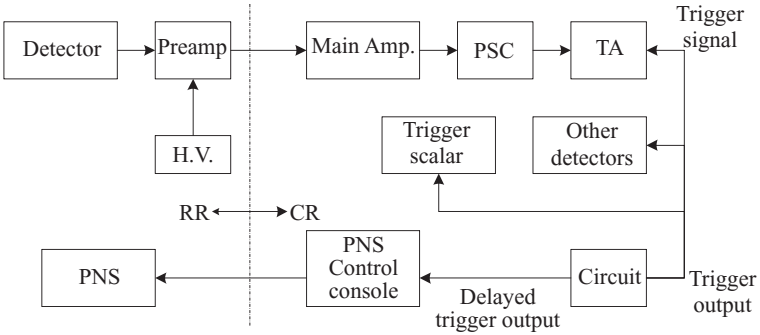

Fig. 5−4 Measurement system

system is set-up. Ensure that the repetition frequency is within 0.5 to 3 pps. Start the time analyzer (TA) counting scalar (CS) for the trigger and timer when the delayed neutron level is constant by injecting pulsed neutrons at approximately 100 pulse. The channel width of the time analyzer (channel width × channel number < repetition frequency) should be within 50 to 100 μs/ch.

(3) Complete the measurement when the pulse injection is within 500 to 2,000 pulse. Record the measurement results by the time analyzer; these should include all the counts, number of triggers, and measurement times (the values of scalar and timer).

(4) Stop the operation of the PNS and withdraw the control rod with approximately 0.1 %$\Delta k/k$ on the basis of the calibration curve of the fully retracted control rod. After reaching the steady state, measure the background count.

(5) Repeat the abovementioned measurement procedure 5 or 6 times around the criticality level.

5−5 Data Processing

(1) Visually determine the decay constant α_c from the decay area of the fundamental mode by plotting the decay curve of all the control rods measured by all the detectors on a semi-log graph paper and by examining the channel of spatial higher-mode disappearance. (Correct the dead time of the detectors and background, etc., if possible. The sensitive measurement time in each channel is presented as [channel width − memory time (4 μs)] × [number of trigger]).

(2) Obtain the relationship between ρ and α by plotting the reactivity ρ that is obtained by plotting the control rod calibration curve in the horizontal

axis and the decay constant α in the vertical axis. Further, determine the prompt neutron decay constant α_c in the critical state by extrapolation.
(3) By using the value of α_c obtained, determine the reactivity in dollar units by using the Simmons-King method by Eq. (5−11).
(4) Determine the reactivity in dollar units by the area ratio method and the extrapolation area ratio method by using Eqs. (5−19) and (5−20), respectively.

5−6 Discussion

As a rule, an experimental report for each member should be prepared. However, the method and results of the experiments and the common terms in each group can be shared and copied (terms (1) through (4) as follows):

(1) Consider how the positions of the neutron generation equipment and detectors affect the higher-mode components.
(2) Confirm whether the reactivity obtained by the period method agrees with that obtained by the Simmons-King method. If they do not agree, determine the underlying reasons.
(3) Confirm whether the reactivity in dollar units obtained by the area ratio method (and extrapolation area ratio method) agrees with that obtained by the Simmons-King method. If they do not agree, determine the underlying reasons.
(4) Determine whether the energy characteristics of the detector are caused by the systematic effect of the measured reactivity, when the experimental data is obtained by detectors with energy characteristics.

References

1. G. R. Keepin, *Physics of Nuclear Kinetics*, Addison-Wesley, (1965).
2. B. E. Simons and J. S. King, *Nucl. Sci. Eng.*, **3**, 595 (1958).
3. S. C. Fultz, *Nucl. Sci. Eng.*, **6**, 313 (1959).
4. N. G. Sjostrand, *Arkiv Fysik*, **11**, 233 (1956).
5. T. Gozaini, *Nukleonik*, **4**, 348 (1962).
6. E. Garelis and J. L. Russel, *Nucl. Sci. Eng.*, **16**, 263 (1963).
7. O. Meyer and E. Garelis, *Development of Pulsed Neutron Application to Power Reactor Start-up Procedures*, GEAP−4644, (1964).
8. A. E. Walter and L. Ruby, *Nukleonik*, **10**, 2 (1948).
9. M. Becker and K. S. Quinsberry, *The Spatial Dependence of Pulsed Neutron, Reactivity Measurements,* Arizona Symposium, (1965).

10. O. Aizawa, *J. Nucl. Sci. Technol.*, **6**, 498 (1969).
11. F. C. Difilippo, N. B. Pieroni, and J. C. Vinez, *Nucl. Sci. Eng.*, **51**, 262 (1973).

Kyoto University Press

NUCLEAR REACTOR PHYSICS EXPERIMENTS

Tsuyoshi Misawa, Hirohiko Unesaki and Cheol Ho Pyeon